Parametric Reduced-Order Models for the Structural Dynamics of Hybrid Electric Vehicle Batteries.

by

Jau-Ching Lu

A dissertation submitted in partial fulfillment
of the requirements for the degree of
Doctor of Philosophy
(Mechanical Engineering)
in The University of Michigan
2018

Doctoral Committee:

Professor Bogdan Epureanu, Chair
Professor Kenn R. Oldham
Professor Armin W. Troesch
Professor Kon-Well Wang

Jau-Ching Lu

jauching@umich.edu

ORCID iD:0000-0002-2899-0750

DEDICATION

To everyone who has helped me and everyone who loves me

ACKNOWLEDGEMENTS

I would like to thank my advisor Professor Bogdan I. Epureanu for his instruction and training during the past 5 years. With his guidance, I learned knowledge in the field of structural dynamics and constructed the parametric reduced-order models for battery packs. He can always point out what I overlooked whenever I met a bug in my codes, while giving me insights to solve a problem. I would like to thank my committee members: Professor Kenn R. Oldham, Professor Armin W. Troesch, and Professor Kon-Well Wang, for their advice during my research.

I would also like to express my gratitude to my lab members in Applied Nonlinear Dynamics of Multi-Scale Systems Lab at the University of Michigan, including the following people: Kiran D'Souza, Mainak Mitra, Hiroshi Yamasaki, Ki-Yong Oh, Seunghun Baek, Woo Chul Nam, Chen Shiyang, Zhiwei Liu, Kejie(Jessy) Chen, Andrea Lupini, Ehsan Mirzakhalili, Amin Ghadami, Himanshu Saxena, Weihan Tang, Adegbenga Odofin, and Chenyu Yi. Special thanks to the lab lunch organizer, Mainak Mitra, the lunch time with lab members at Pierpont Commons is always the best time in a day. Additionally, I appreciate my parents, my girlfriend Tsai-yu Han, my roommate Ming-Yuan Yu, and all my friends for their loves and support.

This research was supported by the Automotive Research Center, a U.S. Army RDECOM center of excellence for modeling and simulation at the University of Michigan.

TABLE OF CONTENTS

LIST OF FIGURES

Figure

LIST OF TABLES

Table

ABSTRACT

A battery pack used in electrified vehicles consists of stacks of nominally identical cells mechanically coupled through foams and spacers. Because of these repeated substructures, the dynamic behavior of a pack is characterized by high modal density (HMD) regions with closely spaced natural frequencies. It is known that with frequencies of excitation in such a HMD region, small commonly occurring structural variations may lead to significant amplification of vibration responses in some cells compared to responses of the nominal design. Intense vibration responses may lead to high stresses and consequently lead to failure of the whole battery pack. Because cells are connected in series, the battery pack fails when one of the cells fails. Consequently, the maximum vibration response for cells is a key metric for the reliability of the battery pack.

To characterize this dynamic behavior, it is necessary to conduct statistical analyses by calculating the vibration response amplitudes for a range of parameters quantifying these structural variations. Since it is time-consuming to conduct a single simulation with full-order finite element models with given structural variation levels, it is time prohibitive to conduct statistical analyses, which involve large numbers of simulations. Moreover, since different arrangements of different types of spacers affect the coupling of cells and are capable mitigating vibration responses of the battery pack, it is essential to search the optimal arrangement of spacers in design process to improve the reliability of battery packs. Since the optimization of the arrangement of spacers involves considerable searching steps and the vibration response amplitudes are calculated at each step, the simulation time is desired to be reduced. This

dissertation focuses on developing parametric reduced-order models (PROMs) to reduce the calculation time and enable statistical analyses and the optimization of the arrangement of spacers.

The structural variations considered in this work are categorized into linear and nonlinear variations. Three linear structural variations are considered: prestress variation (PreV), cell-to-cell variation (C2CV), and spacer-to-spacer variation (S2SV). PreV comes from the preload applied on the battery pack. C2CV refers to each cell that has different structural characteristics compared to its nominal design. S2SV suggests different types of spacers. Two nonlinear structural variations are considered, which come from the nonlinear behavior in cells and foams. The modulus of the elasticity of cells and foams, which include porous material, increase nonlinearly due to the consumption of the porosity under deformation. PROMs are developed to capture all these linear and nonlinear structural variations simultaneously and to predict the vibration responses efficiently and accurately. The results predicted by PROMs are validated by comparison with the full-order model.

The key contributions of this thesis are: (1) the development of novel PROMs for simultaneously capturing linear structural variations including PreV, C2CV, and S2SV, (2) the development of novel PROMs for capturing nonlinear behavior in cells and foams, and (3) the statistical analyses and optimization of the arrangement of spacers using PROMs. The statistical analyses show that the cell-to-cell variations can drastically amplify the vibration response of a cell. Also, the vibration response can be significantly mitigated with the optimized arrangement of spacers.

CHAPTER I

Introduction

1.1 Introduction

1.1.1 Motivation

Automobiles using petroleum causes air pollution and have recently became a global problem[1]. Also, the transportation sector highly depends on the petroleum, whose supply-and-demand balance is straining, and therefore threatens economic stability[2]. Electrified vehicles (EVs) have received considerable attention for their potential of reducing petroleum consumption through efficiency improvements. EVs require onboard battery packs to power their electric drive systems. It is of importance to investigate the design features that can enhance the reliability of a battery pack as a power storage system. There are substantial research interest in performance of battery packs[3, 4, 5, 6]. However, relatively little attention has been paid to their structural dynamics.

Battery packs are subject to road and vehicle vibrations[7], which come from general road surface unevenness, road surface aberrations[8], vehicle drivetrain system, and internal combustion engine[9]. Due to these vibrations, it is necessary to evaluate the fatigue life of battery packs in the initial stage of product design to guarantee its reliability[10]. The impact of mechanical vibration on fatigue life has been studied

extensively in literature[11, 12].

Vibration can cause fatigue damage of different kinds. In the worst case scenario, the cells can burst.

It is known that vibration is one of major causes of battery pack failures[13]. Vibration can cause fatigue damage of different kinds[14, **?**]. In the worst case scenario, the failures of battery packs may lead to severe accidents because the components of rechargeable batteries make them highly flammable and have the potential to spread quickly throughout battery packs which is known as thermal runaway[15, 16, 17]. Many battery fires and incidents used in EVs have been reported. It was reported that in 2011, General Motor Chevrolet Volt Li-ion battery pack caught fire during the National Highway Traffic Safety Administration crash-safty tests before GM recalled approximately 8,000 Volts on the road[18]. It was also reported that in 2012, an explosion of a prototype battery inside a GM laboratory blew at least one eight-inch thick doors[19]. Five people received medical attention after the incident. In 2013, A crash of a Tesla Model S triggered a fire in the EV's battery pack and the company's stock price was down about 10% as a result[20].

The effect of vibration on battery packs is potentially a major cause of durability failures[21]. It is known that even small structural variations in battery packs can significantly amplify the vibration responses. A battery pack is constructed by stacking dozens or even hundreds of nominally identical single cells connected in series coupling through spacers in a spatially repeated layout. The battery pack with such repeated substructures (single cell) features high modal density (HMD) in its natural frequency plot, where bands/groups of natural frequencies can be very close to each other[22, 23, 24, 25].

If the load-induced excitation acting on the battery pack has frequencies in a HMD region, the forced responses may be amplified significantly due to small structural variations from the nominal design of the system[26]. In particular, the system

can exhibit mode localization [27, 28], where the vibration energy is spatially concentrated in a small region of the structure because of the mechanical cross-talk between cells. The mode localization phenomenon can drastically change the amplitude of the vibration response and the location of maximum amplitude, and consequently shortens the fatigue life and decreases the performance of the battery pack. Similar phenomena are also observed in the field of turbomachinery[29, 30]. Because of the high sensitivity of the vibration response of battery packs to small random variations in their structural parameters, statistical methods are needed.

Structural variations in battery packs are classified into two categories: linear and nonlinear structural variations. The linear structural variations are independent of vibration responses of battery packs. The linear structural variations considered in this work involve prestress variation (PreV), cell-to-cell variation (C2CV) at each cell, and spacer-to-spacer variation (S2SV) at each spacer. PreV may exist due to different preloads applied to battery packs during installation or variances in thermal stresses resulting from environmental temperature or charge/discharge cycles. These effects change the equivalent modulus of the elasticity of entire battery packs. Another type of structural variation is the C2CV when different cells in battery packs have different modulus of elasticity compared to the nominal design. Such C2CVs are usually the result of variances in manufacturing process[31], or different state-of-charge in different cells during charge/discharge cycles. The C2CV affects the equivalent modulus of the elasticity of each individual cells[32].

Since small random PreV and C2CV are unavoidable in practice and can radically modify vibration responses, their effects need to be identified during design process. Most commonly statistical analyses are employed to investigate the effect of uncertainties by conducting large numbers of separate simulations with different levels (and distributions) of structural variation as input. However, even a single simulation may require significant computational effort and time for high fidelity full-

order models, depending on the complexity and mesh density of the finite element model (FEM) used. The computational time can be on the order of days of CPU time. Consequently, a statistical analysis may be rendered impractical due to the prohibitive simulation time involved. Additionally, the modes of a pack depend on a nonlinear fashion on each cell's structural variations.

The third type linear structural variation is S2SV. Different types of spacers have different equivalent modulus of elasticity in finite element models (FEMs) and are considered as structural variations between spacers. There are many types of spacer designs for several objectives. First, battery pack spacers are designed to prevent contact between terminals (positive electrode terminal or negative electrode terminal) of adjacent single cells when a load is applied from outside to battery packs and thus prevent short-circuiting of battery packs[33]. Also, cooling medium passages are formed by interposing spacers made of metallic material between two adjacent single cells. The battery packs are cooled by convection currents in these cooling medium passages or by forcibly passing cooling medium therethrough[34, 35]. Spacers are also designed for heating the battery pack due to its poor low-temperature performance. The low temperature increases the internal impedance of batteries and reduces its available energy[36]. Moreover, single cells, which are securely joined together through spacers, must be firmly held to minimize dynamic effects on the vehicle's handling[37, 38].

There are multiple spacers in a battery pack. Replacing any one of spacers from a different type forms a new arrangement of spacers in the battery pack. Since different arrangements of different types of spacers change the mechanical coupling between cells, the vibration response of battery packs can be mitigated. Consequently, the arrangement of spacers can be designed to lower the vibration response, which is a key metric of reliability of battery packs. One of research problems is to optimize the arrangement of spacers, which minimizes the vibration response of a battery pack.

Since the vibration response may be a non-convex nonlinear function of the arrangement of spacers, a genetic algorithm, which is a non-gradient optimization approach, is employed to solve the optimization problem. However, the genetic algorithm may involve multiple random search steps and initial search starting points, each of them requires solving the time-prohibitive full-order model once.

The nonlinear structural variations depend on vibration responses of battery packs. The nonlinear structural variations considered in this work are nonlinear dynamic behavior in cells and foams and are modeled as nonlinear modulus of elasticity. The foams and separators are porous polymeric layers. Nonlinear behavior is observed in these polymers due to the consumption of the porosity under deformation[39, 40, 41, 42, 43]. With the increasing deformation, densification of the polymeric material contributes to the increase of modulus of the elasticity. Solving a nonlinear full-order model, which requires much more computational effort and time than a linear one, becomes computationally impratical.

1.1.2 Background

Different reduction approaches have been studied in literature to reduce simulation time. One popular approach is to represent the modes of system with structural variations in terms of a subset of nominal system modes (SNM)[44], which are defined as the modes of the system without structural variations. The dynamic system matrices (mass, damping, and stiffness) of the system with structural variations are projected using SNM. This projection reduces the order of structural dynamic equations while not requiring the calculation of modes of the system with structural variations. However, the SNM approach requires building and projection of system-level matrices for given structural variations.

Another popular reduction approach is the component mode synthesis (CMS)[45, 46, 47, 48, 49, 50, 51, 52, 53]. CMS approach breaks down a large complex structural

system into several smaller components, which are connected to each other through interfaces. The order of the governing equations of each component is significantly reduced by using CMS modes, which consist of constraint modes and truncated normal modes. The constraint modes are defined by producing a unit displacement on each interface degree of freedom (DOF) with all other interface DOFs fixed. The normal modes are defined as the vibration modes with all interface DOFs fixed, and the truncated normal modes are determined according to the range of frequency of interest. The component-level dynamic system matrices with structural variations are projected on the CMS modes and are assembled through the interface by imposing geometric compatibility and forming the reduced-order system-level matrices. CMS frees the need to build and to project the system-level matrices, but it still needs to build and project the component-level matrices for given structural variations. Also, there is no reduction applied to the number of constraint modes, which is equal to the degrees of freedom (DOFs) on the interfaces between substructures, and the number increases when the mesh density of FEM increases. Consequently, the resulting number of reduced structural dynamic equations increases and the computational time increases. To overcome the issue that the CMS model is dominated by the number of constraint modes, Castanier et al. [54] developed a method to reduce the size of the CMS model by performing an eigenanalysis on the constraint mode partitions of the mass and stiffness matrices. These characteristic constraint modes may then be truncated to yield a smaller model.

SNM and CMS, however, can only be used for a single realization of the model, and is therefore not efficient when there are structural variations that require many realizations. Thus, Balmés [55] introduced design-oriented models called parametric reduced-order models (PROMs). PROMs consider mass and stiffness matrices as functions of a single structural variation, and use interpolation to obtain the projected mass and stiffness matrices in order to avoid building and projecting of matrices for

given structural variations.

There are two levels of structural variations. One is global-level structural variations (such as those induced by prestress variations in the entire pack). The other is component-level structural variations (such as variations in the state of charge of cells, or temperature variations from cell to cell). Previous PROMs are designed to capture system-level structural variations, but they have to be modified to capture component-level variations. Lim et al. [56] developed the component mode mistuning (CMM) method to capture structural variations in substructures. CMM was developed for predicting the vibration response of mistuned bladed disks in turbomachinery. Single stage rotors of turbines consist of sectors that are repeated substructures, and lead to high modal density. Thus, small structural variations in the blades can significantly change the system-level vibration response. However, CMM only captures component-level variations and not system-level variations. Hong et al. [26] developed a method to simultaneously capture global-level and substructure-level variations using interpolation combined with CMS. Nevertheless, their method uses CMS and the computational time can be large if many interface DOFs exist.

Hong et al.[57, 58] developed next-generation parametric reduced-order models (PROMs), which obtain the projected component-level matrices with both system-level and component-level structural variations using interpolation. By using singular value decomposition to condition the transformation matrix in the range of structural variations, the next-generation PROMs are very efficient and accurate for analyzing the vibration response with structural variations, such as thickness changes due to design or damages in substructures. It frees the need to build and project component-level matrices with structural variation. Also, this approach assembles projected component-level matrices simply by addition. This frees the need to enforce geometric compatibility at the interface as in the CMS approach. Moreover, constraint modes are not employed for reduction in PROMs. Consequently, the reduced order

of structural dynamic equations is independent of mesh density.

However, these methods were developed for reduction of linear systems wherein the structural properties are independent of the system responses. As discussed before, the material used for construction of cells and foams is nonlinear and their stiffness and damping depends on the structural displacement. Nonlinear structural dynamic equations may be solved using direct time integration (DTI) techniques[59]. DTI approaches allow analysis of transient system responses but involves computationally expensive calculation processes. Usually, only steady state periodic responses of the structure are of interest in the analysis of vibration amplification due to structural variation. The harmonic balance method (HBM)[60] is a well-known approach to construct the nonlinear structural dynamic equations and to efficiently solve steady state responses. HBM applies fast Fourier transform (FFT) algorithm to project the nonlinear structural dynamic equations into the frequency domain, and the structural displacement is assumed to be the combination of the first few harmonic terms. Nonlinear algebraic equations are constructed wherein the unknowns are the Fourier coefficients of the FFT of the structural displacement. The system is solved using Newton-Raphson method. HBM has been used to simulate bladed disks (blisks) with nonlinear contacts such as blisks with ring dampers [61] and shrouds[62, 63].

1.1.3 Dissertation Outline

This dissertation focuses on developing new nonlinear PROMs which capture both a global-level and multiple component-level structural variations simultaneously while eliminating the need for CMS to significantly reduce the computational time needed to create the low order models. Also, the new nonlinear PROMs integrate the nonlinear hardening/softening effects of materials in battery cells and foams. The vibration responses predicted using PROMs are validated using full-order FEMs. PROMs are computationally efficient and accurate. They are used to conduct statistical analyses

for system with random structural variations and are used for optimization of the arrangement of spacers, which minimizes the vibration responses of battery packs using a genetic algorithm.

In chapter 2, new nonlinear PROMs are proposed to capture PreV and C2CV simultaneously. The transformation matrix, which is constructed using the modes at two extreme PreV levels with zero C2CV for all cells, are conditioned using singular value decomposition to eliminate linearly independent columns. The transformation matrix is employed to reduce the order of system dynamic matrices. The stiffness matrices with structural variations are obtained using linear interpolation with respect to C2CV of each cell. Moreover, cells are mechanically coupled to each other through spacers, and vibration of the battery pack is observed along the first plate-like modes of each cell in the battery pack. The nonlinear behavior in cells are modeled in PROMs based on the observation. The reduced-order nonlinear system dynamic equations are solved using iterative method, and the solutions are validated using time-marching method and algebraic solver.

In chapter 3, the effect of foams are considered and modeled in PROMs. Cells are mechanically coupled to each other through both spacers and foams. Since the change in stiffness of cells due to structural variations is highly affected by both PreV and C2CV of each cell when foams are involved in the battery pack. The stiffness matrices of cells with structural variations are obtained using bi-linear interpolation with respect to PreV and C2CV. Furthermore, the nonlinear behavior in foams is considered and modeled in the new nonlinear PROMs. Since the foams are often polymeric material which are much softer than cells, the vibration of foams is dominated by the two first plate-like modes - one from each neighboring cell. This is the key to modeling the nonlinear behavior in foams. The vibration responses calculated using PROMs are validated with full-order models.

In chapter 4, the effect of different types of spacers, which is considered as S2SV,

is modeled in PROMs. Since the strain distribution on a cell is affected by the stiffness of two neighboring spacers when prestress is applied to the battery pack, the change in stiffness matrix of a cell due to structural variation is a function of four parameters, PreV, C2CV, and two S2SVs of the neighboring spacers. Thus, quadra-linear interpolation method with respect to these four parameters is employed to obtained the stiffness matrix of a cell with structural variations. The method is validated using full-order models. Moreover, the vibration response can be mitigated for the battery pack by designing the arrangement of different types of spacers. The optimal arrangement of spacers is produced using a genetic algorithm.

In chapter 5, conclusions and suggested future work are given.

CHAPTER II

Parametric reduced-order models capturing nonlinear behavior in cells

In this chapter, new nonlinear PROMs are proposed to capture both the system-level and component-level structural variations. Also, the nonlinear behavior in cells are modeled and integrated into PROMs. In Section 2.1, the sources that lead to the change in the vibration response is introduced. In Section 2.2, PROMs capturing linear effects of prestress and cell-to-cell variations are described followed by an iterative method to solve nonlinear forced response of PROMs. In Section 2.3, the structural variations captured by the PROMs are related to a physical model of a battery pack with different states of charge. In Section 2.4, dynamic characteristics of periodic structures and an academic battery pack model are introduced. In Section 2.5, the methods are demonstrated using computational studies of the academic battery pack model. Finally, conclusions are summarized in Section 2.7.

2.1 High modal density and vibration response

Often battery packs are comprised of hundreds of nominally identical cells which stack together and form repeated structures. The repeated structures exhibit high modal density. Figure 2.1 shows the natural frequency versus the mode index for

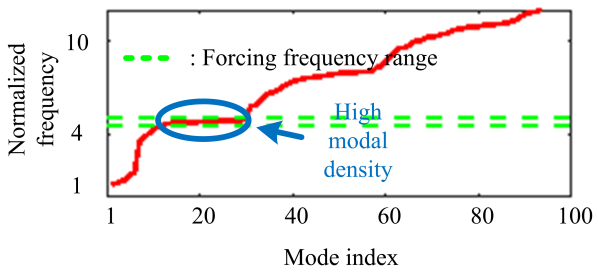

Figure 2.1: The natural frequency plot of the academic battery pack without foams exhibits high modal density regions. (Noted that Fig. 3.2 shows a different natural frequency plot because there are foams in the academic battery pack.)

an academic battery pack which is described in detail in Section 2.4. The results in Fig. 2.1 illustrate high modal density regions which result from the repeated cell structure where there are many modes over a small frequency range. In general, a battery pack has even more repeated cells, and the modal density is even greater.

The vibration response is affected by two types of structural variations: prestress and C2CVs. The prestress variation (Fig. 2.2(a)) comes from the constraints/clamping of battery packs or from thermal stresses resulting from temperature changes due to a charge/discharge or an environmental temperature change [64, 65]. Due to the internal structure of each cell, the prestress can change the equivalent modulus of elasticity of the whole battery pack, and therefore affect the vibration response.

The other type of structural variation is C2CV (Fig. 2.2(b)). Some cells might have slightly different modulus of elasticity which is inevitable due to manufacturing tolerances. Even if all cells are manufactured identically, cells are charged and discharged and have different states of charge over time which leads to different elastic characteristics for individual cells during operation [32, 66].

Knowing what variations lead to an amplification of the maximum amplitude or a change in the location of the maximum amplitude is very useful in the design process. To gain this knowledge, a statistical analysis in the range of variations is required. Efficient models must be used to perform this analysis since conventional full-order

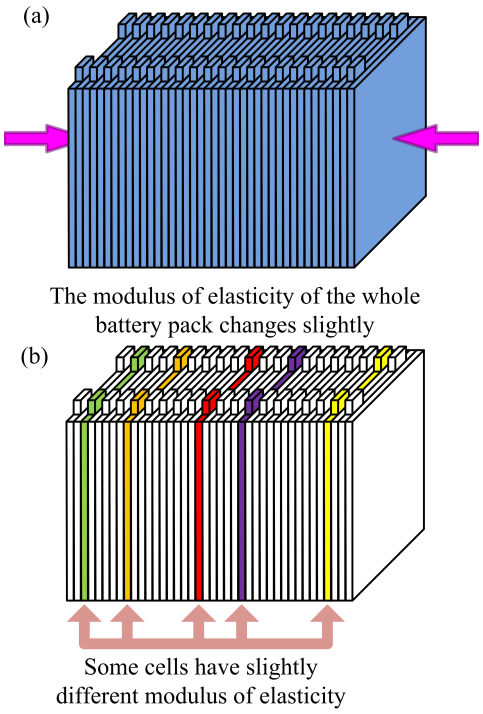

Figure 2.2: Structural variations: (a) prestress variation and (b) cell-to-cell variation.

computations would be prohibitively expensive for thousands of variation cases.

The stiffness of the battery pack is generally affected linearly by the prestress and C2CVs. However, there are also nonlinear material properties of the cell that affect the vibration response. Here, we consider the stiffness of each cell as a nonlinear function of strain. Cubic nonlinearity implies that stiffness varies with the square of the displacement at the central node of each cell. Due to the high modal density, the nonlinear effects also lead to large changes in the vibration response.

2.2 Methodology

To predict the vibration response with structural variations, the linear and nonlinear parts of the model are accounted for. The linear part includes both prestress and C2CVs. The prestress and C2CVs are accounted for in two approaches applied simultaneously. The nonlinear part captures the nonlinear material behavior of cells.

There are two elements to the construction of the fast yet accurate linear PROMs.

The first element is the parameterization of the stiffness matrix. The parameterization of the stiffness matrix reduces the reanalysis time because any variation in the level of prestress and in the cell-to-cell properties (in the parameter range) can be applied without a need for full-order finite element calculations. The second element is the prediction of vibration responses using reduced-order models (ROMs) as opposed to full-order models to reduce the calculation time.

The key to solving the nonlinear problem is the use of an iterative procedure in the frequency domain while ignoring higher order harmonics. The iterative method is similar to harmonic balance and drastically reduces the computational time as compared to time marching approaches.

2.2.1 Linear PROMs

2.2.1.1 Model reduction

In general, structural dynamic equations for a linear proportionally damped system can be written as

$$\boldsymbol{M}\ddot{\boldsymbol{x}} + \beta \boldsymbol{K}_{p,\boldsymbol{s},LI}\dot{\boldsymbol{x}} + \boldsymbol{K}_{p,\boldsymbol{s},LI}\boldsymbol{x} = \boldsymbol{F}, \tag{2.1}$$

where p represents the prestress level, $\boldsymbol{s} = [\ s_1 \quad s_2 \quad \dots \quad s_{N_C}\ ]$ is a vector which contains the C2CV level s_i for each cell i (for $i = 1, 2, \dots, N_C$), with N_C being the number of cells. $\boldsymbol{M}$ is the mass matrix of the battery pack, $\boldsymbol{K}_{p,\boldsymbol{s},LI}$ is the stiffness matrix of the battery pack at prestress level p and C2CV level $\boldsymbol{s}$, $\boldsymbol{F}$ is the excitation force vector, β is the proportional damping coefficient, and $\boldsymbol{x}$ is the vector of physical displacements with respect to the static equilibrium.

The first assumption used to construct PROMs of structures with high modal density is that the modes $\boldsymbol{\phi}_{p,\boldsymbol{s}}$ at a given prestress level p and C2CV level $\boldsymbol{s}$ are linear combinations of the modes at two extreme prestress cases with zero C2CVs

$\boldsymbol{s} = \mathbf{0}$ [44], i.e.

$$span\left(\boldsymbol{\phi}_{p,\boldsymbol{s}}\right) = span\left(\left[\begin{array}{cc} \boldsymbol{\phi}_{p_l,\mathbf{0}} & \boldsymbol{\phi}_{p_u,\mathbf{0}} \end{array}\right]\right), \tag{2.2}$$

where p_l and p_u represent the lower and upper extreme values of prestress variation.

One way to reduce the number of modes in Eq. 2.2 is to consider only modes within a frequency range of interest. Consider that matrices $\boldsymbol{\phi}_{p_l,\mathbf{0}}$ and $\boldsymbol{\phi}_{p_u,\mathbf{0}}$ have m modes (each) within this frequency range of interest. The general transformation matrix $\boldsymbol{T}_G^R$ for a structural variation (in the variation range) is defined as

$$\boldsymbol{T}_G^R = \left[\begin{array}{cc} \boldsymbol{\phi}_{p_l,\mathbf{0}} & \boldsymbol{\phi}_{p_u,\mathbf{0}} \end{array}\right]. \tag{2.3}$$

The general transformation matrix $\boldsymbol{T}_G^R$ can be conditioned and reduced further by using singular value decomposition. In general, some of the modes obtained at prestress levels p_l and p_u can have almost linearly dependent columns. Singular value decomposition can be applied to the general transformation matrix $\boldsymbol{T}_G^R$ to compute an orthogonal basis as

$$\boldsymbol{U}\boldsymbol{S}\boldsymbol{V}^T = svd\left(\boldsymbol{T}_G^R\right), \tag{2.4}$$

where $\boldsymbol{U}$ and $\boldsymbol{V}$ are the left and right singular vectors, and $\boldsymbol{S}$ is a diagonal matrix of singular values. The basis is obtained from a truncated set $\tilde{\boldsymbol{U}}$ of the left singular vectors corresponding to the largest singular values to obtain a new transformation matrix expressed as

$$\boldsymbol{T}^R = \tilde{\boldsymbol{U}}. \tag{2.5}$$

The choice of the cutoff point in terms of the magnitude of the singular values affects the accuracy if it is chosen too high, but it does not affect the numerical stability. Thus, the cutoff value can be estimated by a standard convergence study

where calculations are done at ever lower cutoff values until convergence is obtained. In this study, the corresponding singular values greater than 0.1% of the maximum singular value are included in the transformation matrix. The final version of the transformation used to convert physical coordinates into reduced-order coordinates can be expressed as

$$\boldsymbol{x} = \boldsymbol{T}^R \boldsymbol{q}, \tag{2.6}$$

where $\boldsymbol{q}$ is a vector of reduced-order coordinates. For different levels of prestress and C2CVs, only a single transformation matrix $\boldsymbol{T}^R$ is needed, and there is no need to re-compute $\boldsymbol{T}^R$ when p or $\boldsymbol{s}$ change.

Because the model of the battery pack can have millions of DOFs, to reduce the computational time, the mass matrix, stiffness matrix, and force vector are projected onto reduced-order coordinates by the transformation matrix $\boldsymbol{T}^R$ as

$$\begin{aligned} \boldsymbol{M}^R &= (\boldsymbol{T}^R)^T \boldsymbol{M} \boldsymbol{T}^R, \\ \boldsymbol{K}^R_{p,\boldsymbol{s},LI} &= (\boldsymbol{T}^R)^T \boldsymbol{K}_{p,\boldsymbol{s},LI} \boldsymbol{T}^R, \\ \boldsymbol{F}^R &= (\boldsymbol{T}^R)^T \boldsymbol{F}, \end{aligned} \tag{2.7}$$

and the equations of motion become

$$\boldsymbol{M}^R \ddot{\boldsymbol{q}} + \beta \boldsymbol{K}^R_{p,\boldsymbol{s},LI} \dot{\boldsymbol{q}} + \boldsymbol{K}^R_{p,\boldsymbol{s},LI} \boldsymbol{q} = \boldsymbol{F}^R. \tag{2.8}$$

After the solution $\boldsymbol{q}$ in reduced-order coordinates is obtained, Eq. 2.6 can be used to obtain the solution in full-order coordinates. Conducting the analysis in reduced-order coordinates makes the PROMs very efficient for computing many realizations for different structural variations.

2.2.2 Parameterization

Because the prestress variation level p and the C2CV level $\boldsymbol{s}$ are small, one can expand the stiffness matrix $\boldsymbol{K}^R_{p,\boldsymbol{s},LI}$ at small values of p and $\boldsymbol{s}$ around zero to obtain

$$\begin{aligned}\boldsymbol{K}^R_{p,\boldsymbol{s},LI} = \boldsymbol{K}^R_{0,\boldsymbol{0},LI} + \frac{\partial \boldsymbol{K}^R_{0,\boldsymbol{0},LI}}{\partial p} p \\ + \sum_{i=1}^{N_C} \frac{\partial \boldsymbol{K}^R_{0,\boldsymbol{0},LI}}{\partial s_i} s_i + H.O.T.\end{aligned} \tag{2.9}$$

where $\boldsymbol{K}^R_{0,\boldsymbol{0},LI}$ is the stiffness matrix of the battery pack at prestress variation level $p = 0$ and C2CV level $\boldsymbol{s} = \boldsymbol{0}$. Because the prestress variation level p and the C2CV level $\boldsymbol{s}$ are small, higher order terms in Eq. 2.9 are negligible.

To obtain the matrix $\frac{\partial \boldsymbol{K}^R_{0,\boldsymbol{0},LI}}{\partial p} p$ in Eq. 2.9, assume that the change in stiffness matrix due to small prestress variation is linearly dependent on the prestress variation level p. Therefore, the term $\frac{\partial \boldsymbol{K}^R_{0,\boldsymbol{0},LI}}{\partial p} p$ can be obtained through linear interpolation of p between the two extreme values of prestress $p = p_l$ and $p = p_u$, namely

$$\frac{\partial \boldsymbol{K}^R_{0,\boldsymbol{0},LI}}{\partial p} p = \frac{p - p_l}{p_u - p_l} (\boldsymbol{K}^R_{p_u,\boldsymbol{0},LI} - \boldsymbol{K}^R_{p_l,\boldsymbol{0},LI}), \tag{2.10}$$

where the stiffness matrices $\boldsymbol{K}_{p_l,\boldsymbol{0},LI}$ and $\boldsymbol{K}_{p_u,\boldsymbol{0},LI}$ of the battery pack at two extreme prestress levels $p = p_l$ and $p = p_u$ without C2CV are obtained from full-order FEMs, and are projected on $\boldsymbol{T}^R$ to obtain $\boldsymbol{K}^R_{p_l,\boldsymbol{0},LI}$ and $\boldsymbol{K}^R_{p_u,\boldsymbol{0},LI}$.

Similarly, to obtain the matrix $\frac{\partial \boldsymbol{K}^R_{0,\boldsymbol{0},LI}}{\partial s_i} s_i$ in Eq. 2.9, one can assume that the change in stiffness matrix in cell i due to small C2CV is linearly dependent on the C2CV level s_i. Therefore, the term $\frac{\partial \boldsymbol{K}^R_{0,\boldsymbol{0},LI}}{\partial s_i} s_i$ can be obtained through linear interpolation of s_i between zero C2CV level $s_i = 0$ and the extreme C2CV level $s_i = s_u$ without prestress variations, namely

$$\frac{\partial \boldsymbol{K}^R_{0,\boldsymbol{0},LI}}{\partial s_i} s_i = \frac{s_i - 0}{s_u - 0} (\boldsymbol{K}^R_{i,0,s_u,LI} - \boldsymbol{K}^R_{i,0,0,LI}), \tag{2.11}$$

where the stiffness matrix $\boldsymbol{K}_{i,0,0,LI}$ of cell i at zero prestress level $p = 0$ with zero C2CV $s_i = 0$, and the stiffness matrix $\boldsymbol{K}_{i,0,s_u,LI}$ of cell i at zero prestress level $p = 0$ with an extreme C2CV level $s_i = s_u$ are obtained from the full-order FEMs, and are projected on $\boldsymbol{T}^R$ to obtain $\boldsymbol{K}^R_{i,0,0,LI}$ and $\boldsymbol{K}^R_{i,0,s_u,LI}$. Equation 2.9 can be rewritten as

$$\begin{aligned}\boldsymbol{K}^R_{p,\boldsymbol{s},LI} = \boldsymbol{K}^R_{0,\boldsymbol{0},LI} + \frac{p - p_l}{p_u - p_l}(\boldsymbol{K}^R_{p_u,\boldsymbol{0},LI} - \boldsymbol{K}^R_{p_l,\boldsymbol{0},LI}) \\ + \sum_{i=1}^{N_C} \frac{s_i}{s_u}(\boldsymbol{K}^R_{i,0,s_u,LI} - \boldsymbol{K}^R_{i,0,0,LI}).\end{aligned} \tag{2.12}$$

2.2.3 Nonlinear PROMs

2.2.3.1 Source of nonlinearity

The nonlinear behavior of cells may come from nonlinear material properties as well as the internal structure of the cells. The nonlinear behavior changes the stiffness of cells [40, 42]. Although the nonlinearity is weak, the change in stiffness due to nonlinearity can still lead to significant vibration response change because of the high modal density.

In this work, hardening in the stiffness of cells is considered when the strain increases. Thus, the stiffness matrix $\boldsymbol{K}_{p,\boldsymbol{s}}$ of the battery pack at a certain prestress variation level p and a certain C2CV level $\boldsymbol{s}$ is a function of the strain $\boldsymbol{\epsilon}$. Assume the battery pack is excited by low frequency harmonic forces, and based on the results from the full-order analysis (Fig. 2.3 (a)), each individual cell moves mainly along its first plate-like mode. Therefore, a single value of displacement $x_{i,c}$ at the central node of cell i can determine the strain $\boldsymbol{\epsilon}_i$ in cell i. Thus, the stiffness matrix $\boldsymbol{K}_{p,\boldsymbol{s}}$ of

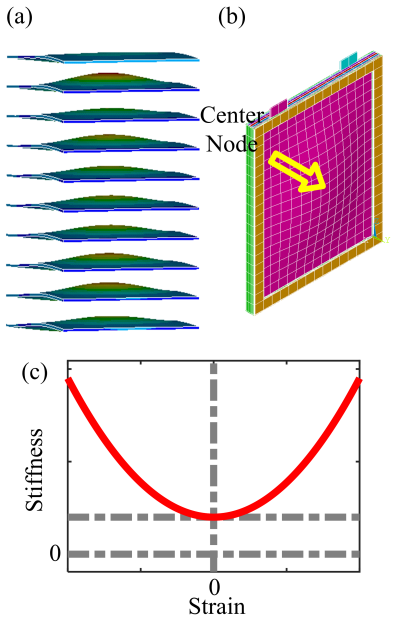

Figure 2.3: (a) Vibration response of the battery pack. (b) The amplitude at the central node of each cell is the largest. (c) The stiffness of cell varies with strain.

each cell can be represented as

$$\begin{aligned} \boldsymbol{K}_{p,\boldsymbol{s}}(\boldsymbol{\epsilon}) &= \boldsymbol{K}_{p,\boldsymbol{s}}([\ \boldsymbol{\epsilon}_1 \quad \dots \quad \boldsymbol{\epsilon}_{N_C}\ ]) \\ &= \boldsymbol{K}_{p,\boldsymbol{s}}([\ x_{1,c} \quad \dots \quad x_{N_C,c}\ ]) \\ &= \boldsymbol{K}_{p,\boldsymbol{s}}(\boldsymbol{x}_c), \end{aligned} \tag{2.13}$$

where $\boldsymbol{x}_c$ is a vector containing the displacement at the central node of each cell.

Next, one may expand the stiffness matrix by Taylor series at small values of $\boldsymbol{x}_c$ around zero to obtain

$$\begin{aligned} \boldsymbol{K}_{p,\boldsymbol{s}}(\boldsymbol{x}_c) = \boldsymbol{K}_{p,\boldsymbol{s}}(\boldsymbol{0}) &+ \sum_{i=1}^{N_C} \frac{\partial \boldsymbol{K}_{p,\boldsymbol{s}}(\boldsymbol{0})}{\partial x_{i,c}} x_{i,c} \\ &+ \sum_{i=1}^{N_C}\sum_{j=1}^{N_C} \frac{\partial^2 \boldsymbol{K}_{p,\boldsymbol{s}}(\boldsymbol{0})}{\partial x_{i,c}\partial x_{j,c}} x_{i,c}x_{j,c} + H.O.T. \end{aligned} \tag{2.14}$$

where $H.O.T.$ represents high order terms.

The stiffness of cells varies with strain as shown in Fig 2.3(c). Because of symmetry, positive and negative values of $x_{i,c}$ contribute equally to the stiffness of cell i. Thus, the odd order terms are neglected in Eq. 2.14. Because cells do not share common elements, the strain in one cell does not directly affect the strain in another cell. Hence $\frac{\partial^2 \boldsymbol{K}_{p,\boldsymbol{s}}(\boldsymbol{0})}{\partial x_{i,c} \partial x_{j,c}} = \boldsymbol{0}$ for $i \neq j$. Also, the contribution of higher order terms is negligible. Thus, the stiffness matrix can be approximated as

$$\boldsymbol{K}_{p,\boldsymbol{s}}(\boldsymbol{x}_c) \approx \boldsymbol{K}_{p,\boldsymbol{s}}(\boldsymbol{0}) + \sum_{i=1}^{N_C} \frac{\partial^2 \boldsymbol{K}_{p,\boldsymbol{s}}(\boldsymbol{0})}{\partial x_{i,c}^2} x_{i,c}^2. \tag{2.15}$$

The first term $\boldsymbol{K}_{p,\boldsymbol{s}}(\boldsymbol{0})$ in Eq. 2.15 accounts for the linear stiffness matrix $\boldsymbol{K}_{p,\boldsymbol{s},LI}$ in Eq. 2.1. The second term in Eq. 2.15 accounts for the nonlinear stiffness of each cell, and is denoted by $\Delta\boldsymbol{\kappa}_{i,p,s_i,NL}$, so that

$$\boldsymbol{K}_{p,\boldsymbol{s}}(\boldsymbol{x}_c) \approx \boldsymbol{K}_{p,\boldsymbol{s},LI} + \sum_{i=1}^{N_C} \Delta\boldsymbol{\kappa}_{i,p,s_i,NL} x_{i,c}^2. \tag{2.16}$$

Note that the matrix $\Delta\boldsymbol{\kappa}_{i,p,s_i,NL} x_{i,c}^2$ of cell i has the same size as $\boldsymbol{K}_{p,\boldsymbol{s},LI}$ and is zero everywhere except at the DOFs corresponding to cell i.

The matrix $\Delta\boldsymbol{\kappa}_{i,p,s_i,NL} x_{i,c}^2$ is a function of prestress level p and C2CV level s_i. One can expand the matrix by multivariable Taylor series at small values of p and s_i around zero to obtain

$$\begin{aligned} \Delta\boldsymbol{\kappa}_{i,p,s_i,NL} x_{i,c}^2 = \Delta\boldsymbol{\kappa}_{i,0,0,NL} x_{i,c}^2 + \frac{\partial \Delta\boldsymbol{\kappa}_{i,0,0,NL}}{\partial p} p x_{i,c}^2 \\ + \frac{\partial \Delta\boldsymbol{\kappa}_{i,0,0,NL}}{\partial s_i} s_i x_{i,c}^2 + H.O.T. \end{aligned} \tag{2.17}$$

Because the nonlinearity considered is weak, the effects of the prestress level p and C2CV level s_i to the nonlinear stiffness are small. Also, the vibration displacement $x_{i,c}$ is small. Therefore, in Eq. 2.17, $p x_{i,c}^2$ and $s x_{i,c}^2$ are second order, and the terms $\frac{\partial \Delta\boldsymbol{\kappa}_{i,0,0,NL}}{\partial p} p x_{i,c}^2$ and $\frac{\partial \Delta\boldsymbol{\kappa}_{i,0,0,NL}}{\partial s_i} s_i x_{i,c}^2$ are negligible. The other higher order terms in

Eq. 2.17 are also negligible. Hence, the $\Delta\boldsymbol{\kappa}_{i,p,s_i,NL}x_{i,c}^2$ in Eq. 2.17 is assumed to be approximately equal to $\Delta\boldsymbol{\kappa}_{i,0,0,NL}x_{i,c}^2$. Equation 2.16 can be rewritten as

$$\boldsymbol{K}_{p,\boldsymbol{s}}(\boldsymbol{x}_c) \approx \boldsymbol{K}_{p,\boldsymbol{s},LI} + \sum_{i=1}^{N_C} \Delta\boldsymbol{\kappa}_{i,0,0_i,NL}x_{i,c}^2. \tag{2.18}$$

2.2.3.2 Equivalent nonlinear stiffness matrix

Consider the equations of motion of the battery pack subject to a single harmonic excitation

$$\begin{aligned} &\boldsymbol{M}\ddot{\boldsymbol{x}} + \beta\boldsymbol{K}_{p,\boldsymbol{s},LI}\dot{\boldsymbol{x}} \\ &\quad + (\boldsymbol{K}_{p,\boldsymbol{s},LI} + \sum_{i=1}^{N_C} \Delta\boldsymbol{\kappa}_{i,0,0,NL}x_{i,c}^2)\boldsymbol{x} \\ &\quad = \boldsymbol{F}_0 \sin(\omega t). \end{aligned} \tag{2.19}$$

We assume that the response is dominated by a single harmonic term at the same frequency as the excitation. Thus, the displacement of cell i can be written as

$$\begin{aligned} x_{i,c} &= X_{i,c}\sin(\omega t), \\ \boldsymbol{x}_i &= \boldsymbol{X}_i \sin(\omega t) \\ &= X_{i,c}\boldsymbol{Y}_i \sin(\omega t), \end{aligned} \tag{2.20}$$

where $x_{i,c}$ and $X_{i,c}$ are complex numbers representing the displacement and its amplitude of vibration at the central node of cell i. $\boldsymbol{x}_i$ and $\boldsymbol{X}_i$ are complex vectors containing displacements and amplitudes of vibration for all DOFs of cell i, and are zero at all other DOFs, $\boldsymbol{Y}_i$ is a vector which equals to $\boldsymbol{x}_i/X_{i,c}$, ω is the excitation frequency.

Because the matrix $\Delta\boldsymbol{\kappa}_{i,0,0,NL}$ of cell i is zero everywhere except at the DOFs of cell i, the contribution of the nonlinear term $\Delta\boldsymbol{\kappa}_{i,0,0,NL}x_{i,c}^2\boldsymbol{x}$ in Eq. 2.19 is equal to

$\Delta\boldsymbol{\kappa}_{i,0,0,NL}x_{i,c}^2\boldsymbol{x}_i$, namely

$$\Delta\boldsymbol{\kappa}_{i,0,0,NL}x_{i,c}^2\boldsymbol{x} = \Delta\boldsymbol{\kappa}_{i,0,0,NL}x_{i,c}^2\boldsymbol{x}_i. \tag{2.21}$$

Substituting Eqs. 2.20 into 2.21, the nonlinear term $\Delta\boldsymbol{\kappa}_{i,0,0,NL}x_{i,c}^2\boldsymbol{x}_i$ in Eq. 2.21 can be expressed as

$$\begin{aligned}
&\Delta\boldsymbol{\kappa}_{i,0,0,NL}x_{i,c}^2\boldsymbol{x}_i \\
&= \Delta\boldsymbol{\kappa}_{i,0,0,NL}\left(X_{i,c}\sin(\omega t)\right)^2 X_{i,c}\boldsymbol{Y}_i\sin(\omega t) \\
&= \Delta\boldsymbol{\kappa}_{i,0,0,NL}X_{i,c}^3\sin^3(\omega t)\boldsymbol{Y}_i \\
&= \Delta\boldsymbol{\kappa}_{i,0,0,NL}X_{i,c}^3\left(\frac{3}{4}\sin(\omega t) - \frac{1}{4}\sin(3\omega t)\right)\boldsymbol{Y}_i \\
&= \Delta\boldsymbol{\kappa}_{i,0,0,NL}\frac{3}{4}X_{i,c}^2\boldsymbol{x}_i \\
&- \frac{1}{4}\Delta\boldsymbol{\kappa}_{i,0,0,NL}X_{i,c}^2\boldsymbol{X}_i\sin(3\omega t).
\end{aligned} \tag{2.22}$$

Neglecting the high frequency term in Eq. 2.22, Eq. 2.19 becomes

$$\begin{aligned}
&\boldsymbol{M}\ddot{\boldsymbol{x}} + \beta\boldsymbol{K}_{p,\boldsymbol{s},LI}\dot{\boldsymbol{x}} \\
&\quad + (\boldsymbol{K}_{p,\boldsymbol{s},LI} + \sum_{i=1}^{N_C}\Delta\boldsymbol{\kappa}_{i,0,0,NL}\frac{3}{4}X_{i,c}^2)\boldsymbol{x} \\
&\quad = \boldsymbol{F}_0\sin(\omega t).
\end{aligned} \tag{2.23}$$

To analyze the vibration response in reduced-order coordinates, the matrix $\Delta\boldsymbol{\kappa}_{i,0,0,NL}$ is projected on $\boldsymbol{T}^R$ as

$$\Delta\boldsymbol{\kappa}_{i,0,0,NL}^R = \left(\boldsymbol{T}^R\right)^T\left(\Delta\boldsymbol{\kappa}_{i,0,0,NL}\right)\boldsymbol{T}^R. \tag{2.24}$$

Equation 2.23 in reduced-order coordinates becomes

$$\begin{aligned} &\boldsymbol{M}^R\ddot{\boldsymbol{q}} + \beta\boldsymbol{K}^R_{p,\boldsymbol{s},LI}\dot{\boldsymbol{q}} \\ &\quad + \left(\boldsymbol{K}^R_{p,\boldsymbol{s},LI} + \sum_{i=1}^{N_C} \Delta\boldsymbol{\kappa}^R_{i,0,0,NL}\frac{3}{4}X^2_{i,c}\right)\boldsymbol{q} \\ &\quad = \boldsymbol{F}^R_0 \sin(\omega t). \end{aligned} \tag{2.25}$$

2.2.3.3 Iterative method

To solve the nonlinear dynamic equations in Eq. 2.25, time marching approaches (e.g., ODE45 in Matlab) or algebraic solvers for nonlinear equations (e.g., FSOLVE in Matlab) can be used, but are computationally expensive. To reduce the computational time, the following iterative method has been developed.

First, the equations of motion Eq. 2.8 are constructed for the linear system, and the linear solution $\boldsymbol{q}_{LI}$ in reduced-order coordinates is obtained. Before starting the iterative method, the initial guess of the nonlinear solution $\boldsymbol{q}_{NL,1}$ is set to be the linear solution $\boldsymbol{q}_{LI}$.

Next, $\boldsymbol{q}_{NL,k}$ is used to update the equivalent nonlinear stiffness matrix $\boldsymbol{K}^R_{i,p,s_i,NL}$ for each cell i in Eq. 2.25 where k is the iteration number. $\boldsymbol{q}_{NL,k+1}$ is obtained by solving the updated equations of motion (Eq. 2.25). Then, the nonlinear solution $\boldsymbol{q}_{NL,k+1}$ and the nonlinear solution $\boldsymbol{q}_{NL,k}$ are compared by calculating

$$\epsilon = \frac{\|\boldsymbol{q}_{NL,k+1} - \boldsymbol{q}_{NL,k}\|}{\|\boldsymbol{q}_{NL,k}\|}. \tag{2.26}$$

The value of ϵ decreases at each iteration, and the process stops when ϵ is below a desired value ϵ_{max}. In this work, ϵ_{max} is set to 1%. If ϵ_{max} is too high, the solution may not be converged. If ϵ_{max} is too low, the computation is slower.

2.2.3.4 Convergence of the iterative method

The iterative method might be unable to converge in some situations because of numerical issues or because of the underlying assumption in Eqs. 2.22 may not hold. For example, the vibration response may contain more than one single harmonic term. In these cases, time marching approaches should be applied to solve the nonlinear equations. However, solving nonlinear equations in the time domain is computationally expensive. Therefore, to solve the nonlinear equations of motion, the iterative approach is applied first. If the iteration approach cannot converge, an algebraic solver is applied. If the algebraic solver cannot converge, then the time marching approach is applied.

2.3 Physical model

The stiffness of the battery pack is affected by charge-discharge cycles. This is because different states of charge lead to different levels of Li-ion intercalation [67], and hence lead to different swelling levels and different mechanical properties of the cells [68, 69]. The overall swelling leads to prestress variation in the battery pack, and therefore changes the stiffness of the battery pack. The different Li-ion intercalation levels in each cell change the mechanical properties of the anodes in the cells, and act like C2CVs.

Therefore, even if the battery pack was already clamped on a vehicle and the prestress and C2CVs of the pack were predetermined, the dynamic responses will still change during charge-discharge cycles.

To predict vibration responses with PROMs, modes and stiffness matrices at two extreme prestress variation levels are extracted from the full-order FEMs. However, most commercial finite element analysis software cannot model the swelling caused by states of charge of cells. Nevertheless, the swelling caused by temperature changes

can be modeled by most commercial finite element analysis software. Therefore, a virtual temperature is introduced to model the swelling caused by states of charge.

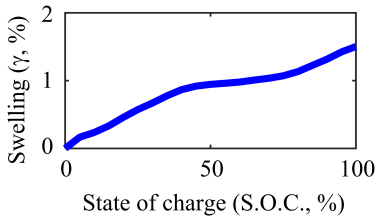

Figure 2.4: Relation between states of charge and swelling.

According to previous experiments [70, 71], the relationship between the state of charge and the swelling of a battery cell studied here is shown on Fig. 2.4. Based on the experimental data, the relation between the virtual temperature of each cell ΔT_i and the Li-ion intercalation swelling can be obtained by using the relation

$$L_a(1 + \gamma_i) = \alpha_T \Delta T_i, \tag{2.27}$$

where L_a is the thickness of the anode before swelling, γ_i is the relative change in the thickness of anode of cell i due to Li-ion intercalation swelling, α_T is the virtual thermal expansion coefficient of the anode, and ΔT_i is the virtual temperature change in cell i. Therefore, changes in states of charge of cells can be related to the prestress on the battery pack. If the stiffness matrices at the two extreme levels of prestress due to state of charge variations are known, the PROMs can be built with the states of charge as input. The material properties with respect to states of charge were measured in experiments. Thus, states of charges can relate to the C2CVs.

There can be temperature gradient field in a battery pack, where the cells at the two ends of the battery pack have a lower temperature, while the cells at the central part of the battery pack have a higher temperature. The temperature gradient field can be modeled by using both the prestress variation and cell-to-cell variations. The prestress variation comes from the thermal swelling as mentioned above. The

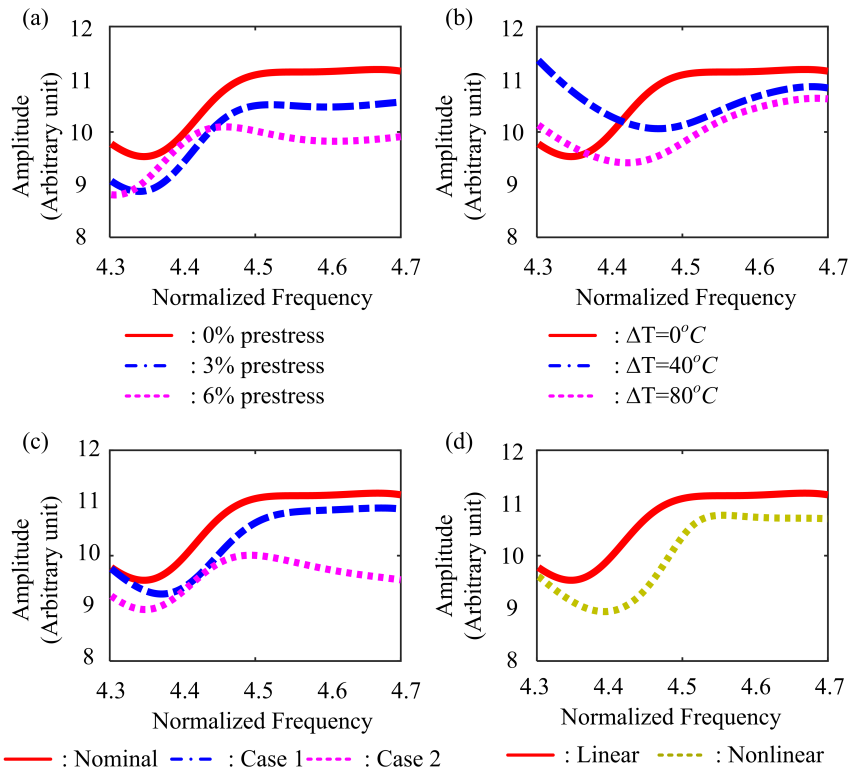

Figure 2.5: The vibration responses at the central node of cell 10 affected by (a) prestress variations due to changes in clamping, (b) prestress variations due to changes in temperature, (c) cell-to-cell variations, and (d) nonlinearity in material.

temperature may have effects on the modulus of elasticity of a cell; thus, each cell may have a different level of cell-to-cell variation. Consequently, the temperature gradient field in the battery pack can be modeled as the cell-to-cell variations.

2.4 Computational model

To demonstrate the proposed approaches, an academic battery pack model was developed with 20 nominally identical cells as shown in Fig. 2.6(a). Each cell is comprised of several components, including a positive current collector, a cathode, a separator, an anode, a negative current collector, a case, and a spacer as shown in Fig. 2.6(b). Cells are stacked together and mechanically coupled through the frames (case and spacer).

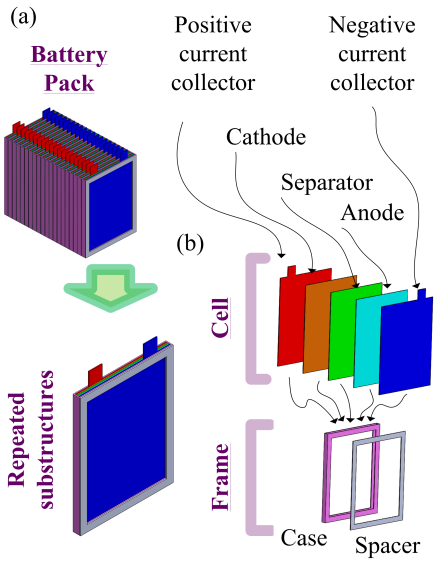

Figure 2.6: (a) Simplified battery pack model with 20 nominally identical cells. (b) Each cell is comprised of several components.

Prestress loads are applied to the pack in the longitudinal direction to compress the structure as shown in Fig. 2.2(a). To study the vibration of the pack due to external loads, harmonic excitation forces are applied to the bottom of the battery pack in the longitudinal direction. Forces are applied instead of displacements, but displacements can be applied as well. The harmonic excitation frequencies are in the range from 4.3 to 4.7 normalized frequency which is in the region of high modal density shown in Fig. 2.1.

For prestress coming from clamping, one side of the battery pack is first fixed, and the other side is compressed by a percentage of the length of the whole battery pack along the longitudinal direction. For prestress coming from temperature, both sides of the battery pack are fixed, and a temperature change is then applied to the whole battery pack. In this work, the prestress ranges from 0% to 6%, and the temperature change ranges from $0°C$ to $80°C$.

To demonstrate the vibration response for different structural variation levels, the vibration response amplitude at the central node of cell 10 is discussed. The central node is chosen because the battery pack is excited by low frequency harmonic forces,

and each individual cell moves similarly to its first fixed-boundary mode (Fig. 2.3 (a)) which has its largest displacement at the central node of the cell (Fig. 2.3 (b)).

To demonstrate the effects of prestress variations due to clamping on the vibration response, 3 different levels of prestress, 0%, 3%, and 6%, are applied. Figure 2.5(a) shows the effect of prestress variations to the vibration response at the central node of cell 10. Because of the high modal density, even though the prestress variation is small, the vibration responses still change drastically. To demonstrate the effects of prestress variations due to changes in temperature, 3 different temperatures, $0°C$, $40°C$, and $80°C$ are applied, and the vibration responses are shown in Fig. 2.5(b). Figures 2.5(a) and (b) show that the vibration responses are significantly different for each level of prestress and temperature.

Similarly, to demonstrate the effects of C2CVs, 2 different cases of modulus of elasticity variations listed in Tab. 2.1 are applied to the academic battery pack model. In this work, the C2CV level of each cell range from -10% to 10% of the nominal modulus of elasticity and are applied to all components of cells, including positive and negative current collectors, an anode, a cathode, and a separator. Results are shown in Fig. 2.5(c). These 2 example cases show that even small variations in just a few cells can cause large changes in the vibration response.

Table 2.1: Two cell-to-cell variation cases

Cell	Case 1	Cell	Case 2
1	5%	4	10%
5	-7%	7	-8%
12	1%	10	3%
16	3%	19	-5%

To demonstrate the effect of the weak nonlinearity, one can project the matrix $\Delta\boldsymbol{\kappa}_{i,0,0,NL}$ on the first plate-like mode and obtain the scalar $\Delta\boldsymbol{\kappa}^N_{i,0,0,NL}$. One can also project the matrix $\Delta\boldsymbol{K}_{i,0,s_u,LI} = \boldsymbol{K}_{i,0,s_u,LI} - \boldsymbol{K}_{i,0,0,LI}$ on the first plate-like mode of cell i and obtain the scalar $\Delta K^N_{i,0,s_u,LI}$ where the C2CV level s_i is applied to all components of cell i. Because $\Delta\kappa^N_{i,0,0,NL}$ and $\Delta K^N_{i,0,s_u,LI}$ are scalar, they are proportional to each

other, namely

$$\Delta\kappa^N_{i,0,0,NL} = \frac{\mu}{L^2}\Delta K^N_{i,0,s_u,LI}, \tag{2.28}$$

where L is the thickness of the cell and μ is a dimensionless scalar determined by the material properties of the cells.

Because vibration responses of the battery pack are dominated by the first plate-like mode for each cell i, the modes $\boldsymbol{\phi}_{p_l,0}$ and $\boldsymbol{\phi}_{p_u,0}$ (used in transformation matrix $\boldsymbol{T}^R$) are dominated by the first plate-like mode. Let $\boldsymbol{T}^R_i$ be the matrix equal to $\boldsymbol{T}^R$ at the DOF of cell i and be zeros everywhere else. Because the modes are dominated by the the first plate-like mode, $\boldsymbol{T}^R_i$ can be written as

$$\begin{aligned}
\boldsymbol{T}^R_i &= \begin{bmatrix} \boldsymbol{T}^R_{i,1} & \dots & \boldsymbol{T}^R_{i,m} \end{bmatrix} \\
&\approx \begin{bmatrix} \boldsymbol{\phi}_{i,N}\rho_{i,1} & \dots & \boldsymbol{\phi}_{i,N}\rho_{i,m} \end{bmatrix} \\
&= \boldsymbol{\phi}_{i,N}\begin{bmatrix} \rho_{i,1} & \dots & \rho_{i,m} \end{bmatrix} \\
&= \boldsymbol{\phi}_{i,N}\boldsymbol{\rho}_i
\end{aligned} \tag{2.29}$$

where $\boldsymbol{T}^R_{i,j}$ is the j^{th} column of $\boldsymbol{T}^R_i$, $\boldsymbol{\phi}_{i,N}$ is the first plate-like mode of cell i, $\rho_{i,j}$ is a scalar factor represents how much $\boldsymbol{\phi}_{i,N}$ involves in $\boldsymbol{T}^R_{i,j}$, and $\boldsymbol{\rho}_i$ is a row vectors collecting $\rho_{i,j}$.

Thus, the matrix $\Delta\boldsymbol{\kappa}^R_{i,0,0,NL}$ due to the weak nonlinearity in reduced-order coordinates is proportional to the matrix $\Delta\boldsymbol{K}^R_{i,0,s_u,LI}$ due to a small extreme C2CV level s_u

in reduced-order coordinates (the C2CV is applied to all components of cell i), i.e.,

$$\begin{aligned}
\Delta\boldsymbol{\kappa}^R_{i,0,0,NL} &= \left(\boldsymbol{T}_i^R\right)^T \Delta\boldsymbol{\kappa}_{i,0,0,NL}\boldsymbol{T}_i^R \\
&\approx \left(\boldsymbol{\phi}_{i,N}\boldsymbol{\rho}_i\right)^T \Delta\boldsymbol{\kappa}_{i,0,0,NL}\boldsymbol{\phi}_{i,N}\boldsymbol{\rho}_i \\
&= \boldsymbol{\rho}_i^T\boldsymbol{\phi}_{i,N}^T\Delta\boldsymbol{\kappa}_{i,0,0,NL}\boldsymbol{\phi}_{i,N}\boldsymbol{\rho}_i \\
&= \boldsymbol{\rho}_i^T\Delta\kappa^N_{i,0,0,NL}\boldsymbol{\rho}_i \\
&= \boldsymbol{\rho}_i^T\tfrac{\mu}{L^2}\Delta K^N_{i,0,s_u,LI}\boldsymbol{\rho}_i \\
&\approx \tfrac{\mu}{L^2}\Delta\boldsymbol{K}^R_{i,0,s_u,LI}
\end{aligned} \tag{2.30}$$

$\frac{\mu}{L^2} = 0.002$ in Eq. 2.24 and $\epsilon_{max} = 1\%$ are applied. Results are shown in Fig. 2.5(d) and show the importance of small nonlinearity.

For the academic battery pack model, the frequency range of interest is from 4.3 to 4.7 normalized frequency, which contains the first high modal density region shown in Fig. 2.1. Only the first 200 modes for each extreme prestress level are chosen to capture the dynamic behavior in Eq. 2.3. After singular value decomposition, the basis for the transformation matrix $\boldsymbol{T}^R$ has 390 modes. By using $\boldsymbol{T}^R$ for the academic pack model in Eq. 2.5, the projected stiffness matrices are reduced to 390×390 while the full-order matrices have a size of $159,666 \times 159,666$.

2.5 Validation

2.5.1 Linear validation

The vibration response at the central node of cell 10 computed using the full-order FEM and a PROM with prestress and C2CVs are plotted in Figs. 2.7(a) and (b). The prestress variation level is 3%, and the distribution of C2CVs are listed in Tab. 2.1.

Figures 2.7(a) and (b) show that PROM predictions agree very well with the full-order FEM results. The solid line indicates the full-order FEM predictions and the dashed line indicates PROM predictions. The average computational time over a

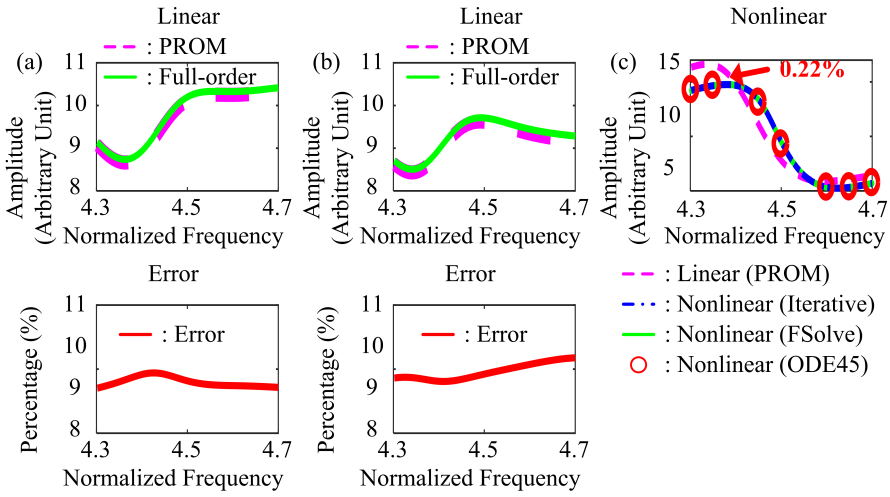

Figure 2.7: Validation results: (a) linear, cell 10, 3% prestress variation & case 1 cell-to-cell variation, (b) linear, cell 10, 3% prestress variation & case 2 cell-to-cell variation, and (c) nonlinear, cell 7, 3% prestress variation & case 2 cell-to-cell variation.

frequency range for reanalysis using PROMs is 0.47 second and using full-order FEM is 32.74 second. The average computational time is reduced by a factor of 69.66.

This computational gain can increase if a finer finite element mesh is used. That is because the computational time of the full-order FEM increases with the mesh density. However, the computational time of a PROM depends on the number of modes selected, which is related to the physics of the system. The physics remains the same when the mesh density is higher, and is captured by the same number of PROM coordinates. Therefore, the computational gain is expected to be even greater for more realistic FEMs of industrial battery packs.

2.5.2 Nonlinear validation

The linear and nonlinear vibration responses at the central node of cell 7 with PreV and C2CV in the frequency range of interest are shown in Fig. 2.7. The dashed line shows the linear response, the dashdot line shows the nonlinear response computed by the iterative method, the solid line shows the nonlinear response computed by the algebraic solver, and circles show the nonlinear response computed by the time

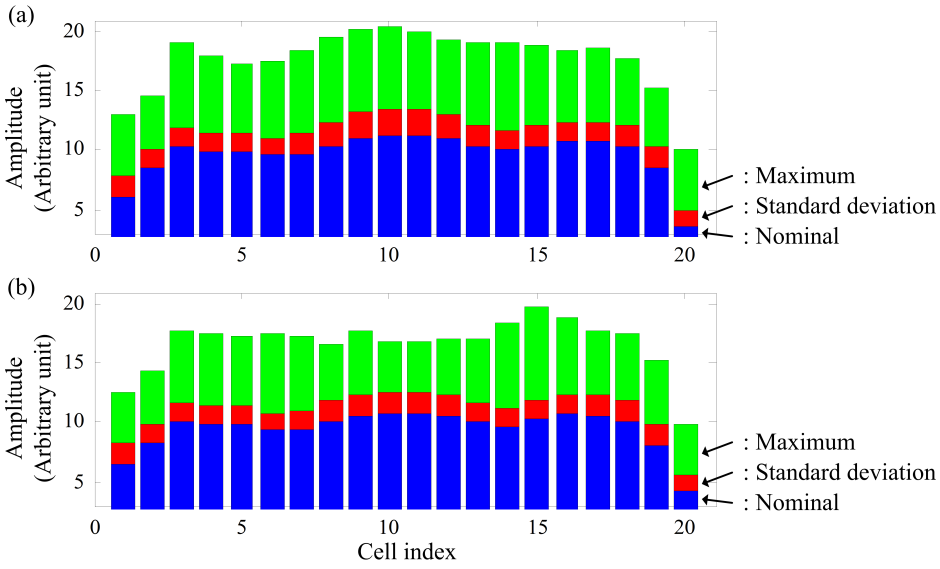

Figure 2.8: (a) Linear and (b) nonlinear statistical analyses for 1,000 cell-to-cell variation cases.

marching method. Because the time marching approach is very time-consuming, only amplitudes at a few frequencies are provided. The maximum nonlinear amplitude drops about 12.4% compared to the linear response. By setting ϵ_{max} to 1%, the errors in the results between the iterative method and the time marching method are below 3% in this simulation, but the computational time of the iterative method is much shorter than the time marching approach. In this work, the average computation time over a frequency range for reanalysis using iterative method is 0.2 seconds, using the algebraic solver is 180 seconds, and using the time marching method is 13,000 seconds. The average computational time is reduced by a factor of 65,000 comparing the iterative method and the time marching method.

The results computed by the algebraic solver and the iterative method also agree very well. The algebraic solver is computationally slower than the iterative method, but still much faster than the time marching method.

2.6 Statistical analysis

In the battery pack, a single cell with intense vibrations may lead to the failure of the whole battery pack. Thus, the maximum response level for any cell in a battery pack is a key reliability metric. However, in order to consider the effects of random structural variations, a statistical analysis is needed. Thus, a Monte Carlo simulation was performed using the 390-DOF PROMs to predict the vibration response for 1,000 C2CV cases. For each single C2CV case, the average C2CVs over the 20 cells was zero and was within $\pm 10\%$ of the nominal modulus of elasticity. Harmonic forces over the frequency range from 4.3 to 4.7 normalized frequency were applied to the bottom of the battery pack along the longitudinal direction.

Figures 2.8(a) and (b) show the results of linear and nonlinear Monte Carlo statistical analyses. Let $X_{0,i}$ denotes the maximum amplitude at the central node of cell i over the frequency range for the nominal C2CV case, $X_{std,i}$ denotes the standard deviation of the maximum amplitude at the central node of cell i over the frequency range for 1,000 C2CV cases, and $X_{max,i}$ denotes the maximum of the maximum amplitude at the central node of cell i over the frequency range for 1,000 C2CV cases. In Fig. 2.8, at cell i, the lower bar shows $X_{0,i}$, the middle bar shows $X_{0,i} + X_{std,i}$, and the upper bar shows $X_{max,i}$.

The results in Fig. 2.8 show that the C2CVs can lead to higher response levels for all cells as compared to the nominal case. In the linear case, the increase of the amplitude of cell 10 is almost 80% compared to the nominal case. Therefore, neglecting the effect of C2CVs might lead to a serious underprediction of the maximum stress, and thus an overprediction of the battery pack reliability. In the nonlinear case, the largest amplitude of cell 10 increases by 20.7% compared to the linear case. Thus, the nonlinear effects cannot be neglected either.

2.7 Conclusions

The structural dynamics of battery packs used in electrified vehicles are affected by PreV, C2CV, and sometimes nonlinear material properties. The battery pack is comprised of nominally identical cells which exhibit high modal density. The vibration response can change drastically because of the high modal density that causes vibration localization. Analysis of the vibration response of the pack with structural variations and nonlinear materials is essential for fatigue life predictions. Although statistical analyses are required to understand the effects of structural variations, typical FEMs of industrial battery packs can easily have millions of DOFs, and thus statistical analyses is computationally prohibitive.

To overcome this difficulty, an accurate and computationally efficient numerical method was developed to predict the vibration response with structural variations and nonlinear materials. A simplified academic battery pack with 20 nominally identical cells is used to demonstrate the proposed approach. The linear PROMs were developed based on 2 key assumptions: (1) modes of the structure with structural variations are linear combinations of modes at the two extreme PreV levels and no C2CV, and (2) the stiffness of the structure with variations can be expressed as an interpolation based on stiffness matrices at the extreme PreV and C2CV levels. The nonlinear PROMs are developed based on the assumption that the nonlinearity is weak.

By reducing the order of the model and interpolating the stiffness matrices, PROMs can be generated efficiently, and full-order analysis can be avoided. The 159,666-DOF system in this work was reduced to a 390-DOF system by a single transformation matrix. Such low order models cannot be constructed by other existing methods like CB-CMS or sub-structuring. Also, by solving the nonlinear equations using an iterative method, the nonlinear vibration response was obtained efficiently.

In addition, for linear system, the vibration responses predicted from the PROMs

match very well those from the full-order FEM. However, the simulation time was reduced by a factor of 69.66. For nonlinear system, the vibration responses predicted from the iterative method also match very well with those from the time marching approach. However, there is a reduction in simulation time by a factor of 65,000 compared to time-marching.

Moreover, in the presented work, the PROMs simultaneously capture the effects of the PreV variation in the overall system, the C2CV in each cell, and nonlinear material properties of the cells. The statistical analyses show that the amplitude of the cells can be drastically changed due to small structural variations.

CHAPTER III

Parametric reduced-order models capturing nonlinear behavior in foams

In this chapter, augmented nonlinear PROMs are developed for battery packs, which simultaneously capture the effects of linear structural variations as well as the nonlinear behavior in both cells and foams. In Sec. 3.1, the effects of structural variations on the dynamic responses of battery packs in a HMD region are discussed. In Sec. 3.2, formulation of augmented nonlinear PROMs for modeling structural variations and nonlinear behavior of materials are described. In Sec. 3.3, numerical results calculated from the dynamic simulation of PROMs and full-order models are compared. In Sec. 3.4, statistical analyses are performed and used to illustrate the effect the linear and nonlinear structural variations. Finally, the conclusions of this study are presented in Sec. 3.5.

3.1 Effect of High Modal Density

To demonstrate the ideas proposed in this paper, an academic FEM of a battery pack was designed as shown in Fig. 3.1(a). This model is comprised of 20 nominally identical cells. Fig. 3.1(b) shows that each cell is comprised of several different components, including positive and negative current collectors, a cathode, an anode,

a separator, and a case. The cells are stacked together and mechanically coupled through foams and spacers.

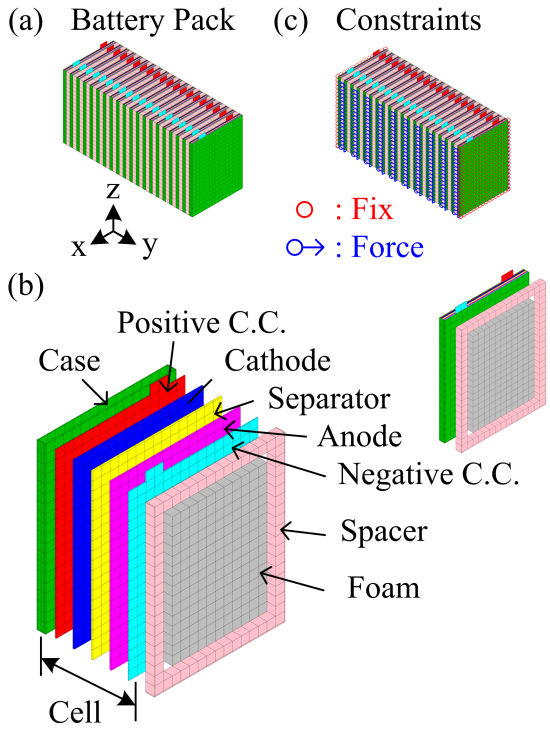

Figure 3.1: (a) The academic battery pack model. (b) A cell is comprised of positive and negative current collectors, an anode, a cathode, a separator, and a case. (c) Constraints applied to the two ends of the pack (red circles), and harmonic force is applied to the bottom and two sides of the pack along y-direction (blue circles and arrows).

The battery pack usually contains hundreds of cells. The cells are stacked together, and the battery pack is comprised of these repeated substructures. Due to this spatially periodic construction, the natural frequency plot of the battery pack exhibits HMD regions as shown in Fig. 3.2. The normalized frequencies are calculated through dividing natural frequencies by its lowest natural frequency. In general, the higher the number of repeated cells in the pack is, the wider the HMD region is. If excitation frequencies lie in a HMD region, a small structural variation can lead to drastic changes in vibration responses.

The PreV level of battery packs is defined as how much the overall length of the

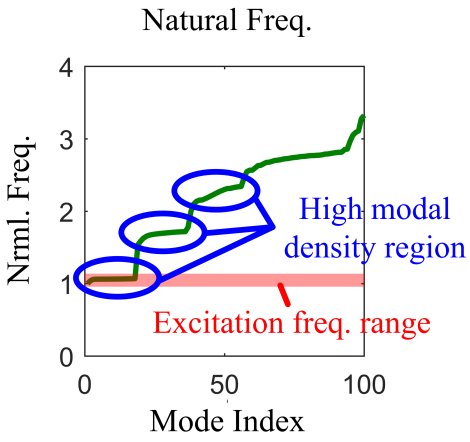

Figure 3.2: The natural frequency plot of the academic battery pack with foams exhibits high modal density regions. (Noted that Fig. 2.1 shows a different natural frequency plot because there is no foam in the academic battery pack.)

battery pack pack in y-direction shown in Fig. 3.1(a) is shorter than the nominal design due to preload. For example, the battery pack, whose length in y-direction is shorter than the nominal design by 5% due to preload, has PreV level equals to 5%. The effects of PreV on the vibration responses of battery packs are discussed in literatures[57, 72]. The C2CV level of a cell is defined as the variational percentage on modulus of elasticity of the cell compared to its nominal design. For example, a cell, whose modulus of elasticity is 5% higher than the nominal design, has C2CV level equals to 5%. The C2CV level is randomly generated from normal distribution, where the mean is 0% and the standard deviation is chosen to be 3.33% to make 99.7% of C2CV levels that are in the range of -10% to 10% as shown in Fig 3.3.

Fig. 3.4 shows the effect of different C2CV cases applied to the nominal design of the academic battery pack model. The excitation is a single harmonic force applied to the bottom and two sides of the battery pack model, which is constrained at the two ends as shown in Fig. 3.1(c). The excitation frequency indicated by red horizontal rectangular area in Fig. 3.2 lies in the first HMD region.

Fig. 3.4(a) shows vibration responses of each separator in the battery pack. The

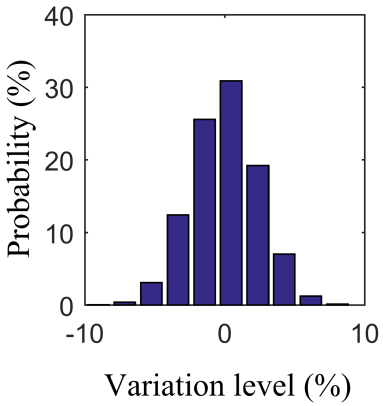

Figure 3.3: Distribution of cell-to-cell variation levels.

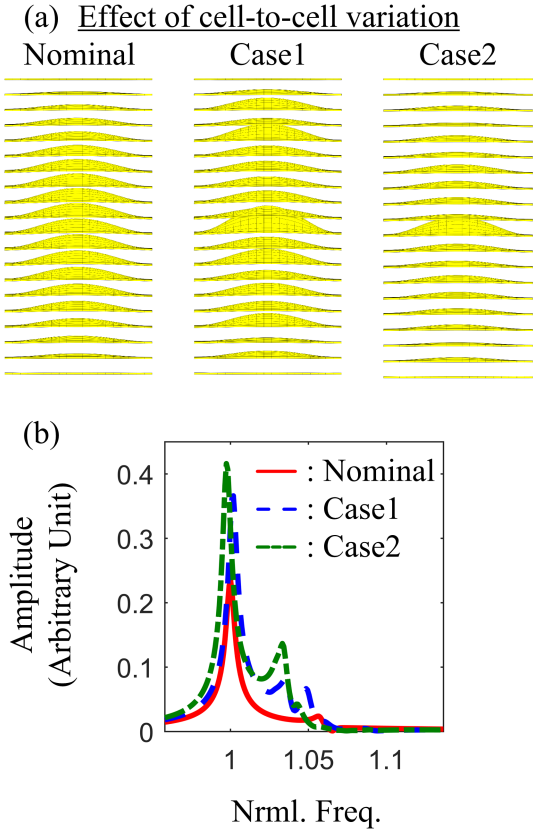

Figure 3.4: The effect of cell-to-cell variations.

separators are chosen to show vibration responses because they are at the central node of each cell and are representative of vibration response of cells. The peak amplitude of vibration response is observed at the central node of each cell, and the vibration response of a cell is dominated by its first plate-like mode. In the nominal case, the

amplitude of vibration are in the small-large-small pattern from one end to the other end of the battery pack. However, in case 1 and case 2, the patterns have changed. Fig. 3.4(b) shows the amplitude of vibration at the central node of cell 10 through a frequency range. The frequency and amplitude of the peak change significantly due to C2CV.

The nonlinear material properties in cells and foams are considered in FEM. The modulus of elasticity of an element E_{el} is assumed to be a quadratic function of strain of the element ϵ_{el} as shown in Fig. 3.5. The strain of the element ϵ_{el} can be approximated as the equivalent strain ϵ_{eq} gives the same strain energy density U [73].

$$\epsilon_{el} = \epsilon_{eq} = \sqrt{\frac{2U}{E_{el}(\epsilon_{eq})}} = \sqrt{\boldsymbol{x}_{el}^T \frac{\boldsymbol{K}_{el}(\epsilon_{eq})}{E_{el}(\epsilon_{eq}) \cdot V_{el}} \boldsymbol{x}_{el}} \tag{3.1}$$

where E_{el} is the modulus of elasticity of the element and is a function of ϵ_{eq}, $\boldsymbol{x}_{el}$ is a vector of displacement at DOFs of the element, $\boldsymbol{K}_{el}$ is the stiffness matrix of the element and a function of ϵ_{eq}, and V_{el} is the volume of the element. Because $\boldsymbol{K}_{el}$ is proportional to E_{el}, Eq. 3.1 can to be evaluted at zero strain,

$$\epsilon_{el} = \epsilon_{eq} = \sqrt{\boldsymbol{x}_{el}^T \frac{\boldsymbol{K}_{el,LI}}{E_{el,LI} \cdot V_{el}} \boldsymbol{x}_{el}} \tag{3.2}$$

where $\boldsymbol{K}_{el,LI}$ is the linear stiffness matrix evaluated at zero strain, and $E_{el,LI}$ is the modulus of elasticity evaluated at zero strain. Since E_{el} is assumed to be a quadratic function of ϵ_{el}, $\boldsymbol{K}_{el}$ is also a quadratic function of ϵ_{el},

$$\begin{aligned} \boldsymbol{K}_{el} &= \frac{\boldsymbol{K}_{el,LI}}{E_{el,LI}} \left(E_{el,LI} + \xi_{el} \epsilon_{el}^2 \right) \\ &= \boldsymbol{K}_{el,LI} + \frac{\boldsymbol{K}_{el,LI}}{E_{el,LI}} \xi_{el} \epsilon_{el}^2 \end{aligned} \tag{3.3}$$

where ξ_{el} is the nonlinear coefficient of element material properties, $\boldsymbol{K}_{el,LI}$ is the linear part of stiffness matrix, and $\Delta \boldsymbol{K}_{el,NL}$ is the nonlinear part of stiffness matrix. Denote

the nonlinear part of stiffness of matrix of element as $\Delta \boldsymbol{K}_{el,NL}$.

$$\Delta \boldsymbol{K}_{el,NL} \equiv \frac{\boldsymbol{K}_{el,LI}}{E_{el,LI}} \xi_{el} \epsilon_{el}^2 \equiv \Delta \boldsymbol{\kappa}_{el,NL} \epsilon_{el}^2 \tag{3.4}$$

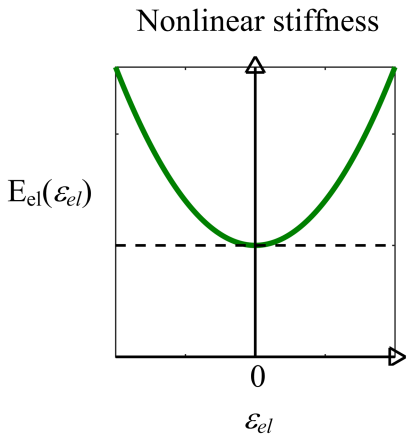

Figure 3.5: The stiffness increases when the strain increases.

Fig. 3.6(a) compares vibration responses with and without nonlinear structural variations. The linear structural variations refer to PreV and C2CV, which are independent of ϵ_{el} . In contrast, the nonlinear structural variations refer to the variations depending on ϵ_{el}. Fig. 3.6(b) shows that the peak amplitude of vibration is lowered about 30% due to nonlinearity.

For the vibration of a cell along its first plate-like mode, the strain distribution of the cell can be captured by the modal amplitude α as shown in Fig. 3.7. This observation is the key to constructing nonlinear PROMs because the stiffness matrix of the cell can be represented as function of a single parameter α .

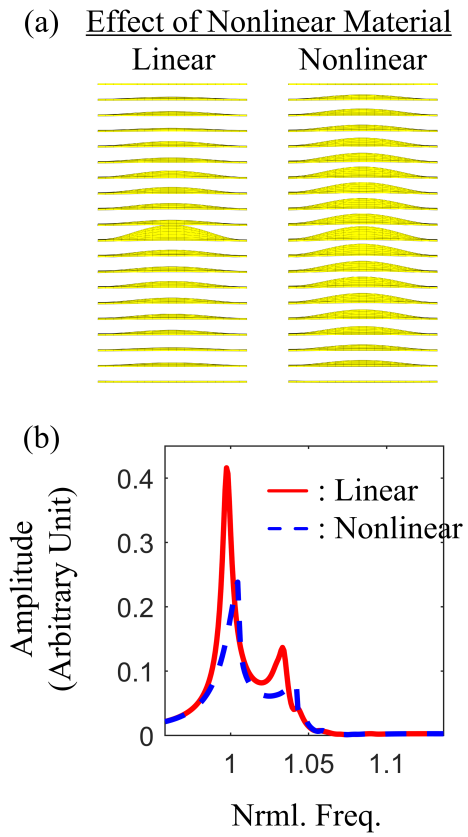

Figure 3.6: The effect of nonlinear material.

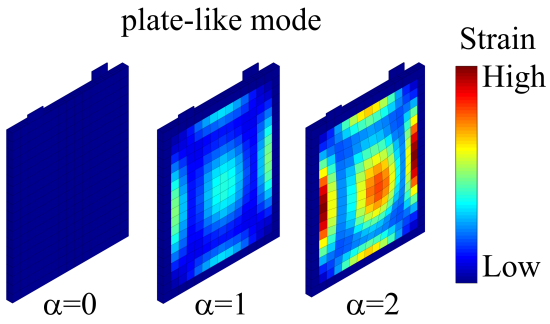

Figure 3.7: The strain distribution of a cell vibrating along different amplitudes of the plate-like mode is a function of the modal amplitude α

3.2 Methodology

3.2.1 Structural Dynamic Equations

The structural dynamic equations of the battery pack can be represented as

$$\boldsymbol{M}\ddot{\boldsymbol{x}} + \boldsymbol{C}\dot{\boldsymbol{x}} + \boldsymbol{K}\dot{\boldsymbol{x}} = \boldsymbol{f} \tag{3.5}$$

where $\boldsymbol{M}$ is mass matrix, $\boldsymbol{C}$ is damping matrix, $\boldsymbol{K}$ is stiffness matrix, $\boldsymbol{f}$ is external excitation force vector, and $\boldsymbol{x}$ is displacement vector.

The battery pack is subjected to structural variations. The PreV level p varies between a lower bound p_l and an upper bound p_u. The C2CV level s_i of cell i varies between a lower bound s_{il} and an upper bound s_{iu}. The vectors $\boldsymbol{s}_l$ and $\boldsymbol{s}_u$ represent the collection of the lower and upper bounds of C2CV levels for all cells. The vector $\boldsymbol{s}$ represents the collection of the C2CV levels for all cells. The nominal case is defined as $p = p_l$ and $\boldsymbol{s} = \boldsymbol{0}$.

$$
\begin{aligned}
p &\in \begin{bmatrix} p_l & p_u \end{bmatrix}, \; p_l \leq p_u \\
s &\in \begin{bmatrix} s_{il} & s_{iu} \end{bmatrix}, \; s_{il} \leq 0 \leq s_{iu} \\
\boldsymbol{s}_l &= \begin{bmatrix} s_{1l} \\ \vdots \\ s_{N_c l} \end{bmatrix}, \; \boldsymbol{s}_u = \begin{bmatrix} s_{1u} \\ \vdots \\ s_{N_c u} \end{bmatrix}, \; \boldsymbol{s} = \begin{bmatrix} s_1 \\ \vdots \\ s_{N_c} \end{bmatrix}
\end{aligned}
\tag{3.6}
$$

where N_c is the number of cells.

The stiffness matrix $\boldsymbol{K}$ is a function of linear structural variations and nonlinear dynamic behavior in cells and foams. The linear structural variations are assumed to be small. The nonlinear parts of stiffness matrix are assumed to be independent of linear structural variations. With these two assumptions, $\boldsymbol{K}$ is approximated as

$$
\boldsymbol{K} \approx \boldsymbol{K}_{p,\boldsymbol{s},LI} + \Delta \boldsymbol{K}_{C,NL} + \Delta \boldsymbol{K}_{F,NL} \tag{3.7}
$$

where $\boldsymbol{K}_{p,\boldsymbol{s},LI}$ is the stiffness matrix capturing linear structural variations at PreV level p and C2CV level $\boldsymbol{s}$, $\Delta \boldsymbol{K}_{C,NL}$ is the stiffness matrix capturing nonlinear dynamic behavior in cells, and $\Delta \boldsymbol{K}_{F,NL}$ is the stiffness matrix capturing nonlinear dynamic behavior in foams.

Assume that the damping matrix $\boldsymbol{C}$ is proportional to the stiffness matrix. The

proportional damping coefficients of all components are equal except foams, which are assumed to have a higher damping coefficient. β_f denotes the damping coefficient of foams, and β_g denotes the damping coefficient of all other components. $\boldsymbol{C}$ can be represented as

$$\begin{aligned}\boldsymbol{C} =&\beta_g \boldsymbol{K}_{p,\boldsymbol{s},LI} + (\beta_f - \beta_g)\frac{\boldsymbol{K}_{F10\%,p,\boldsymbol{s},LI} - \boldsymbol{K}_{p,\boldsymbol{s},LI}}{10\%} \\ &+ \beta_g \Delta\boldsymbol{K}_{C,NL} + \beta_f \Delta\boldsymbol{K}_{F,NL} \\ \approx&\beta_g \boldsymbol{K}_{p,\boldsymbol{s},LI} + (\beta_f - \beta_g)\frac{\boldsymbol{K}_{F10\%,p,\boldsymbol{0},LI} - \boldsymbol{K}_{p,\boldsymbol{0},LI}}{10\%} \\ &+ \beta_g \Delta\boldsymbol{K}_{C,NL} + \beta_f \Delta\boldsymbol{K}_{F,NL}\end{aligned} \tag{3.8}$$

where $\boldsymbol{K}_{F10\%,p,\boldsymbol{s},LI}$ is the stiffness matrix for the system with all foams having stiffness 10% higher than the nominal design of foams at PreV level p and C2CV level $\boldsymbol{s}$. The purpose of the term $(\beta_f - \beta_g)\frac{\boldsymbol{K}_{F10\%,p,\boldsymbol{s},LI} - \boldsymbol{K}_{p,\boldsymbol{s},LI}}{10\%}$ is to replace the contribution of foams in $\beta_g \boldsymbol{K}_{p,\boldsymbol{s},LI}$ from β_g to β_f. Since C2CV and the 10% stiffness change of foam are both small, $\boldsymbol{K}_{F10\%,p,\boldsymbol{s},LI} - \boldsymbol{K}_{p,\boldsymbol{s},LI}$ is approximated to be $\boldsymbol{K}_{F10\%,p,\boldsymbol{0},LI} - \boldsymbol{K}_{p,\boldsymbol{0},LI}$ in Eq. 3.8.

The structural dynamic equations of battery packs can have tens of thousands of DOFs depending on the complexity and mesh density of FEM. To reduce the order of structural dynamic equations, several reduction techniques are employed.

3.2.2 Order Reduction

The transformation matrix $\boldsymbol{T}^R$ is constructed to reduce the order of structural dynamic equations. The first assumption is that vibration responses at PreV level p and C2CV level $\boldsymbol{s}$ can be captured by the truncated modes $\boldsymbol{\phi}_{p,\boldsymbol{s}}$ whose natural frequencies are close to the frequency range of interest. Moreover, assume that the truncated modes $\boldsymbol{\phi}_{p,\boldsymbol{s}}$ are linear combinations of truncated modes $\boldsymbol{\phi}_{p_l,\boldsymbol{0}}$ at PreV level p_l and C2CV level $\boldsymbol{0}$ and truncated modes $\boldsymbol{\phi}_{p_u,\boldsymbol{0}}$ at PreV level p_u and C2CV level $\boldsymbol{0}$,

i.e.

$$span(\boldsymbol{\phi}_{p,\boldsymbol{s}}) = span(\begin{bmatrix} \boldsymbol{\phi}_{p_l,\mathbf{0}} & \boldsymbol{\phi}_{p_u,\mathbf{0}} \end{bmatrix}) \tag{3.9}$$

The assumption in Eq. 3.9 is valid when the frequency range of interest is in a high modal density region and structural variations are small. The general transformation matrix $\boldsymbol{T}_G^R$ is defined as

$$\boldsymbol{T}_G^R = \begin{bmatrix} \boldsymbol{\phi}_{p_l,\mathbf{0}} & \boldsymbol{\phi}_{p_u,\mathbf{0}} \end{bmatrix}. \tag{3.10}$$

Because the PreV bounds p_l and p_u are close, the modes $\boldsymbol{\phi}_{p_l,\mathbf{0}}$ and $\boldsymbol{\phi}_{p_u,\mathbf{0}}$ can have approximately linearly independent columns. Gauss-Jordan elimination (*rref* command in Matlab) is employed to eliminate these columns in $\boldsymbol{T}_G^R$.

$$\boldsymbol{T}^R = rref(\boldsymbol{T}_G^R) \tag{3.11}$$

The order of structural dynamic equations is reduced by projection using $\boldsymbol{x} = \boldsymbol{T}^R\boldsymbol{q}$.

$$\boldsymbol{M}^R\ddot{\boldsymbol{q}} + \boldsymbol{C}^R\dot{\boldsymbol{q}} + \boldsymbol{K}^R\dot{\boldsymbol{q}} = \boldsymbol{f}^R \tag{3.12}$$

where

$$
\begin{aligned}
\boldsymbol{M}^R &= (\boldsymbol{T}^R)^T \boldsymbol{M} \boldsymbol{T}^R \\
\boldsymbol{C}^R &= (\boldsymbol{T}^R)^T \boldsymbol{C} \boldsymbol{T}^R \\
&= (\boldsymbol{T}^R)^T (\beta_g \boldsymbol{K}_{p,\boldsymbol{s},LI} + (\beta_f - \beta_g) \frac{\boldsymbol{K}_{F10\%,p,\boldsymbol{0},LI} - \boldsymbol{K}_{p,\boldsymbol{0},LI}}{10\%} \\
&\quad + \beta_g \Delta \boldsymbol{K}_{C,NL} + \beta_f \Delta \boldsymbol{K}_{F,NL}) \boldsymbol{T}^R \\
&= \beta_g \boldsymbol{K}^R_{p,\boldsymbol{s},LI} + (\beta_f - \beta_g) \frac{\boldsymbol{K}^R_{F10\%,p,\boldsymbol{0},LI} - \boldsymbol{K}^R_{p,\boldsymbol{0},LI}}{10\%} \\
&\quad + \beta_g \Delta \boldsymbol{K}^R_{C,NL} + \beta_f \Delta \boldsymbol{K}^R_{F,NL} \\
\boldsymbol{K}^R &= (\boldsymbol{T}^R)^T \boldsymbol{K} \boldsymbol{T}^R \\
&= (\boldsymbol{T}^R)^T (\boldsymbol{K}_{p,\boldsymbol{s},LI} + \Delta \boldsymbol{K}_{C,NL} + \Delta \boldsymbol{K}_{F,NL}) \boldsymbol{T}^R \\
&= \boldsymbol{K}^R_{p,\boldsymbol{s},LI} + \Delta \boldsymbol{K}^R_{C,NL} + \Delta \boldsymbol{K}^R_{F,NL} \\
\boldsymbol{f}^R &= (\boldsymbol{T}^R)^T \boldsymbol{f}
\end{aligned}
\tag{3.13}
$$

3.2.3 Derivation of Linear PROMs

The reduced-order stiffness matrix $\boldsymbol{K}^R_{p,\boldsymbol{s},LI}$ at PreV level p and C2CV level $\boldsymbol{s}$ in Eq. 3.13 can be expanded by Taylor series around $\boldsymbol{s} = 0$.

$$
\begin{aligned}
\boldsymbol{K}^R_{p,\boldsymbol{s},LI} &= \boldsymbol{K}^R_{p,\boldsymbol{0},LI} + \sum_{i=1}^{N_c} \frac{\partial \boldsymbol{K}^R_{p,s_i,LI}}{\partial s_i} s_i + H.O.T. \\
&\approx \boldsymbol{K}^R_{p,\boldsymbol{0},LI} + \sum_{i=1}^{N_c} \frac{\partial \boldsymbol{K}^R_{p,s_i,LI}}{\partial s_i} s_i
\end{aligned}
\tag{3.14}
$$

where $H.O.T.$ are high order terms and are negligible because s_i is small.

To obtain $\boldsymbol{K}^R_{p,\boldsymbol{0},LI}$ in Eq. 3.14, one first constructs the stiffness matrices $\boldsymbol{K}_{p_u,\boldsymbol{0},LI}$ and $\boldsymbol{K}_{p_l,\boldsymbol{0},LI}$ at the extreme PreV levels p_u and p_l without C2CV using finite element analyses and project the stiffness matrices using $\boldsymbol{T}^R$.

$$
\begin{aligned}
\boldsymbol{K}_{p_u,\boldsymbol{0},LI} &= (\boldsymbol{T}^R)^T \boldsymbol{K}_{p_u,\boldsymbol{0},LI} \boldsymbol{T}^R \\
\boldsymbol{K}_{p_l,\boldsymbol{0},LI} &= (\boldsymbol{T}^R)^T \boldsymbol{K}_{p_l,\boldsymbol{0},LI} \boldsymbol{T}^R
\end{aligned}
\tag{3.15}
$$

For any PreV level p between p_u and p_l, linear interpolation is employed to obtain $\boldsymbol{K}^R_{p,\mathbf{0},LI}$.

$$\boldsymbol{K}^R_{p,\mathbf{0},LI} = \frac{p - p_l}{p_u - p_l}(\boldsymbol{K}^R_{p_u,\mathbf{0},LI} - \boldsymbol{K}^R_{p_l,\mathbf{0},LI}) + \boldsymbol{K}^R_{p_l,\mathbf{0},LI} \tag{3.16}$$

Similarly, to obtain stiffness matrices $\frac{\partial \boldsymbol{K}^R_{p,s_i,LI}}{\partial s_i} s_i$ in Eq. 3.14, one obtain the stiffness matrices $\boldsymbol{K}_{p_l,s_{il},LI}$, $\boldsymbol{K}_{p_l,s_{iu},LI}$, $\boldsymbol{K}_{p_u,s_{il},LI}$, and $\boldsymbol{K}_{p_u,s_{iu},LI}$ at the extreme PreV levels and C2CV levels using finite element analyses. Then, these four stiffness matrices are projected using $\boldsymbol{T}^R$.

$$\begin{aligned}
\boldsymbol{K}^R_{p_l,s_{il},LI} &= (\boldsymbol{T}^R)^T \boldsymbol{K}_{p_l,s_{il},LI} \boldsymbol{T}^R \\
\boldsymbol{K}^R_{p_l,s_{iu},LI} &= (\boldsymbol{T}^R)^T \boldsymbol{K}_{p_l,s_{iu},LI} \boldsymbol{T}^R \\
\boldsymbol{K}^R_{p_u,s_{il},LI} &= (\boldsymbol{T}^R)^T \boldsymbol{K}_{p_u,s_{il},LI} \boldsymbol{T}^R \\
\boldsymbol{K}^R_{p_u,s_{iu},LI} &= (\boldsymbol{T}^R)^T \boldsymbol{K}_{p_u,s_{iu},LI} \boldsymbol{T}^R
\end{aligned} \tag{3.17}$$

Because there are two linear structural variations, p and s_i, are involved in the stiffness matrix $\frac{\partial \boldsymbol{K}^R_{p,s_i,LI}}{\partial s_i} s_i$, two steps of linear interpolation are employed. The first step is the linear interpolation of stiffness matrices with respect to PreV level.

$$\begin{aligned}
\Delta \boldsymbol{K}^R_{p,s_{il},LI} &= \frac{p - p_l}{p_u - p_l}(\boldsymbol{K}^R_{p_u,s_{il},LI} - \boldsymbol{K}^R_{p_l,s_{il},LI}) \\
\Delta \boldsymbol{K}^R_{p,s_{iu},LI} &= \frac{p - p_l}{p_u - p_l}(\boldsymbol{K}^R_{p_u,s_{iu},LI} - \boldsymbol{K}^R_{p_l,s_{iu},LI}).
\end{aligned} \tag{3.18}$$

The second step is the linear interpolation of stiffness matrices with respect to C2CV level.

$$\frac{\partial \boldsymbol{K}^R_{p,s_i,LI}}{\partial s_i} s_i = \frac{s_i}{s_{iu} - s_{il}}(\Delta \boldsymbol{K}^R_{p,s_{iu},LI} - \Delta \boldsymbol{K}^R_{p,s_{il},LI}). \tag{3.19}$$

The terms $\boldsymbol{K}^R_{p,\mathbf{0},LI}$ and $\frac{\partial \boldsymbol{K}^R_{p,s_i,LI}}{\partial s_i} s_i$ in Eq. 3.14 can be obtained using linear interpolations instead of running time-consuming finite element analyses. Furthermore, the linear interpolations are conducted in the reduced-order coordinate which make PROMs be computationally efficient.

To obtain $\boldsymbol{K}^R_{F10\%,p,\mathbf{0},LI}$ in Eq. 3.13, one first obtains the stiffness matrices $\boldsymbol{K}_{F10\%,p_u,\mathbf{0},LI}$

and $\boldsymbol{K}_{F10\%,p_l,\mathbf{0},LI}$ at the extreme PreV levels without C2CV using finite element analyses where the stiffness of foams are 10% higher than the nominal design of foams and project them using $\boldsymbol{T}^R$.

$$\begin{aligned}\boldsymbol{K}_{F10\%,p_u,\mathbf{0},LI} &= (\boldsymbol{T}^R)^T \boldsymbol{K}_{F10\%,p_u,\mathbf{0},LI} \boldsymbol{T}^R \\ \boldsymbol{K}_{F10\%,p_l,\mathbf{0},LI} &= (\boldsymbol{T}^R)^T \boldsymbol{K}_{F10\%,p_l,\mathbf{0},LI} \boldsymbol{T}^R\end{aligned} \tag{3.20}$$

Similar to Eq. 3.16, linear interpolation is employed to obtain the stiffness matrix $\boldsymbol{K}^R_{F10\%,p,\mathbf{0},LI}$ at PreV level p and C2CV level $\mathbf{0}$.

$$\begin{aligned}\boldsymbol{K}^R_{F10\%,p,\mathbf{0},LI} = &\frac{p-p_l}{p_u-p_l}(\boldsymbol{K}^R_{F10\%,p_u,\mathbf{0},LI} - \boldsymbol{K}^R_{F10\%,p_l,\mathbf{0},LI}) \\ &+ \boldsymbol{K}^R_{F10\%,p_u,\mathbf{0},LI}\end{aligned} \tag{3.21}$$

The reduced-order linear damping matrix $\boldsymbol{C}^R_{p,\boldsymbol{s},LI}$ can be represented as

$$\boldsymbol{C}^R_{p,\boldsymbol{s},LI} = \beta_g \boldsymbol{K}^R_{p,\boldsymbol{s},LI} + (\beta_f - \beta_g)\frac{\boldsymbol{K}^R_{F10\%,p,\mathbf{0},LI} - \boldsymbol{K}^R_{p,\mathbf{0},LI}}{10\%} \tag{3.22}$$

One can use PreV level p and C2CV level $\boldsymbol{s}$ as input to construct $\boldsymbol{K}^R_{p,\boldsymbol{s},LI}$ and $\boldsymbol{C}^R_{p,\boldsymbol{s},LI}$ and form the linear part of reduced-order structural dynamic equations in Eq. 3.12.

$$\boldsymbol{M}^R\ddot{\boldsymbol{q}} + \boldsymbol{C}^R_{p,\boldsymbol{s},LI}\dot{\boldsymbol{q}} + \boldsymbol{K}^R_{p,\boldsymbol{s},LI}\dot{\boldsymbol{q}} = \boldsymbol{f}^R \tag{3.23}$$

Linear vibration responses can be solved using Eq. 3.23.

3.2.4 Derivation of Nonlinear PROMs

The modulus of elasticity of an element of cells and foams is assumed to be a quadratic function of strain of the element. Since the stiffness matrix of an element linearly depends on the modulus of elasticity of the element, it's also a quadratic function of strain of the element. Denote $\boldsymbol{K}_{el}$ as the stiffness matrix of an element

and ϵ_{el} as strain of the element .

$$\boldsymbol{K}_{el}(\epsilon_{el}) = \boldsymbol{K}_{el,LI} + \Delta\boldsymbol{\kappa}_{el,NL}\epsilon_{el}^2 \tag{3.24}$$

where $\boldsymbol{K}_{el}$ the stiffness matrix of an element, and ϵ_{el} is strain of the element which can be evaluated using Eq. 3.2.

3.2.4.1 Nonlinear Cells

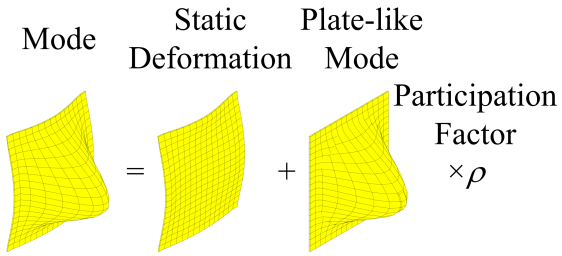

Figure 3.8: Deconstruct modes into static deformation $\boldsymbol{\Phi}_{C_i}^S$ and plate-like mode $\boldsymbol{\phi}_{C_i}^N$ multiplied by participation factor $\boldsymbol{\rho}_i$.

The first plate-like mode of each cell dominating vibration responses is observed in Fig. 3.4(a) and Fig. 3.6(a). Denote the vibration response at DOFs of cell i as $\boldsymbol{x}_{C_i}$ and modes at DOFs of cell i as $\boldsymbol{T}_{C_i}^R$ in $\boldsymbol{T}^R$. Because the first plate-like mode dominates, the modes $\boldsymbol{T}_{C_i}^R$ can be deconstructed into two parts as shown in Fig. 3.8, the static deformation $\boldsymbol{\Phi}_{C_i}^S$ and the plate-like mode $\boldsymbol{\phi}_{C_i}^N$ multiplied by the participation factor $\boldsymbol{\rho}_i$ which represents how much the first plate-like mode is involved in each column of $\boldsymbol{T}_{C_i}^R$.

$$\boldsymbol{x}_{C_i} = \boldsymbol{T}_{C_i}^R\boldsymbol{q} \approx \left(\boldsymbol{\Phi}_{C_i}^S + \boldsymbol{\phi}_{C_i}^N\boldsymbol{\rho}_i\right)\boldsymbol{q} \tag{3.25}$$

The first plate-like mode $\boldsymbol{\phi}_{C_i}^N$ is obtained by employing zero displacement constraints at DOFs of boundaries of single cell FEM of cell i without linear and nonlinear structural variations. The static deformation $\boldsymbol{\Phi}_{C_i}^S$ is obtained by employing displacements along the modes $\boldsymbol{T}_{C_i}^R$ at DOFs of boundaries of the single cell FEM and calculating

the corresponding displacement at internal DOFs. From Eq. 3.25,

$$\boldsymbol{T}_{C_i}^R - \boldsymbol{\Phi}_{C_i}^S \approx \boldsymbol{\phi}_{C_i}^N \boldsymbol{\rho}_i \tag{3.26}$$

Multiply both sides by $(\boldsymbol{\phi}_{C_i}^N)^T \boldsymbol{K}_{C_i,LI}$, where $\boldsymbol{K}_{C_i,LI}$ is the stiffness matrix of the single cell FEM.

$$(\boldsymbol{\phi}_{C_i}^N)^T \boldsymbol{K}_{C_i,LI}(\boldsymbol{T}_{C_i}^R - \boldsymbol{\Phi}_{C_i}^S) \approx (\boldsymbol{\phi}_{C_i}^N)^T \boldsymbol{K}_{C_i,LI} \boldsymbol{\phi}_{C_i}^N \boldsymbol{\rho}_i \tag{3.27}$$

Denote $\Lambda_i = (\boldsymbol{\phi}_{C_i}^N)^T \boldsymbol{K}_{C_i,LI} \boldsymbol{\phi}_{C_i}^N$ which represents the eigenvalue of the first plate-like mode. The participation factor $\boldsymbol{\rho}_i$ can be calculated by

$$\boldsymbol{\rho}_i \approx \Lambda_i^{-1} (\boldsymbol{\phi}_{C_i}^N)^T \boldsymbol{K}_{C_i,LI}(\boldsymbol{T}_{C_i}^R - \boldsymbol{\Phi}_{C_i}^S) \tag{3.28}$$

In Eq. 3.25, because the plate-like mode $\boldsymbol{\phi}_{C_i}^N \boldsymbol{\rho}_i$ dominates, the static deformation $\boldsymbol{\Phi}_{C_i}^S$ is negligible.

$$\begin{aligned} \boldsymbol{x}_{C_i} &\approx \boldsymbol{\phi}_{C_i}^N \boldsymbol{\rho}_i \boldsymbol{q} = \boldsymbol{\phi}_{C_i}^N \alpha_i \\ \alpha_i &\equiv \boldsymbol{\rho}_i \boldsymbol{q} \end{aligned} \tag{3.29}$$

where α_i is a scalar variable which represents the modal amplitude of the first plate-like mode of cell i. The vibration response $\boldsymbol{x}_{el,C_i}$ at DOFs of an element of cell i becomes

$$\boldsymbol{x}_{el} = \boldsymbol{x}_{el,C_i} \approx \boldsymbol{\phi}_{el,C_i}^N \alpha_i \tag{3.30}$$

where $\boldsymbol{\phi}_{el,C_i}^N$ is the first plate-like mode at DOFs of an element in cell i. Substitute Eq. 3.30 into Eq. 3.2 and Eq. 3.4, one can obtain

$$\begin{aligned} &\Delta \boldsymbol{K}_{el,C_i,NL} \equiv \Delta \boldsymbol{\kappa}_{el,C_i,NL} \epsilon_{el,C_i}^2 \\ =&\Delta \boldsymbol{\kappa}_{el,C_i,NL} \frac{(\boldsymbol{\phi}_{el,C_i}^N)^T \boldsymbol{K}_{el,C_i,LI} \boldsymbol{\phi}_{el,C_i}^N}{E_{el,C_i} \cdot V_{el,C_i}} \alpha_i^2 \\ \equiv&\Delta \bar{\boldsymbol{\kappa}}_{el,C_i,NL} \alpha_i^2 \end{aligned} \tag{3.31}$$

where C_i denotes cell i, $\Delta \boldsymbol{K}_{el,C_i,NL}$ is the nonlinear part of stiffness matrix of an element of cell i in Eq. 3.4, and $\Delta \bar{\boldsymbol{\kappa}}_{el,C_i,NL}$ is a constant matrix with respect to ϵ_{el,C_i}.

The nonlinear part of stiffness matrix $\Delta \boldsymbol{K}_{C_i,NL}$ can be constructed by assembling $\Delta \boldsymbol{K}_{el,C_i,NL}$ for all elements of cell i.

$$\begin{aligned} \Delta \boldsymbol{K}_{C_i,NL} &= \sum_{el} \Delta \boldsymbol{K}_{el,C_i,NL} \\ &= \sum_{el} \Delta \bar{\boldsymbol{\kappa}}_{el,C_i,NL} \alpha_i^2 = \Delta \bar{\boldsymbol{\kappa}}_{C_i,NL} \alpha_i^2 \end{aligned} \tag{3.32}$$

Because α_i is identical for all elements of the single cell FEM, it can be pulled out of the assembly in Eq. 3.32.

In Eq. 3.32, $\Delta \boldsymbol{K}_{C_i,NL}$ for a given displacement can be obtained using finite element analyses of the single cell FEM of cell i where the element stiffness matrices are updated using Eq. 3.2. By employing displacement along the first plate-like mode $\boldsymbol{\phi}_{C_i}^N$ on the single cell FEM with modal amplitude $\bar{\alpha}$, $\Delta \bar{\boldsymbol{\kappa}}_{C_i,NL}$ can be obtained using Eq. 3.32.

$$\Delta \bar{\boldsymbol{\kappa}}_{C_i,NL} = \frac{1}{\bar{\alpha}^2} \Delta \boldsymbol{K}_{C_i,NL}|_{\alpha_i = \bar{\alpha}} \tag{3.33}$$

Knowing $\Delta \bar{\boldsymbol{\kappa}}_{C_i,NL}$ in Eq. 3.32, $\Delta \boldsymbol{K}_{C_i,NL}$ can be obtained for given α_i without using a full-order model.

$\Delta \boldsymbol{K}_{C,NL}^R$ in Eq. 3.13 capturing the nonlinear behavior of cells can be obtained by projecting and summing up the nonlinear part of stiffness matrices for all cells for given α_i.

$$\begin{aligned} \Delta \boldsymbol{K}_{C,NL}^R &= \sum_{i=1}^{N_c} (\boldsymbol{T}_{C_i}^R)^T \Delta \boldsymbol{K}_{C_i,NL} \boldsymbol{T}_{C_i}^R \\ &= \sum_{i=1}^{N_c} (\boldsymbol{T}_{C_i}^R)^T \Delta \bar{\boldsymbol{\kappa}}_{C_i,NL} \alpha_i^2 \boldsymbol{T}_{C_i}^R \\ &= \sum_{i=1}^{N_c} \Delta \boldsymbol{\kappa}_{C_i,NL}^R \alpha_i^2 \end{aligned} \tag{3.34}$$

3.2.4.2 Nonlinear Foams

By following similar strategy of modeling nonlinear behavior in cells, the nonlinear behavior in foams is modeled. The difference between modeling cells and foams is that foams are much softer material than cells. Consequently, the deformation of a foam is dominated by the two neighboring cells as shown in Fig. 3.9. With the assumption that the vibration response of a cell is dominated by its first plate-like mode, the vibration response of a foam is dominated by the first plate-like modes of two neighboring cells.

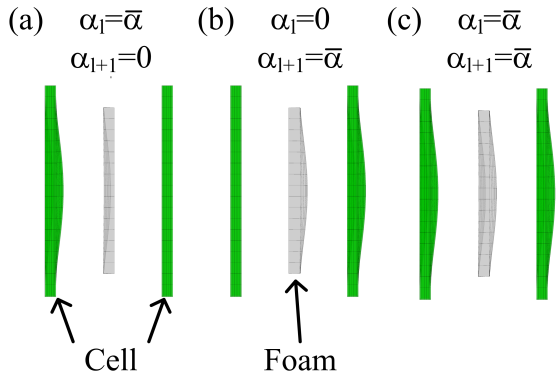

Figure 3.9: Apply the displacement along the plate-like modes with 3 different set of amplitudes (a), (b), and (c).

Denote the vibration response at DOFs of foam l as $\boldsymbol{x}_{F_l}$ and modes at DOFs of foam l as $\boldsymbol{T}^R_{F_l}$ in $\boldsymbol{T}^R$. Because there are two first plate-like modes dominate, the modes $\boldsymbol{T}^R_{F_l}$ are deconstructed into three parts, the static deformation $\boldsymbol{\Phi}^S_{F_l}$, the participation factor $\boldsymbol{\rho}_l$ and the first plate-like mode $\boldsymbol{\phi}^N_{F_l}$ of cell l at DOFs of foam l, and the participation factor $\boldsymbol{\rho}_{l+1}$ and the first plate-like mode $\boldsymbol{\phi}^N_{F_{l+1}}$ of cell $l+1$ at DOFs of foam l.

$$\boldsymbol{x}_{F_l} = \boldsymbol{T}^R_{F_l}\boldsymbol{q} \approx \left(\boldsymbol{\Phi}^S_{F_l} + \boldsymbol{\phi}^N_{F_l}\boldsymbol{\rho}_l + \boldsymbol{\phi}^N_{F_{l+1}}\boldsymbol{\rho}_{l+1}\right)\boldsymbol{q} \tag{3.35}$$

In Eq. 3.35, since the first plate-like modes $\boldsymbol{\phi}^N_{F_l}\boldsymbol{\rho}_l$ and $\boldsymbol{\phi}^N_{F_{l+1}}\boldsymbol{\rho}_{l+1}$ dominate, the

static deformation $\boldsymbol{\Phi}^S_{F_l}$ is negligible.

$$\begin{aligned} \boldsymbol{x}_{F_l} &\approx \boldsymbol{\phi}^N_{F_l}\boldsymbol{\rho}_l\boldsymbol{q} + \boldsymbol{\phi}^N_{F_{l+1}}\boldsymbol{\rho}_{l+1}\boldsymbol{q} = \boldsymbol{\phi}^N_l\alpha_l + \boldsymbol{\phi}^N_{l+1}\alpha_{l+1} \\ \alpha_l &= \boldsymbol{\rho}_l\boldsymbol{q} \\ \alpha_{l+1} &= \boldsymbol{\rho}_{l+1}\boldsymbol{q} \end{aligned} \tag{3.36}$$

where α_l and α_{l+1} are scalar variables which represent modal amplitudes. The vibration response $\boldsymbol{x}_{el,F_l}$ at DOFs of an element of foam l becomes

$$\boldsymbol{x}_{el,F_l} \approx \boldsymbol{\phi}^N_{el,F_l}\alpha_l + \boldsymbol{\phi}^N_{el,F_{l+1}}\alpha_{l+1} \tag{3.37}$$

where $\boldsymbol{\phi}^N_{el,F_l}$ and $\boldsymbol{\phi}^N_{el,F_{l+1}}$ are the first plate-like modes from cell l and cell $l+1$ at DOFs of an element of foam l. Substitute Eq. 3.37 into Eq. 3.2 and Eq. 3.4, one can obtain

$$\begin{aligned} \Delta\boldsymbol{K}_{el,F_l,NL} =& \Delta\boldsymbol{\kappa}_{el,F_l,NL}\epsilon^2_{el,F_l} \\ =& \Delta\boldsymbol{\kappa}_{el,F_l,NL}\frac{(\boldsymbol{\phi}^N_{el,F_l})^T\boldsymbol{K}_{el,F_l,LI}\boldsymbol{\phi}^N_{el,F_l}}{E_{el,F_l}\cdot V_{el,F_l}}\alpha_l^2 \\ &+\Delta\boldsymbol{\kappa}_{el,F_l,NL}\frac{(\boldsymbol{\phi}^N_{el,F_{l+1}})^T\boldsymbol{K}_{el,F_l,LI}\boldsymbol{\phi}^N_{el,F_{l+1}}}{E_{el,F_l}\cdot V_{el,F_l}}\alpha_{l+1}^2 \\ &+\Delta\boldsymbol{\kappa}_{el,F_l,NL}\frac{(\boldsymbol{\phi}^N_{el,F_l})^T\boldsymbol{K}_{el,F_l,LI}\boldsymbol{\phi}^N_{el,F_{l+1}}}{E_{el,F_l}\cdot V_{el,F_l}}2\alpha_l\alpha_{l+1} \\ \equiv& \begin{pmatrix} \Delta\bar{\boldsymbol{\kappa}}_{1,el,F_l,NL}\alpha_l^2 \\ +\Delta\bar{\boldsymbol{\kappa}}_{2,el,F_l,NL}\alpha_{l+1}^2 \\ +\Delta\bar{\boldsymbol{\kappa}}_{3,el,F_l,NL}\alpha_l\alpha_{l+1} \end{pmatrix} \end{aligned} \tag{3.38}$$

where F_l denotes foam l, $\Delta\boldsymbol{K}_{el,F_l,NL}$ is the nonlinear part of stiffness matrix of an element of foam l in Eq. 3.4, and $\Delta\bar{\boldsymbol{\kappa}}_{1,el,F_l,NL}$, $\Delta\bar{\boldsymbol{\kappa}}_{2,el,F_l,NL}$, and $\Delta\bar{\boldsymbol{\kappa}}_{3,el,F_l,NL}$ are constant matrices with respect to ϵ_{el,F_l}.

The nonlinear part of stiffness matrix $\Delta\boldsymbol{K}_{F_l,NL}$ can be constructed by assembling

$\Delta \boldsymbol{K}_{el,F_l,NL}$ for all elements of foam l.

$$\begin{aligned}
\Delta \boldsymbol{K}_{F_l,NL} &= \sum_{el} \Delta \boldsymbol{K}_{el,F_l,NL} \\
&= \sum_{el} \begin{pmatrix} \Delta \bar{\boldsymbol{\kappa}}_{1,el,F_l,NL} \alpha_l^2 \\ +\Delta \bar{\boldsymbol{\kappa}}_{2,el,F_l,NL} \alpha_{l+1}^2 \\ +\Delta \bar{\boldsymbol{\kappa}}_{3,el,F_l,NL} \alpha_l \alpha_{l+1} \end{pmatrix} \\
&= \begin{pmatrix} \Delta \bar{\boldsymbol{\kappa}}_{1,F_l,NL} \alpha_l^2 \\ +\Delta \bar{\boldsymbol{\kappa}}_{2,F_l,NL} \alpha_{l+1}^2 \\ +\Delta \bar{\boldsymbol{\kappa}}_{3,F_l,NL} \alpha_l \alpha_{l+1} \end{pmatrix}
\end{aligned} \tag{3.39}$$

In Eq. 3.39, $\Delta \boldsymbol{K}_{F_l,NL}$ for a given displacement can be obtained using full-order model of the single foam FEM of foam l where the element stiffness matrices are updated using Eq. 3.2. By employing displacement along the first plate-like modes $\boldsymbol{\phi}_{F_l}^N$ and $\boldsymbol{\phi}_{F_{l+1}}^N$ on the single foam FEM with three modal amplitude cases:

$$(\alpha_l, \alpha_{l+1}) = \begin{cases} (\ \bar{\alpha} \ , \ 0 \ ) \\ (\ 0 \ , \ \bar{\alpha} \ ) \\ (\ \bar{\alpha} \ , \ \bar{\alpha} \ ) \end{cases} \tag{3.40}$$

$\Delta \bar{\boldsymbol{\kappa}}_{1,F_l,NL}$, $\Delta \bar{\boldsymbol{\kappa}}_{2,F_l,NL}$, and $\Delta \bar{\boldsymbol{\kappa}}_{3,F_l,NL}$ are obtained using Eq. 3.39.

$$\begin{aligned}
\Delta \bar{\boldsymbol{\kappa}}_{1,F_l,NL} &= \frac{1}{\bar{\alpha}^2} \Delta \boldsymbol{K}_{F_l,p_l,0,NL} \big|_{\substack{\alpha_l=\bar{\alpha} \\ \alpha_{l+1}=0}} \\
\Delta \bar{\boldsymbol{\kappa}}_{2,F_l,NL} &= \frac{1}{\bar{\alpha}^2} \Delta \boldsymbol{K}_{F_l,NL} \big|_{\substack{\alpha_l=0 \\ \alpha_{l+1}=\bar{\alpha}}} \\
\Delta \bar{\boldsymbol{\kappa}}_{3,F_l,NL} &= \frac{1}{\bar{\alpha}^2} \begin{pmatrix} \Delta \boldsymbol{K}_{F_l,NL} \big|_{\substack{\alpha_l=\bar{\alpha} \\ \alpha_{l+1}=\bar{\alpha}}} \\ -\Delta \bar{\boldsymbol{\kappa}}_{1,F_l,NL} \bar{\alpha}^2 - \Delta \bar{\boldsymbol{\kappa}}_{2,F_l,NL} \bar{\alpha}^2 \end{pmatrix}
\end{aligned} \tag{3.41}$$

Knowing $\Delta \bar{\boldsymbol{\kappa}}_{1,F_l,NL}$, $\Delta \bar{\boldsymbol{\kappa}}_{2,F_l,NL}$, and $\Delta \bar{\boldsymbol{\kappa}}_{3,F_l,NL}$ in Eq. 3.39, $\Delta \boldsymbol{K}_{F_l,NL}$ can be obtained

for given α_l and α_{l+1} without using full-order model.

$\Delta \boldsymbol{K}^R_{F,NL}$ in Eq. 3.13 capturing the nonlinear behavior of foams can be obtained by projecting and summing up the nonlinear part of stiffness matrices for all foams for given α_i.

$$\begin{aligned}
\Delta \boldsymbol{K}^R_{F,NL} &= \sum_{l=1}^{N_f} (\boldsymbol{T}^R_{F_l})^T \Delta \boldsymbol{K}_{F_l,NL} \boldsymbol{T}^R_{F_l} \\
&= \sum_{l=1}^{N_f} (\boldsymbol{T}^R_{F_l})^T \begin{pmatrix} \Delta \boldsymbol{\kappa}_{1,F_l,NL} \alpha_l^2 \\ +\Delta \boldsymbol{\kappa}_{2,F_l,NL} \alpha_{l+1}^2 \\ +\Delta \boldsymbol{\kappa}_{3,F_l,NL} \alpha_l \alpha_{l+1} \end{pmatrix} \boldsymbol{T}^R_{F_l} \\
&= \sum_{l=1}^{N_f} \begin{pmatrix} \Delta \boldsymbol{\kappa}^R_{1,F_l,NL} \alpha_l^2 \\ +\Delta \boldsymbol{\kappa}^R_{2,F_l,NL} \alpha_{l+1}^2 \\ +\Delta \boldsymbol{\kappa}^R_{3,F_l,NL} \alpha_l \alpha_{l+1} \end{pmatrix}
\end{aligned} \tag{3.42}$$

where N_f is the number of foams.

3.2.4.3 Equivalent Nonlinear Stiffness Matrix for Cells

In Eq. 3.5, assume that the force $\boldsymbol{f}$ is a single harmonic excitation with amplitude $\boldsymbol{F}$ and frequency ω, and the vibration response $\boldsymbol{x}_{C_i}$ at DOFs of cell i has only a single harmonic term with amplitude $\boldsymbol{X}_{C_i}$,

$$\begin{aligned}
\boldsymbol{f} &= \boldsymbol{F} \sin \omega t \\
\boldsymbol{x}_{C_i} &= \boldsymbol{X}_{C_i} \sin \omega t
\end{aligned} \tag{3.43}$$

Consequently, the modal amplitude in Eq. 3.29 is a single harmonic term and can be represented as

$$\boldsymbol{x}_{C_i} \approx \boldsymbol{\phi}^N_{C_i} \alpha_i = \boldsymbol{\phi}^N_{C_i} A_i \sin \omega t \tag{3.44}$$

where

$$\alpha_i = A_i \sin \omega t \tag{3.45}$$

A_i is the amplitude of α_i. Substitute Eq. 3.32, $\boldsymbol{x}_{C_i}$ in Eq. 3.43, and α_i in Eq. 3.45 into the nonlinear part of stiffness matrix at DOFs of cell i in Eq. 3.5.

$$\begin{aligned}
&\Delta \boldsymbol{K}_{C_i,NL} \boldsymbol{x}_{C_i} \\
&= \Delta \bar{\boldsymbol{\kappa}}_{C_i,NL} \alpha_i^2 \boldsymbol{x}_{C_i} \\
&= \Delta \bar{\boldsymbol{\kappa}}_{C_i,NL} A_i^2 \sin^2 \omega t \boldsymbol{X}_{C_i} \sin \omega t \\
&= \Delta \bar{\boldsymbol{\kappa}}_{C_i,NL} A_i^2 \boldsymbol{X}_{C_i} \sin^3 \omega t
\end{aligned} \tag{3.46}$$

Expand $\sin^3 \omega t$ and neglect the higher frequency term $\sin(3\omega t)$), one can obtain

$$\begin{aligned}
&\Delta \boldsymbol{K}_{C_i,NL} \boldsymbol{x}_{C_i} \\
&= \Delta \bar{\boldsymbol{\kappa}}_{C_i,NL} A_i^2 \boldsymbol{X}_{C_i} \begin{pmatrix} \frac{3}{4} \sin \omega t \\ +\frac{1}{4} \sin(3\omega t) \end{pmatrix} \\
&\approx \Delta \bar{\boldsymbol{\kappa}}_{C_i,NL} A_i^2 \boldsymbol{X}_{C_i} \left(\frac{3}{4} \sin \omega t \right) \\
&= \frac{3}{4} \Delta \bar{\boldsymbol{\kappa}}_{C_i,NL} A_i^2 \boldsymbol{X}_{C_i} \sin \omega t \\
&= \frac{3}{4} \Delta \bar{\boldsymbol{\kappa}}_{C_i,NL} A_i^2 \boldsymbol{x}_{C_i}
\end{aligned} \tag{3.47}$$

The equivalent stiffness matrix $\Delta \boldsymbol{K}_{Eq,C_i,NL}$ of cell i can be defined as

$$\Delta \boldsymbol{K}_{Eq,C_i,NL} \equiv \frac{3}{4} \Delta \bar{\boldsymbol{\kappa}}_{C_i,NL} A_i^2 \tag{3.48}$$

Substitute Eq. 3.48 into Eq. 3.34.

$$\begin{aligned}\Delta \boldsymbol{K}^R_{Eq,C,NL} &\equiv \sum_{i=1}^{N_c} (\boldsymbol{T}^R_{C_i})^T \Delta \boldsymbol{K}_{Eq,C_i,NL} \boldsymbol{T}^R_{C_i} \\ &= \sum_{i=1}^{N_c} (\boldsymbol{T}^R_{C_i})^T \frac{3}{4} \Delta \bar{\boldsymbol{\kappa}}_{C_i,NL} A_i^2 \boldsymbol{T}^R_{C_i} \\ &= \frac{3}{4} \sum_{i=1}^{N_c} \Delta \bar{\boldsymbol{\kappa}}^R_{C_i,NL} A_i^2\end{aligned} \tag{3.49}$$

In Eq. 3.34, α_i and $\Delta \boldsymbol{K}^R_{C,,NL}$ are functions of time t. In contrast, in Eq. 3.49, A_i and $\Delta \boldsymbol{K}^R_{Eq,C,,NL}$ are independent of time t but with an coefficient $\frac{3}{4}$. By using the equivalent stiffness strategy, the nonlinear part of stiffness matrix of cells in the system equations Eq. 3.12 can be constructed using time-independent stiffness matrix $\Delta \boldsymbol{K}^R_{Eq,C,NL}$.

3.2.4.4 Equivalent Nonlinear Stiffness Matrix for Foams

Similar to the derivation of the equivalent nonlinear stiffness matrix for cells, Eq. 3.36 can be rewritten as

$$\boldsymbol{x}_{F_l} = \boldsymbol{X}_{F_l} \sin \omega t \tag{3.50}$$

where

$$\begin{aligned}\alpha_l &= A_l \sin \omega t \\ \alpha_{l+1} &= A_{l+1} \sin \omega t\end{aligned} \tag{3.51}$$

Substitute Eq. 3.39, Eq. 3.50, and Eq. 3.51 into the nonlinear part of stiffness matrix at DOFs of foam l in Eq. 3.5. The equivalent stiffness matrix $\Delta \boldsymbol{K}_{Eq,F_l,NL}$ of foam l can be defined as

$$\Delta \boldsymbol{K}_{Eq,F_l,NL} \boldsymbol{x}_{F_l} \equiv \frac{3}{4} \begin{pmatrix} \Delta \bar{\boldsymbol{\kappa}}_{1,F_l,NL} A_l^2 \\ +\Delta \bar{\boldsymbol{\kappa}}_{2,F_l,NL} A_{l+1}^2 \\ +\Delta \bar{\boldsymbol{\kappa}}_{3,F_l,NL} A_l A_{l+1} \end{pmatrix} \boldsymbol{x}_{F_l}. \tag{3.52}$$

Substitute Eq. 3.52 into Eq. 3.42.

$$\begin{aligned}\Delta \boldsymbol{K}^R_{Eq,F,NL} &= \sum_{l=1}^{N_f} (\boldsymbol{T}^R_{F_l})^T \Delta \boldsymbol{K}_{Eq,F_l,NL} \boldsymbol{T}^R_{F_l} \\ &= \sum_{l=1}^{N_f} (\boldsymbol{T}^R_{F_l})^T \frac{3}{4} \begin{pmatrix} \Delta \bar{\boldsymbol{\kappa}}_{1,F_l,NL} A_l^2 \\ +\Delta \bar{\boldsymbol{\kappa}}_{2,F_l,NL} A_{l+1}^2 \\ +\Delta \bar{\boldsymbol{\kappa}}_{3,F_l,NL} A_l A_{l+1} \end{pmatrix} \boldsymbol{T}^R_{F_l} \\ &= \frac{3}{4} \sum_{l=1}^{N_f} \begin{pmatrix} \Delta \bar{\boldsymbol{\kappa}}^R_{1,F_l,NL} A_l^2 \\ +\Delta \bar{\boldsymbol{\kappa}}^R_{2,F_l,NL} A_{l+1}^2 \\ +\Delta \bar{\boldsymbol{\kappa}}^R_{3,F_l,NL} A_l A_{l+1} \end{pmatrix}\end{aligned} \tag{3.53}$$

Note that $\Delta \boldsymbol{K}^R_{Eq,F,NL}$ is independent of time t.

3.2.5 Construction of PROMs

There are two parts of PROMs, the linear and nonlinear parts. To construct PROMs, both parts need finite element analyses. However, once PROMs are built, there is no need to conduct full-order model again to predict vibration responses.

To construct the linear PROMs, eight different cases of structural variation are employed to the battery pack FEM, and the corresponding stiffness matrices and

modes are calculated.

$$
\begin{aligned}
&p = p_l,\ \boldsymbol{s} = \mathbf{0},\ \text{regular foams} && \rightarrow \boldsymbol{K}_{p_l,\mathbf{0},LI},\ \boldsymbol{\phi}_{p_l,\mathbf{0}} \\
&p = p_u,\ \boldsymbol{s} = \mathbf{0},\ \text{regular foams} && \rightarrow \boldsymbol{K}_{p_u,\mathbf{0},LI},\ \boldsymbol{\phi}_{p_u,\mathbf{0}} \\
&p = p_l,\ \boldsymbol{s} = \boldsymbol{s}_l,\ \text{regular foams} && \rightarrow \boldsymbol{K}_{p_l,\boldsymbol{s}_l,LI} \\
&p = p_u,\ \boldsymbol{s} = \boldsymbol{s}_l,\ \text{regular foams} && \rightarrow \boldsymbol{K}_{p_u,\boldsymbol{s}_l,LI} \\
&p = p_l,\ \boldsymbol{s} = \boldsymbol{s}_u,\ \text{regular foams} && \rightarrow \boldsymbol{K}_{p_l,\boldsymbol{s}_u,LI} \\
&p = p_u,\ \boldsymbol{s} = \boldsymbol{s}_u,\ \text{regular foams} && \rightarrow \boldsymbol{K}_{p_u,\boldsymbol{s}_u,LI} \\
&p = p_l,\ \boldsymbol{s} = \mathbf{0},\ 10\%\ \text{stiffer foams} && \rightarrow \boldsymbol{K}_{F10\%,p_l,\mathbf{0},LI} \\
&p = p_l,\ \boldsymbol{s} = \mathbf{0},\ 10\%\ \text{stiffer foams} && \rightarrow \boldsymbol{K}_{F10\%,p_u,\mathbf{0},LI}
\end{aligned}
\tag{3.54}
$$

Next, the transformation matrix $\boldsymbol{T}^R$ is constructed using Eq. 3.10 and Eq. 3.11. The stiffness matrices in Eq. 3.54 are then projected using $\boldsymbol{T}^R$.

The stiffness matrix $\boldsymbol{K}^R_{p,\boldsymbol{s},LI}$ and the damping matrix $\boldsymbol{C}^R_{p,\boldsymbol{s},LI}$ at a given PreV level p and C2CV level $\boldsymbol{s}$ can be obtained by linear interpolation in Eq. 3.16, Eq. 3.18, Eq. 3.19, and Eq. 3.21. Finally, the linear structural dynamic equations Eq. 3.23 are constructed.

To construct the nonlinear PROMs for cell i, the displacement along the plate-like mode with modal amplitude $\bar{\alpha}$ is employed on the single cell FEM, and the corresponding $\Delta\bar{\boldsymbol{\kappa}}_{C_i,NL}$ is calculated using Eq. 3.33. Similarly, to construct the nonlinear PROMs for foam l, the displacement along the plate-like modes is employed on the two neighboring cells og foam l, and the corresponding $\Delta\bar{\boldsymbol{\kappa}}_{1,F_l,NL}$, $\Delta\bar{\boldsymbol{\kappa}}_{2,F_l,NL}$, and $\Delta\bar{\boldsymbol{\kappa}}_{3,F_l,NL}$ are calculated using Eq. 3.41. The stiffness matrix $\boldsymbol{K}^R$ and damping matrices $\boldsymbol{C}^R$ are built using Eq. 3.13 and the nonlinear structural dynamic equations Eq. 3.12 can be constructed and solved.

3.2.6 Iterative Method

The steady state vibration responses can be solved using the reduced-order structural dynamic equations Eq. 3.12. Time marching approaches, such as ODE45 in Matlab, can be used to solve the nonlinear structural dynamic equations but are computationally expensive. To improve the computational efficiency, the following iterative method has been developed.

To initiate the iterative method, the linear vibration response is solved using of the linear structural dynamic equations Eq. 3.23. Assume that the excitation $\boldsymbol{f}^R$ and vibration response $\boldsymbol{q}_{LI}$ in the reduced-order coordinate are single harmonic terms.

$$\begin{aligned} \boldsymbol{f}^R &= \boldsymbol{F}^R \sin(\omega t) \\ \boldsymbol{q}_{LI} &= \boldsymbol{Q}_{LI} \sin(\omega t) \end{aligned} \tag{3.55}$$

where $\boldsymbol{F}^R$ is the amplitude of $\boldsymbol{f}^R$, and $\boldsymbol{Q}_{LI}$ is the amplitude of $\boldsymbol{q}_{LI}$ and is a vector of complex numbers. The amplitude of vibration response $\boldsymbol{Q}_{LI}$ can be solved by

$$\boldsymbol{Q}_{LI} = \left(\boldsymbol{K}^R_{p,\boldsymbol{s},LI} - \omega^2 \boldsymbol{M}^R + j\boldsymbol{C}^R_{p,\boldsymbol{s},LI}\right)^{-1} \boldsymbol{F}^R \tag{3.56}$$

Denote $\boldsymbol{Q}_r$ as the solution solved in each iteration in the iterative method where the subscript r represents the iteration counts. $\boldsymbol{Q}_{LI}$ is used as the initial guess for the solution of the nonlinear structural dynamic equations.

For each iteration, the current solution $\boldsymbol{Q}_r$ is employed to update α_i for all cells using Eq. 3.29.

$$\alpha_i = \boldsymbol{\rho}_i \boldsymbol{Q}_r \tag{3.57}$$

Since α_i is a complex number, the amplitude A_i can be obtained by

$$A_i = \sqrt{\alpha_i^H \alpha_i}. \tag{3.58}$$

Knowing A_i, the equivalent stiffness matrix $\Delta \boldsymbol{K}^R_{Eq,C,NL}$ capturing the nonlinear dynamic behavior in cells can be updated using Eq. 3.49. For the system with nonlinear foams, the equivalent stiffness matrix $\Delta \boldsymbol{K}^R_{Eq,F,NL}$ capturing the nonlinear dynamic behavior in foams can be updated using Eq. 3.53. Next, the overall stiffness matrix $\boldsymbol{K}^R$ and damping matrix $\boldsymbol{C}^R$ are updated using Eq. 3.13. The updated solution $\boldsymbol{Q}_{r+1}$ can be solved using Eq. 3.12.

$$\boldsymbol{Q}_{r+1} = \left(\boldsymbol{K}^R - \omega^2 \boldsymbol{M}^R + j\boldsymbol{C}^R\right)^{-1} \boldsymbol{F}^R \tag{3.59}$$

As the iteration proceeds, the new solution $\boldsymbol{Q}_{r+1}$ and old solution $\boldsymbol{Q}_r$ are compared.

$$\sigma_r = \frac{\|\boldsymbol{Q}_{r+1} - \boldsymbol{Q}_r\|}{\|\boldsymbol{Q}_r\|} \tag{3.60}$$

The ratio σ_r decreases at each iteration and the solution $\boldsymbol{Q}_r$ gradually converges to the true vibration response. The iteration stops when σ_r meet the criteria σ_{max}.

$$\sigma_r \leq \sigma_{max} \tag{3.61}$$

The choice of σ_{max} is critical. If σ_{max} is too low, the iterative method takes many iterations to converge. If σ_{max} is too high, the solution $\boldsymbol{Q}_r$ may not converge to the true solution.

3.3 Validation

To demonstrate the proposed approaches, the academic battery pack model described in Fig. 3.1 is used. The FEM of the academic battery pack has about 180,000 DOFs. In contrast, PROMs have only 36 DOFs. In Eq. 3.6, the lower and upper bounds of PreV level are $p_l = 0\%$ and $p_u = 6\%$. Also, the lower and upper bounds of C2CV level are $s_{il} = -10\%$ and $s_{iu} = 10\%$. The number of cells is $N_c = 20$, and the

number of foams is $N_f = 19$. To solve the nonlinear structural dynamic equations, the convergence criteria is chosen to be $\sigma_{max} = 0.1\%$.

3.3.1 Linear Validation

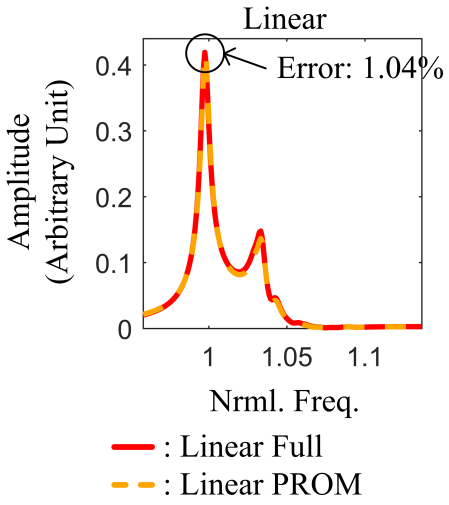

Figure 3.10: The linear validation results for system with prestress variation and cell-to-cell variations. The results calculated using full-order model and PROMs are compared.

To validate PROMs with linear structural variations, the PreV level is chosen to be at $p = 3\%$, which is at the middle of its lower and upper bounds. The C2CV level is randomly generated from -10% to 10% with normal distribution and zero mean as shown in Fig 3.3. Fig. 3.10 shows the linear vibration responses calculated using PROMs (orange dashed line) and full-order model (red solid line). The amplitude of the vibration response at the central node of cell 10 is measured. Fig. 3.10 shows that the vibration response predicted by PROMs follows the response predicted by the full-order model very well. The error of the peak value is only about 1%. However, the computational time is very different . Tab. 3.1 shows the average computational time for the full-order model and PROMs to predict the vibration response at a frequency.

The average computational gain of linear case is 1,674 and can increase if the mesh of FEM becomes finer. It is because the computational time of the full-order model

Table 3.1: Average computational time of linear system

	Full	PROMs
Linear	385(s)	0.23(s)

increases with the mesh density. However, the computational time of PROMs depends on the number of modes selected, which is related to the physics of the system. If physics of the system remains the same but the mesh become finer, the number of modes selected is still the same. Thus, the computational time for PROMs remains similar, but the time for the full-order model is expected to be increased. Therefore, the computational gain increases.

3.3.2 Nonlinear Validation

To validate PROMs with both linear and nonlinear structural variations simultaneously, the same linear structural variations as in the linear validation are employed, and 3 different cases of nonlinear structural variations are discussed. Similar to the linear validation, the amplitude of the vibration response at the central node of cell 10 is measured. Fig. 3.11 shows nonlinear vibration responses calculated using PROMs (blue dashed line) and full-order model (green dotted line), and the linear vibration response (red sold line). Fig. 3.11(a) shows the vibration response of system with nonlinear cells. Fig. 3.11(b) shows the vibration response of system with nonlinear foams. And Fig. 3.11(c) shows the vibration response of system with both nonlinear cells and foams simultaneously. The errors between PROMs prediction and the full-order model results at the peak of the vibration results are less than 1%. The average computational time shown in Tab. 3.2 are very different between full-order model and PROMs.

Table 3.2: Average computational time of nonlinear system

	Full	PROMs
Nonlinear	3240(s)	2.33(s)

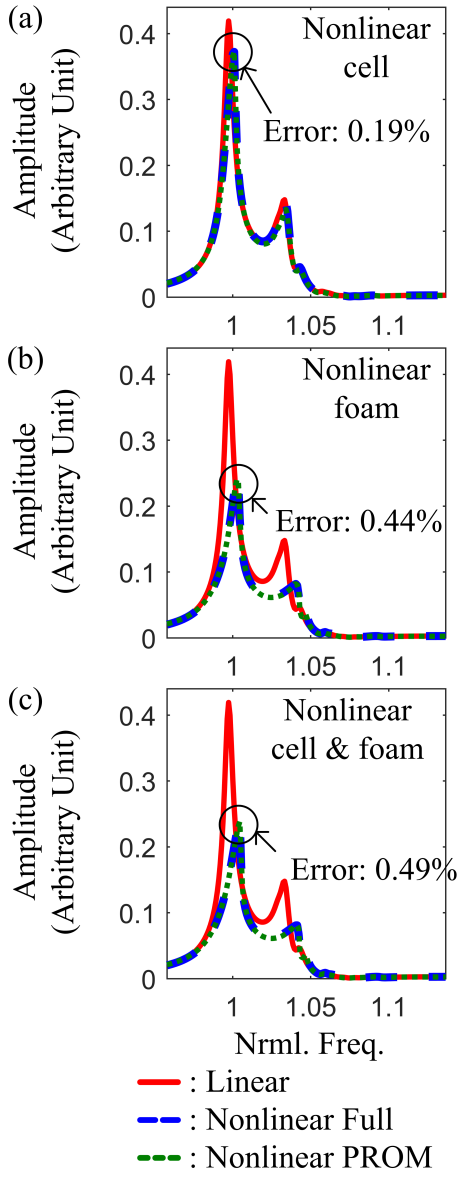

Figure 3.11: The nonlinear validation results for system with (a) nonlinear cells, (b) nonlinear foams, (c) and nonlinear cells and foams.

Fig. 3.11 also shows that the effects of nonlinear cells and foams to the vibration responses are significant. In this example, Fig. 3.11(a) shows that peak value is lowered about 10% for system with nonlinear cells. However, Fig. 3.11(b) shows that peak value is lowered about 50% for system with nonlinear foams. It's a coincidence in this example that the effect of nonlinear foams has greater impact on the vibration response than nonlinear cells. There are many factors affect the amplification factor of

the peak value of vibration responses for the nonlinear system. First, the amplification factor is different cell-by-cell. Also, different C2CV cases show different amplification factors. Moreover, the effect of nonlinearity are affected by the nonlinear coefficient ξ_{el} described in Eq. 3.3.

3.4 Statistical Analysis

The battery pack is comprised of stacking cells and exhibits high modal density. When the excitation frequency is in a high modal density region, small structural variations in cells can amplify the vibration response in some cells. Because the intense vibration response in a single cell may lead to the failure of the whole battery pack, the maximum vibration response for any cell in a battery pack is a key reliability metric.

Because C2CV level is random, statistical analyses are needed and Monte Carlo simulations are performed with 1,000 C2CV cases. The same single harmonic force is employed at the academic battery pack FEM. For each C2CV case, the vibration responses at the central node of each cell are collected, and the corresponding maximum vibration response χ_i of cell i over the range of excitation frequency is calculated for each cell. The circled peak values in Fig. 3.10 and Fig. 3.11 show examples of the maximum vibration response of cell 10. Next, the average and standard deviation of χ_i over 1,000 C2CV cases are calculated.

Fig. 3.12 illustrates the Monte Carlo simulation results. Fig. 3.12(a) shows the results of linear system and Fig. 3.12(b) shows the results of system with nonlinear cells and foams simultaneously. The values of χ_i for each random C2CV case is marked as cyan asterisk. The red circles represent the average χ_i over 1,000 C2CV cases, and the standard deviations plus their average values are labeled. The green vertical bars represent χ_i of the nominal system.

Fig. 3.12 shows that the C2CV lead to the amplification of vibration responses

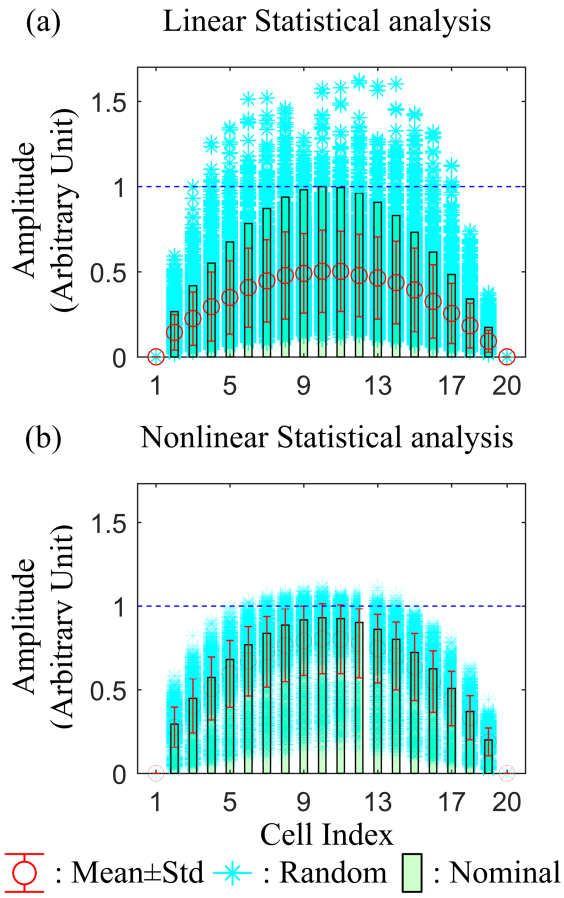

Figure 3.12: The Monte Carlo simulation results of 1,000 random cell-to-cell variation cases. (a) Linear system (b) System with nonlinear cells and foams.

compared to the nominal system. Fig. 3.12(a) shows that the maximum amplification factor at cell 10 is more than 50% compared to the nominal case. Fig. 3.12(b) also shows about 20% maximum amplification factor at cell 10. Therefore, neglecting the effect of C2CV might lead to a serious underprediction of the maximum stress, and thus an overprediction of the battery pack reliability. The overall amplification factors for the nonlinear system are significantly smaller than the one for the linear system in this example. Thus, neglecting the effect of nonlinearity might also lead to incorrect prediction of vibration responses.

With the nonlinearity, the vibration responses are mitigated. Also, the amplification effects of vibration response due to cell-to-cell variations are mitigated as

shown in Fig. 3.12 where the spread range of cyan stars of the nonlinear system are much narrower than the linear system. It is because the stiffness of cells and foams increases with deformation and the deformation is suppressed; thus, the amplification of vibration responses are mitigated.

3.5 Conclusions

The battery packs used in electrified vehicles are comprised of repeated stacking cells. The system with repeated substructures exhibits high modal density, and thus a small structural variation in the system can lead to drastically changes in vibration responses. There are two types of structural variations. The linear structural variations considered here are the PreV and the C2CV, and the nonlinear structural variations come from the nonlinear dynamic behavior in cells and foams.

Because the vibration response of battery packs is an essential metric for the fatigue life and reliability, the statistical analysis is required to investigate the effect of random structural variations. However, typical full-order model can easily have millions of DOFs, and thus statistical analyses is computationally prohibitive. Thus, PROMs are proposed to overcome this difficulty. PROMs can accurately and efficiently predict vibration responses of battery packs with multiple structural variations simultaneously.

PROMs are developed based on the assumptions that (1) the vibration modes of the system with structural variations are the linear combination of modes of the system at two extreme PreV levels, (2) the stiffness matrices of the system with structural variations can be obtained by linear interpolation of stiffness matrices at extreme PreV and C2CV levels, (3) the modulus of elasticity of a nonlinear element is a quadratic function of strain of the element, (4) the vibration response of a cell is dominated by the first plate-like mode of the cell, and (5) foams are much softer than the two neighboring cells.

Once PROMs are built, to predict the vibration response of the battery pack with structural variations, the full-order model can be avoided, and statistical analyses are enabled. The effect of nonlinear dynamic behavior in cells and foams are captured in the nonlinear structural dynamic equations. The nonlinear vibration responses can be efficiently solved using the iterative method. The average simulation time of linear PROMs is 1,674 times faster than the full-order model, and time of nonlinear PROMs is 1,392 times faster. The errors at the peak values of the vibration response are about 1% between PROMs and full-order model. The Monte Carlo analysis shows that the linear and nonlinear responses are amplified due to small C2CV. Also, the effects of nonlinearity should be considered for the prediction of vibration responses.

CHAPTER IV

Optimization of arrangement of spacers using parametric reduced-order models

In this chapter, different types of spacers are considered as S2SV and are captured by PROMs. Adjusting the arrangement of different types of spacers in the battery pack changes the mechanical coupling between cells and hence may mitigate vibration responses. The optimized arrangement of different types of spacers is found using a genetic algorithm, and the vibration response is lowered. In Sec. 4.1, the academic battery pack model is introduced. In Sec. 4.2, formulation of PROMs for modeling structural variations including PreV, C2CV, and S2SV are described. In Sec. 4.3, numerical results calculated from the dynamic simulation of PROMs and full-order models are compared. The effects of S2SV are discussed using statistical analyses. In Sec. 4.4, the optimization of the arrangement of spacers is performed, and the results are shown. Finally, the conclusions of this study are presented in Sec. 4.5.

4.1 Academic Battery Pack FEM

The academic battery pack FEM, which constitutes 20 nominally identical cells and 19 nominally identical spacers, in Fig. 4.1(a) is proposed to demonstrate the idea of PROMs. Each cell has several components including positive and negative current

collectors, a cathode, an anode, a separator, and a case as shown in Fig. 4.1(c). The cells couple to each other through spacers and foams. The stiffness of spacers is assumed to be much higher than cells, while the stiffness of foams is assumed to be much lower than cells. The academic battery pack is constrained at both ends of the pack as shown in Fig. 4.1(b). The excitation is a single harmonic force and is employed along the y-direction at two sides and bottom of the battery pack.

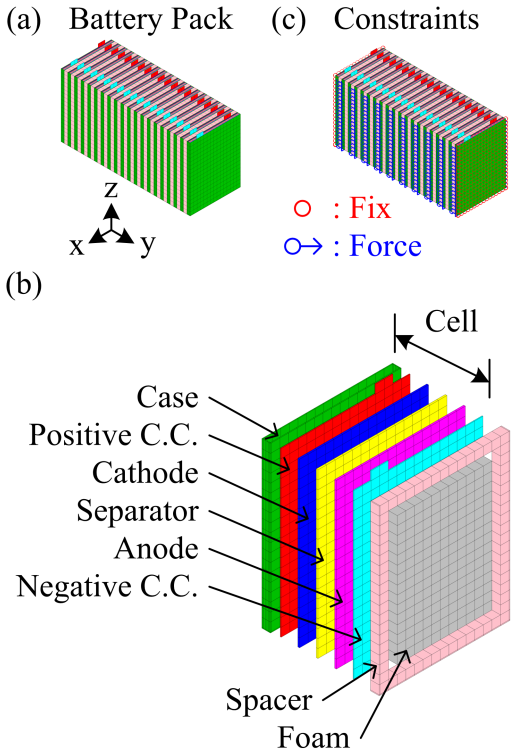

Figure 4.1: (a) The academic battery FEM which constitutes 20 nominally identical cells and 19 nominally identical spacers. (b) Constraint and forcing nodes. (c) A cell is comprised of positive and negative current collectors, a cathode, an anode, a separator, and a case. Cells couples to each other through spacers and foams.

Fig. 4.2 shows the natural frequency plot which exhibits high modal density regions due to repeated substructures in the academic battery pack. The frequency of the excitation force lies in the range of the first high modal density region as shown in the red rectangular in Fig. 4.2. Small structural variations employed at such system lead to significant vibration response change[26, 72].

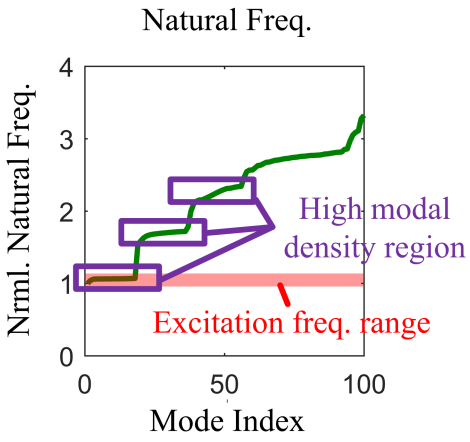

Figure 4.2: The academic battery pack shows high modal density regions due to repeated substructures.

The modulus of elasticity of elements of a cell is considered to be affected by the prestress applied to the battery pack and the C2CV level of the cell. Because a cell is sandwiched between two spacers as shown in Fig. 4.3. Because spacers are much harder than cells, the strain distribution of a cell highly depends on the S2SV levels of two adjacent spacers (e.g. the modulus of elasticity of cell i depends on S2SV levels of spacer i and $i-1$). In contrast, the effect from foams to cells is negligible because foams are much softer than cells. This is the key to constructing PROMs with PreV, C2CV, and S2SV simultaneously. Note that the modulus of elasticity of elements of a spacer is assumed to only depend on its S2SV level and PreV level, and independent of the C2CV levels of the adjacent cells because cells are much softer than spacers. For this research, only two types of spacers, type 1 and type 2, with different modulus of elasticity are considered.

4.2 Methodology

4.2.1 Structural Dynamic Equations

The battery pack is subjected to structural variations. The PreV level p varies between a lower bound p_l and an upper bound p_u. The C2CV level s_i of cell i varies

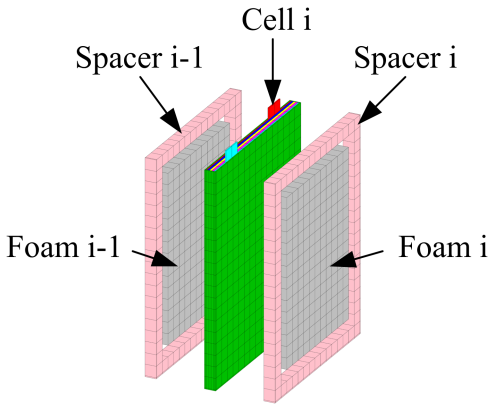

Figure 4.3: The modulus of elasticity of elements of cell i is affected by S2SVs of spacer i and $i-1$.

between a lower bound s_{il} and an upper bound s_{iu}. Since there are only two types of spacers, the S2SV level z_i of spacer i is either z_{il} or z_{iu}. The vectors $\boldsymbol{s}_l$ and $\boldsymbol{s}_u$ represent the collection of the lower and upper bounds of C2CV levels for all cells. The vector $\boldsymbol{s}$ represents the collection of the C2CV levels for all cells. The vectors $\boldsymbol{z}_l$ and $\boldsymbol{z}_u$ represent the collection of the two types of S2SV levels for spacers. The vector $\boldsymbol{z}$ represents the collection of the S2SV levels for all spacers. The nominal case is defined as $p = p_l$, $\boldsymbol{s} = \boldsymbol{0}$, and $\boldsymbol{z} = \boldsymbol{z}_l$.

$$
\begin{aligned}
& p \in \begin{bmatrix} p_l & p_u \end{bmatrix}, \; p_l \leq p_u \\
& s \in \begin{bmatrix} s_{il} & s_{iu} \end{bmatrix}, \; s_{il} \leq 0 \leq s_{iu} \\
& z = z_{il} \quad \text{or} \quad z_{iu} \;, \; z_{il} \leq z_{iu} \\
& \boldsymbol{s}_l = \begin{bmatrix} s_{1l} \\ \vdots \\ s_{N_c l} \end{bmatrix}, \; \boldsymbol{s}_u = \begin{bmatrix} s_{1u} \\ \vdots \\ s_{N_c u} \end{bmatrix}, \; \boldsymbol{s} = \begin{bmatrix} s_1 \\ \vdots \\ s_{N_c} \end{bmatrix} \\
& \boldsymbol{z}_l = \begin{bmatrix} z_{1l} \\ \vdots \\ z_{N_s l} \end{bmatrix}, \; \boldsymbol{z}_u = \begin{bmatrix} z_{1u} \\ \vdots \\ z_{N_s u} \end{bmatrix}, \; \boldsymbol{z} = \begin{bmatrix} z_1 \\ \vdots \\ z_{N_s} \end{bmatrix},
\end{aligned}
\tag{4.1}
$$

where N_c is the number of cells and N_s is the number of spacers.

The structural dynamic equations of the battery pack can be represented as

$$\boldsymbol{M}\ddot{\boldsymbol{x}} + \boldsymbol{C}_{p,\boldsymbol{s},\boldsymbol{z}}\dot{\boldsymbol{x}} + \boldsymbol{K}_{p,\boldsymbol{s},\boldsymbol{z}}\dot{\boldsymbol{x}} = \boldsymbol{f} \tag{4.2}$$

where $\boldsymbol{M}$ is mass matrix, $\boldsymbol{C}_{p,\boldsymbol{s},\boldsymbol{z}}$ and $\boldsymbol{K}_{p,\boldsymbol{s},\boldsymbol{z}}$ are damping and stiffness matrices at PreV level p, C2CV level $\boldsymbol{s}$ and S2SV level $\boldsymbol{z}$, $\boldsymbol{f}$ is external excitation force vector, and $\boldsymbol{x}$ is displacement vector.

The damping matrix $\boldsymbol{C}$ is assumed to be proportional to the stiffness matrix. The proportional damping coefficients of all components are equal except foams, which are assumed to have a higher damping coefficient. β_f denotes the damping coefficient of foams, and β_g denotes the damping coefficient of all other components. $\boldsymbol{C}$ can be represented as

$$\begin{aligned}\boldsymbol{C}_{p,\boldsymbol{s},\boldsymbol{z}} =& \beta_g \boldsymbol{K}_{p,\boldsymbol{s},\boldsymbol{z}} + (\beta_f - \beta_g)\frac{\boldsymbol{K}_{F10\%,p,\boldsymbol{s},\boldsymbol{z}} - \boldsymbol{K}_{p,\boldsymbol{s},\boldsymbol{z}}}{10\%} \\ \approx& \beta_g \boldsymbol{K}_{p,\boldsymbol{s},\boldsymbol{z}} + (\beta_f - \beta_g)\frac{\boldsymbol{K}_{F10\%,p,\boldsymbol{0},\boldsymbol{z}_l} - \boldsymbol{K}_{p,\boldsymbol{0},\boldsymbol{z}_l}}{10\%}\end{aligned} \tag{4.3}$$

where $\boldsymbol{K}_{F10\%,p,\boldsymbol{s},\boldsymbol{z}}$ is the stiffness matrix for the system with all foams having stiffness 10% higher than the nominal design of foams at PreV level p, C2CV level $\boldsymbol{s}$ and S2SV $\boldsymbol{z}$. The purpose of the term $(\beta_f - \beta_g)\frac{\boldsymbol{K}_{F10\%,p,\boldsymbol{s},\boldsymbol{z}} - \boldsymbol{K}_{p,\boldsymbol{s},\boldsymbol{z}}}{10\%}$ is to replace the contribution of foams in $\beta_g \boldsymbol{K}_{p,\boldsymbol{s},\boldsymbol{z}}$ from β_g to β_f. Since C2CV and the 10% stiffness change of foam are both small , and foams are much softer than other components in the battery pack, $\boldsymbol{K}_{F10\%,p,\boldsymbol{s},\boldsymbol{z}} - \boldsymbol{K}_{p,\boldsymbol{s},\boldsymbol{z}}$ is approximated to be $\boldsymbol{K}_{F10\%,p,\boldsymbol{0},\boldsymbol{z}_l} - \boldsymbol{K}_{p,\boldsymbol{0},\boldsymbol{z}_l}$ in Eq. 4.3.

The structural dynamic equations of battery packs can have tens of thousands of DOFs, depending on the complexity and mesh density of FEM. To reduce the order of structural dynamic equations, several reduction techniques are employed.

4.2.2 Order Reduction

The transformation matrix $\boldsymbol{T}^R$ is constructed to reduce the order of structural dynamic equations. The first assumption is that vibration responses at PreV level p, C2CV level $\boldsymbol{s}$, and S2SV level $\boldsymbol{z}$ can be captured by the truncated modes $\boldsymbol{\phi}_{p,\boldsymbol{s},\boldsymbol{z}}$ whose natural frequencies are close to the frequency range of interest. The second assumption is that the truncated modes $\boldsymbol{\phi}_{p,\boldsymbol{s},\boldsymbol{z}}$ are linear combinations of four sets of truncated modes at different extreme PreV, C2CV, and S2SV levels

$$span(\boldsymbol{\phi}_{p,\boldsymbol{s},\boldsymbol{z}}) = span(\begin{bmatrix} \boldsymbol{\phi}_{p_l,\boldsymbol{0},\boldsymbol{z}_l} & \boldsymbol{\phi}_{p_u,\boldsymbol{0},\boldsymbol{z}_l} & \boldsymbol{\phi}_{p_l,\boldsymbol{0},\boldsymbol{z}_u} & \boldsymbol{\phi}_{p_u,\boldsymbol{0},\boldsymbol{z}_u} \end{bmatrix}). \tag{4.4}$$

The assumption in Eq. 4.4 is valid when the frequency range of interest is in a high modal density region and structural variations are small. The general transformation matrix $\boldsymbol{T}_G^R$ is defined as

$$\boldsymbol{T}_G^R = \begin{bmatrix} \boldsymbol{\phi}_{p_l,\boldsymbol{0},\boldsymbol{z}_l} & \boldsymbol{\phi}_{p_u,\boldsymbol{0},\boldsymbol{z}_l} & \boldsymbol{\phi}_{p_l,\boldsymbol{0},\boldsymbol{z}_u} & \boldsymbol{\phi}_{p_u,\boldsymbol{0},\boldsymbol{z}_u} \end{bmatrix}. \tag{4.5}$$

Because the structural variations are small, the modes $\boldsymbol{\phi}_{p_l,\boldsymbol{0},\boldsymbol{z}_l}$, $\boldsymbol{\phi}_{p_u,\boldsymbol{0},\boldsymbol{z}_l}$, $\boldsymbol{\phi}_{p_u.\boldsymbol{0},\boldsymbol{z}_u}$, and $\boldsymbol{\phi}_{p_u,\boldsymbol{0},\boldsymbol{z}_u}$ can have approximately linearly independent columns. Gauss-Jordan elimination (*rref* command in Matlab) is employed to eliminate these columns in $\boldsymbol{T}_G^R$

$$\boldsymbol{T}^R = rref(\boldsymbol{T}_G^R). \tag{4.6}$$

The order of structural dynamic equations is reduced by projection using $\boldsymbol{x} = \boldsymbol{T}^R\boldsymbol{q}$

$$\boldsymbol{M}^R\ddot{\boldsymbol{q}} + \boldsymbol{C}_{p,\boldsymbol{s},\boldsymbol{z}}^R\dot{\boldsymbol{q}} + \boldsymbol{K}_{p,\boldsymbol{s},\boldsymbol{z}}^R\dot{\boldsymbol{q}} = \boldsymbol{f}^R, \tag{4.7}$$

where

$$
\begin{aligned}
\boldsymbol{M}^R &= (\boldsymbol{T}^R)^T \boldsymbol{M} \boldsymbol{T}^R \\
\boldsymbol{C}^R_{p,\boldsymbol{s},\boldsymbol{z}} &= (\boldsymbol{T}^R)^T \boldsymbol{C}_{p,\boldsymbol{s},\boldsymbol{z}} \boldsymbol{T}^R \\
&= (\boldsymbol{T}^R)^T (\beta_g \boldsymbol{K}_{p,\boldsymbol{s},\boldsymbol{z}} + (\beta_f - \beta_g) \frac{\boldsymbol{K}_{F10\%,p,\boldsymbol{0},\boldsymbol{z}_l} - \boldsymbol{K}_{p,\boldsymbol{0},\boldsymbol{z}_l}}{10\%}) \boldsymbol{T}^R \\
&= \beta_g \boldsymbol{K}^R_{p,\boldsymbol{s},\boldsymbol{z}} + (\beta_f - \beta_g) \frac{\boldsymbol{K}^R_{F10\%,p,\boldsymbol{0},\boldsymbol{z}_l} - \boldsymbol{K}^R_{p,\boldsymbol{0},\boldsymbol{z}_l}}{10\%} \\
\boldsymbol{K}^R_{p,\boldsymbol{s},\boldsymbol{z}} &= (\boldsymbol{T}^R)^T \boldsymbol{K}_{p,\boldsymbol{s},\boldsymbol{z}} \boldsymbol{T}^R \\
\boldsymbol{f}^R &= (\boldsymbol{T}^R)^T \boldsymbol{f}
\end{aligned}
\tag{4.8}
$$

4.2.3 Derivation of PROMs

The stiffness matrix $\boldsymbol{K}_{C_i,p,s_i,z_i,z_{i-1}}$ of cell i is a function of four parameters, PreV level p, C2CV level s_i, and S2SV level z_i and z_{i-1} of the adjacent spacers. It only has values at DOFs of cell i of $\boldsymbol{K}_{p,\boldsymbol{s},\boldsymbol{z}}$ and is zeros elsewhere as shown in Fig. 4.4. Similarly, the stiffness matrix $\boldsymbol{K}_{S_i,p,z_i}$ of spacer i is a function of two parameters, PreV level p and S2SV level z_i. It only has values at two off-diagonal blocks at DOFs of the spacer i of $\boldsymbol{K}_{p,\boldsymbol{s},\boldsymbol{z}}$ and is zeros elsewhere as shown in Fig. 4.4.

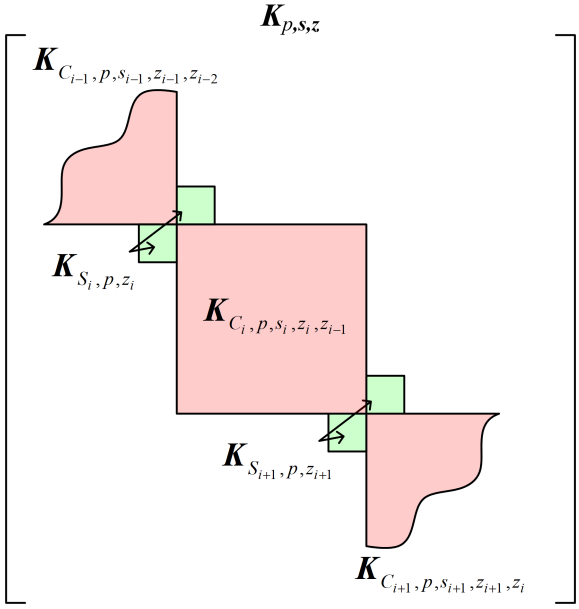

Figure 4.4: Definitions of $\boldsymbol{K}_{C_i}$ and $\boldsymbol{K}_{S_i}$.

The change in stiffness matrix $\Delta \boldsymbol{K}_{C_i,p,s_i,z_i,z_{i-1}}$ of cell i due to C2CV and S2SV levels and the change in stiffness matrix $\Delta \boldsymbol{K}_{S_i,p,z_i}$ of spacer i due to S2SV levels are defined as

$$\begin{aligned} \Delta \boldsymbol{K}_{C_i,p,s_i,z_i,z_{i-1}} &= \boldsymbol{K}_{C_i,p,s_i,z_i,z_{i-1}} - \boldsymbol{K}_{C_i,p,0,z_l} \\ \Delta \boldsymbol{K}_{S_i,p,z_i} &= \boldsymbol{K}_{S_i,p,z_i} - \boldsymbol{K}_{S_i,p,z_l}. \end{aligned} \tag{4.9}$$

The order of $\Delta \boldsymbol{K}_{C_i,p,s_i,z_i,z_{i-1}}$ and $\Delta \boldsymbol{K}_{S_i,p,z_i}$ can be reduced by projection using $\boldsymbol{T}^R$

$$\begin{aligned} \Delta \boldsymbol{K}^R_{C_i,p,s_i,z_i,z_{i-1}} &= (\boldsymbol{T}^R)^T \Delta \boldsymbol{K}_{C_i,p,s_i,z_i,z_{i-1}} \boldsymbol{T}^R \\ \Delta \boldsymbol{K}^R_{S_i,p,z_i} &= (\boldsymbol{T}^R)^T \Delta \boldsymbol{K}_{S_i,p,z_i} \boldsymbol{T}^R. \end{aligned} \tag{4.10}$$

The reduced-order stiffness matrix $\boldsymbol{K}^R_{p,\boldsymbol{s},\boldsymbol{z}}$ of the battery pack in Eq. 4.8 can be represented as the summation of the stiffness matrix considering only PreV $\boldsymbol{K}^R_{p,\boldsymbol{0},\boldsymbol{0}}$, the change in stiffness matrices of cells $\Delta \boldsymbol{K}^R_{C_i,p,s_i,z_i,z_{i-1}}$ due to C2CV and S2SV, and the change in stiffness matrices of spacers $\Delta \boldsymbol{K}^R_{S_i,p,z_i}$ due to S2SV

$$\boldsymbol{K}^R_{p,\boldsymbol{s},\boldsymbol{z}} = \boldsymbol{K}^R_{p,\boldsymbol{0},\boldsymbol{z}_l} + \sum_{i=1}^{N_c} \Delta \boldsymbol{K}^R_{C_i,p,s_i,z_i,z_{i-1}} + \sum_{i=1}^{N_s} \Delta \boldsymbol{K}^R_{S_i,p,z_i}. \tag{4.11}$$

The stiffness matrix $\boldsymbol{K}^R_{p,\boldsymbol{0},\boldsymbol{z}_l}$ in Eq. 4.11 can be expanded by Taylor series with respected to PreV level p.

$$\boldsymbol{K}^R_{p,\boldsymbol{0},\boldsymbol{z}_l} = \boldsymbol{K}^R_{p_l,\boldsymbol{0},\boldsymbol{z}_l} + \frac{\partial \boldsymbol{K}^R_{p_l,\boldsymbol{0},\boldsymbol{z}_l}}{\partial p}(p - p_l) + H.O.T., \tag{4.12}$$

where H.O.T. represents high order terms and are negligible since $p - p_l$ is assumed to be small, and the term $\frac{\partial \boldsymbol{K}^R_{p_l,\boldsymbol{0},\boldsymbol{z}_l}}{\partial p}$ can be obtained using linear interpolation.

$$\boldsymbol{K}^R_{p,\boldsymbol{0},\boldsymbol{z}_l} \approx \boldsymbol{K}^R_{p_l,\boldsymbol{0},\boldsymbol{z}_l} + \frac{\boldsymbol{K}^R_{p_u,\boldsymbol{0},\boldsymbol{z}_l} - \boldsymbol{K}^R_{p_l,\boldsymbol{0},\boldsymbol{z}_l}}{p_u - p_l}(p - p_l), \tag{4.13}$$

where the stiffness matrices $\boldsymbol{K}^R_{p_u,\boldsymbol{0},\boldsymbol{z}_l}$ and $\boldsymbol{K}^R_{p_l,\boldsymbol{0},\boldsymbol{z}_l}$ at the extreme PreV levels p_u and

p_l are obtained using finite element analyses followed by projection using $\boldsymbol{T}^R$.

$$\begin{aligned} \boldsymbol{K}^R_{p_u,\mathbf{0},\boldsymbol{z}_l} &= (\boldsymbol{T}^R)^T \boldsymbol{K}_{p_u,\mathbf{0},\boldsymbol{z}_l} \boldsymbol{T}^R \\ \boldsymbol{K}^R_{p_l,\mathbf{0},\boldsymbol{z}_l} &= (\boldsymbol{T}^R)^T \boldsymbol{K}_{p_l,\mathbf{0},\boldsymbol{z}_l} \boldsymbol{T}^R \end{aligned} \tag{4.14}$$

Following similar strategy, $\Delta\boldsymbol{K}^R_{C_i,p,s_i,z_i,z_{i-1}}$ in Eq. 4.11, which is a function of four parameters with small variations, can be obtained using quadra-linear interpolation. $\Delta\boldsymbol{K}^R_{C_i,p,s_i,z_i,z_{i-1}}$ can be represented using a quadra-linear function.

$$\Delta\boldsymbol{K}^R_{C_i,p,s_i,z_i,z_{i-1}} \approx \begin{bmatrix} 1 & p & s_i & \dots & s_i z_i z_{i-1} & p s_i z_i z_{i-1} \end{bmatrix} \begin{bmatrix} \mathbb{K}^R_{C_i,1} \\ \mathbb{K}^R_{C_i,2} \\ \vdots \\ \mathbb{K}^R_{C_i,15} \\ \mathbb{K}^R_{C_i,16} \end{bmatrix}, \tag{4.15}$$

where $\mathbb{K}^R_{C_i,j}$ for $j = 1\ 16$, which are unknown coefficient matrices, can be solved by plugging in 16 different sets of parameters (p, s_i, z_i, z_{i-1}), where the value of each parameter is either its lower and upper bound, to Eq. 4.15.

$$\begin{bmatrix} \mathbb{K}^R_{C_i,1} \\ \mathbb{K}^R_{C_i,2} \\ \vdots \\ \mathbb{K}^R_{C_i,15} \\ \mathbb{K}^R_{C_i,16} \end{bmatrix} = \boldsymbol{B}^{-1}_{C_i} \begin{bmatrix} \Delta\boldsymbol{K}^R_{C_i,p_l,s_{il},z_{il},z_{i-1,l}} \\ \Delta\boldsymbol{K}^R_{C_i,p_u,s_{il},z_{il},z_{i-1,l}} \\ \vdots \\ \Delta\boldsymbol{K}^R_{C_i,p_l,s_{iu},z_{iu},z_{i-1,u}} \\ \Delta\boldsymbol{K}^R_{C_i,p_u,s_{iu},z_{iu},z_{i-1,u}} \end{bmatrix}, \tag{4.16}$$

where $\boldsymbol{B}_{C_i}$ is a 16-by-16 matrix

$$\boldsymbol{B}_{C_i} = \begin{bmatrix} 1 & p_l & s_{il} & \dots & z_{il} & z_{i-1,l} \\ 1 & p_u & s_{il} & \dots & z_{il} & z_{i-1,l} \\ & & \vdots & & & \\ 1 & p_l & s_{iu} & \dots & s_{iu}z_{iu}z_{i-1,u} & p_l s_{iu} z_{iu} z_{i-1,u} \\ 1 & p_u & s_{iu} & \dots & s_{iu}z_{iu}z_{i-1,u} & p_u s_{iu} z_{iu} z_{i-1,u} \end{bmatrix}. \tag{4.17}$$

After knowing $\mathbb{K}^R_{C_i,j}$ vectors, $\Delta\boldsymbol{K}^R_{C_i,p,s_i,z_i,z_{i-1}}$ can be obtained using Eq. 4.15 for given (p, s_i, z_i, z_{i-1}) values within their bounds.

Similarly, $\Delta\boldsymbol{K}^R_{S_i,p,s_i}$ is a function of two parameters with small variations, can be obtained using bi-linear function. $\Delta\boldsymbol{K}^R_{S_i,p,s_i}$ can be represented using a bi-linear function.

$$\Delta\boldsymbol{K}^R_{S_i,p,z_i} \approx \begin{bmatrix} 1 & p_i & z_i & z_i z_{i-1} \end{bmatrix} \begin{bmatrix} \mathbb{K}_{S_i,1} \\ \mathbb{K}_{S_i,2} \\ \mathbb{K}_{S_i,3} \\ \mathbb{K}_{S_i,4} \end{bmatrix}, \tag{4.18}$$

where $\mathbb{K}_{S_i,j}$ for $j = 1\ 4$, which are unknown coefficient matrices, can be solved by plugging in 4 different sets of parameters p, z_i at their extreme values to Eq. 4.18

$$\begin{bmatrix} \mathbb{K}^R_{S_i,1} \\ \mathbb{K}^R_{S_i,2} \\ \mathbb{K}^R_{S_i,3} \\ \mathbb{K}^R_{S_i,4} \end{bmatrix} = \boldsymbol{B}^{-1}_{S_i} \begin{bmatrix} \Delta\boldsymbol{K}^R_{S_i,p_l,z_{il},z_{i-1,l}} \\ \Delta\boldsymbol{K}^R_{S_i,p_u,z_{il},z_{i-1,u}} \\ \Delta\boldsymbol{K}^R_{S_i,p_l,z_{iu},z_{i-1,l}} \\ \Delta\boldsymbol{K}^R_{S_i,p,z_{iu},z_{i-1,u}} \end{bmatrix} \tag{4.19}$$

where $\boldsymbol{B}_{S_i}$ is a 4-by-4 matrix

$$\boldsymbol{B}_{S_i} = \begin{bmatrix} 1 & p_l & z_{il} & p_l z_{il} \\ 1 & p_u & z_{il} & p_u z_{il} \\ 1 & p_l & z_{iu} & p_l z_{iu} \\ 1 & p_u & z_{iu} & p_u z_{iu} \end{bmatrix}. \tag{4.20}$$

After knowing $\mathbb{K}^R_{S_i,j}$ vectors, $\Delta \boldsymbol{K}^R_{S_i,p,z_i}$ can be obtained using Eq. 4.18 for given (p, z_i) values within their bounds.

$\boldsymbol{K}^R_{p,\boldsymbol{s},\boldsymbol{z}}$ in the reduced-order system dynamic equations Eq. 4.7 can be obtained using Eq. 4.11 by linear interpolation Eq. 4.13, bi-linear interpolation Eq. 4.18, and quadra-linear interpolation Eq. 4.18 for given structural variations. $\boldsymbol{C}^R_{p,\boldsymbol{s},\boldsymbol{z}}$, which can be obtained using Eq. 4.8, is also required to construct Eq. 4.7. The stiffness matrices $\boldsymbol{K}_{F10\%,p,\boldsymbol{0},\boldsymbol{z}_l}$ in Eq. 4.8 can be obtained using linear interpolation with respect to p. One first obtains the stiffness matrices $\boldsymbol{K}_{F10\%,p_u,\boldsymbol{0},\boldsymbol{z}_l}$ and $\boldsymbol{K}_{F10\%,p_l,\boldsymbol{0},\boldsymbol{z}_l}$ at the extreme PreV levels using finite element analyses where the stiffness of foams are 10% higher than the nominal design of foams and project them using $\boldsymbol{T}^R$

$$\begin{aligned} \boldsymbol{K}^R_{F10\%,p_u,\boldsymbol{0},\boldsymbol{z}_l} &= (\boldsymbol{T}^R)^T \boldsymbol{K}_{F10\%,p_u,\boldsymbol{0},\boldsymbol{z}_l} \boldsymbol{T}^R \\ \boldsymbol{K}^R_{F10\%,p_l,\boldsymbol{0},\boldsymbol{z}_l} &= (\boldsymbol{T}^R)^T \boldsymbol{K}_{F10\%,p_l,\boldsymbol{0},\boldsymbol{z}_l} \boldsymbol{T}^R \end{aligned}. \tag{4.21}$$

Similar to Eq. 4.13, linear interpolation is employed to obtain the stiffness matrix $\boldsymbol{K}^R_{F10\%,p,\boldsymbol{0},\boldsymbol{z}_l}$ at PreV level p

$$\begin{aligned} \boldsymbol{K}^R_{F10\%,p,\boldsymbol{0},\boldsymbol{z}_l} = &\frac{p - p_l}{p_u - p_l} (\boldsymbol{K}^R_{F10\%,p_u,\boldsymbol{0},\boldsymbol{z}_l} - \boldsymbol{K}^R_{F10\%,p_l,\boldsymbol{0},\boldsymbol{z}_l}) \\ &+ \boldsymbol{K}^R_{F10\%,p_u,\boldsymbol{0},\boldsymbol{z}_l} \end{aligned}. \tag{4.22}$$

4.3 Validation

To demonstrate the proposed approaches, the academic battery pack model described in Fig. 4.1 is used. The FEM of the academic battery pack has about 180,000 DOFs. In contrast, PROMs have only 72 DOFs. In Eq. 4.1, the lower and upper bounds of PreV level are $p_l = 0\%$ and $p_u = 6\%$. The lower and upper bounds of C2CV level are $s_{il} = -10\%$ and $s_{iu} = 10\%$. The lower and upper bounds of S2SV level are $z_{il} = 0\%$ and $z_{iu} = 50\%$. The number of cells is $N_c = 20$, and the number of spacers is $N_s = 19$.

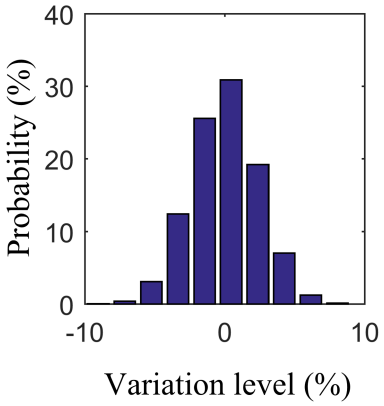

Figure 4.5: The cell-to-cell variation level distribution.

To validate PROMs with linear structural variations, the PreV level is chosen to be at $p = 3\%$, which is at the middle of its lower and upper bounds. The C2CV level is randomly generated from -10% to 10% with normal distribution and zero mean as shown in Fig 4.5. Since there are 19 spacers, a random integer number, which is randomly generated with uniform distribution with in $1 \sim 2^{19}$ as shown in Fig. 4.6, is binarized to generated 19 S2SV levels for each S2SV case.

Since the vibration response of cells in the battery pack are dominated by the first plate-like mode[72], the maximum amplitude of the vibration of each node occurs at the central node of each cell. Fig. 4.7 shows the vibration response at the central node of cell 10 calculated using PROMs (orange dashed line) and full-order FEM

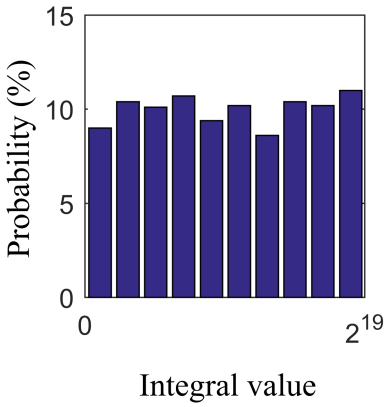

Figure 4.6: The spacer-to-spacer variation level distribution.

(red solid line). Fig. 4.7 shows that the vibration response predicted by PROMs follows the response predicted by the full-order model very well. The error of the peak value is only about 1.44%. However, the computational time is very different . Tab. 4.1 shows the average computational time for the full-order model and PROMs to predict the vibration response at a frequency.

Table 4.1: Average computational time

	Full	PROMs
Linear	420(s)	0.13(s)

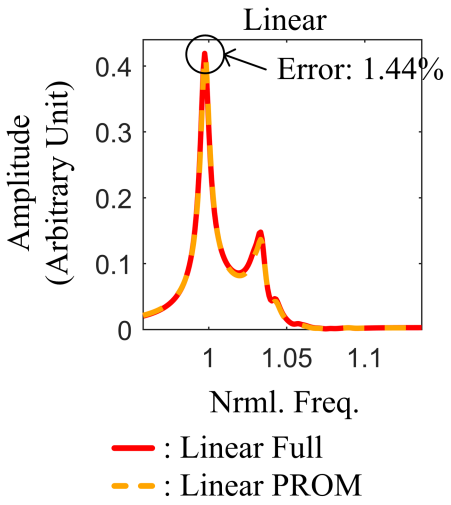

Figure 4.7: Vibration response calculated using PROMs and full-order FEM with PreV, C2CV, and S2SV.

The average computational gain of linear case is 3,230 and can increase if the mesh of FEM becomes finer. It is because the computational time of the full-order model increases with the mesh density. However, the computational time of PROMs depends on the number of modes selected, which is related to the physics of the system. If physics of the system remains the same but the mesh become finer, the number of modes selected is still the same. Thus, the computational time for PROMs remains similar, but the time for the full-order model is expected to be increased. Therefore, the computational gain increases.

4.4 Optimization

Since cells are mechanically coupled to each other through spacers, the arrangement of different types of spacers can change the vibration response of the battery pack. There are 19 spaces for 2 types of spacers in the academic battery pack and therefore there are 2^{19} S2SV cases, which represent combinations of the arrangement of spacers. The simulation of an arrangement of spacer needs significant computational effort and time using full-order model, thus PROMs are employed to predict the vibration response. Monte Carlo simulations are performed using PROMs with 1,000 S2SV cases to demonstrate the effect of the arrangement of spacers.

For each S2SV case, the vibration response at the central of each cell are collected, and the corresponding maximum value ξ_i of cell i over the range of excitation frequency is calculated for each cell. The circled peak value in Fig. 4.7 shows an example of ξ_{10}. Next, the average and standard deviation of ξ_i for $i = 1 \sim N_c$ over 1,000 S2SV cases are calculated, and the results are shown in Fig. 4.8.

The battery pack fails if one of cells fails since cells are connected in series. The cell which has the maximum vibration response has the highest possibility of failure. Consequently, the objective is to minimize ξ_i over 20 cells. Mathematically, the cost

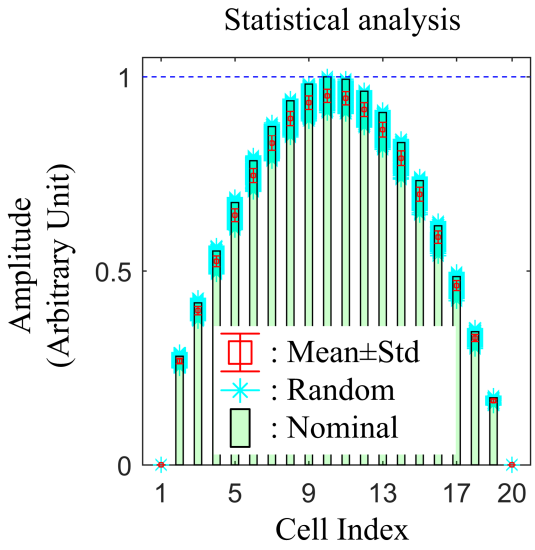

Figure 4.8: Statistical analysis for 1,000 spacer-to-spacer variation cases.

function is written as

$$\begin{aligned} &minimize: && \underset{\boldsymbol{z}}{max}\ \underset{i=1\sim N_s}{max}\ \xi_i(\boldsymbol{z}) \\ &\text{Subject to}: && z_i = \{z_{il}, z_{iu}\},\ i = 1 \sim N_s \end{aligned} \tag{4.23}$$

The cost function $\underset{i=1\sim N_s}{max}\ \xi_i(\boldsymbol{z})$ represents the maximum vibration response over 20 cells over a frequency range. The variable $\boldsymbol{z}$ represents the arrangement of spacers. z_i is either z_{il} or z_{iu} since each spacer is either type 1 or type 2.

Because the cost function is a non-convex and nonlinear function of the variable $\boldsymbol{z}$ with discrete-valued variables, a genetic algorithm which is a non-gradient based method is employed to search for the optimized solution. Since the genetic algorithm is based on random search, the optimization problem is solved for eight times and the best solution is obtained among the eight optimized solutions. A single optimization problem solved using a genetic algorithm may require tens of thousands of simulations due to random search. The simulation time for the optimization problem is reduced using PROMs. Fig. 4.9(a) shows the best solution where the first 14 spacers are type 1 and the last 5 spacers are type 2. Fig. 4.9(b) compares the vibration response at

the central node of cell 10 between nominal and the best arrangements of spacers. The peak of the vibration response drops 8.5% with the best arrangement.

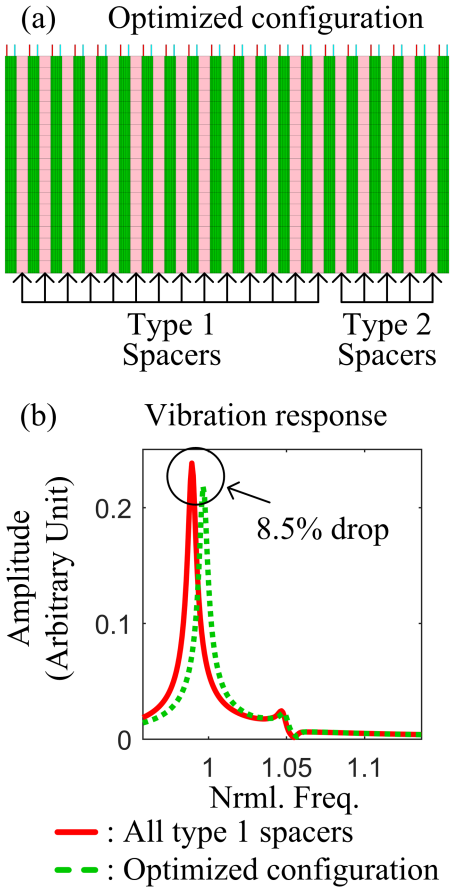

Figure 4.9: (a) The optimized arrangement of spacers. (b) The vibration response at cell 10 with nominal and optimized arrangement of spacers.

The vibration response can be significantly amplified due to small structural variations when the frequency of excitation lies in a high modal density region. Fig. 4.10 shows the Monte Carlo simulations of vibration response for the battery pack with 1,000 cases of random C2CV. Similar to Fig. 4.8, the vibration response at the central of each cell is measured and the corresponding maximum value ξ_i is calculated for all cells. Fig. 4.10(a) shows the results for battery pack with nominal arrangement of spacers, while Fig. 4.10(b) shows the results with optimized arrangement. The average value and standard deviation of ξ_i are marked on Fig. 4.10 are generally reduced due to the optimized arrangement of spacers, which reduces the risk of failure of cells.

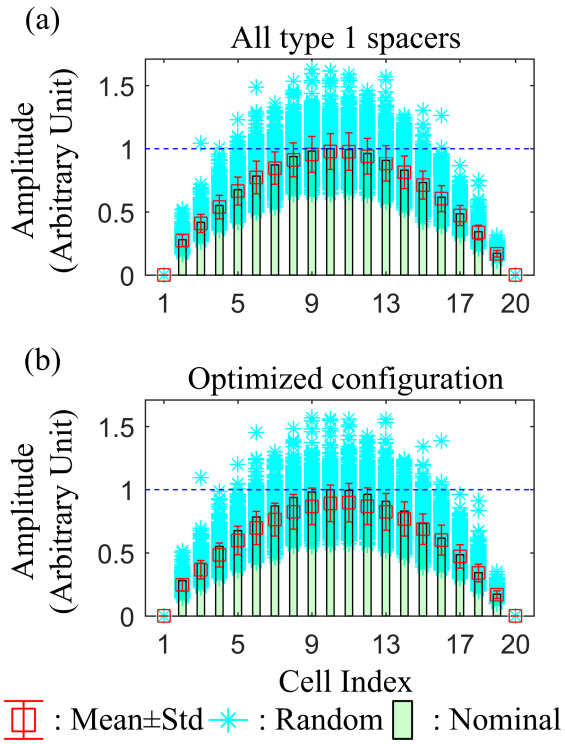

Figure 4.10: Statistical analysis for 1,000 cell-to-cell variation cases with (a) nominal and (b) optimized arrangement of spacers

4.5 Conclusion

The battery pack constitute a plural of nominally identical cells, which mechanically coupled to each other through spacers and foams. The natural frequency plot of the battery pack shows high modal density regions because of repeated substructures. A small structural variation may cause significant change in vibration response when the frequency of excitation lies in a high modal density region. The small structural variations considered here are PreV, C2CV, and S2SV.

Because the vibration response of battery packs is an essential metric for the fatigue life and reliability, the statistical analysis is required to investigate the effect of random structural variations. Also, the arrangement of different type of spacers can mitigate the vibration response and the optimized arrangement can be solved using a genetic algorithm which requires solving the vibration response multiple times for

different arrangement of spacers in the random search process. However, typical full-order model can easily have millions of DOFs, and thus multiple simulations are computationally prohibitive. Thus, PROMs are proposed to overcome this difficulty. PROMs can accurately and efficiently predict vibration responses of battery packs with PreV, C2CV, and S2SV simultaneously. Once PROMs are built, to predict the vibration response of the battery pack with structural variations, the full-order model can be avoided. The average simulation time of PROMs is 3,230 times faster than the full-order model.

The Monte Carlo analysis of the battery pack with random S2SV shows that the arrangement of different types of spacers can lower the vibration response. Moreover, the average vibration response for the battery pack with random C2CV is also lowered with the optimized arrangement of spacers. PROMs, which predict vibration response with random structural variations efficiently, improves the design capability of battery packs and shorten the time of design process.

CHAPTER V

Summary and future works

5.1 Summary

Battery packs are widely used on EVs and experience road and vehicle vibrations which shorten the fatigue life of battery packs. The amplitude of vibration response is a key factor of reliability of battery packs. Battery packs are comprised of multiple nominally identical cells and show high modal density in their natural frequency plot. An academic battery pack model which is comprised of 20 cells was introduced to demonstrate high modal density regions. In Chap 2, the academic battery pack without foams was investigated. In Chap 3 and 4, the academic battery pack with foams was studied.

The vibration response of a battery pack with small structural variations may change significantly when the frequency of excitation applied to the battery pack lies in a high modal density region compared to the nominal design of the battery pack. The structural variations considered in this dissertation includes linear and nonlinear variations. The linear variations involve PreV, C2CV, and S2SV, where stiffness matrices of elements in the FEM of battery packs are independent of deformation. In contrast, the nonlinear behavior in cells and foams exhibit hardening effects of material property in deformed elements of FEM of battery packs. The structural variations have significant influence on the vibration response of battery packs and

their effect needs to be identified in the design process of battery packs. The structural variations are random in a range and requires statistical analyses. However, even a full-order model analysis, which is required for a given structural variation case, is computationally prohibitive.

PROMs, which capture both linear and nonlinear structural variations simultaneously, are developed to reduce computational time of full-order analysis while maintaining high accuracy. PROMs obtain stiffness matrices of components with linear structural variations using interpolation. The nonlinear behavior in cells and foams is modeled in PROMs based on the observation that the vibration responses of the battery pack are dominated by the first plate-like mode of each cell.

With PROMs as a design tool, statistical analyses were performed to discuss that effects of small random structural variations are not negligible. The results show that maximum amplitudes of vibration responses of each cell in a frequency range can be amplified drastically, and the location of maximum vibration amplitude in academic battery packs can change from one cell to another. The results also show that different arrangements of spacers can mitigate vibrations responses of battery packs. Consequently, an optimization of the arrangement of spacers was performed using PROMs to minimize the vibration response of the battery pack.

In Chapter II, the proposed nonlinear PROMs was used to capture the PreV of the battery pack, the C2CV of each cell, and the nonlinear behavior in cells. Since cells are mechanically coupled through spacers and the stiffness matrices of cells are dependent on C2CV, the stiffness matrix of a cell was obtained using linear interpolation with respect to C2CV of that cell. The order of the system dynamic equations with structural variations was reduced by the transformation matrix, which was constructed from modes from two extreme cases of PreV levels. The nonlinear PROMs was built based on the observation that cells essentially vibrate along their first plate-like modes, while the strain distribution of a cell is a function of a single

parameter, the modal amplitude of its first plate-like mode. The nonlinear PROMs was solved using the iterative method, which was validated by using a time-marching method and an algebraic solver.

In Chapter III, the effect of foams were modeled. The FEMs of the battery pack were re-designed with cells mechanically coupled through spacers and foams. Since stiffness matrices of cells are dependent on both PreV and C2CV when foams are involved, the stiffness matrix of a cell is obtained using bi-linear interpolation with respect to PreV and C2CV. The key to constructing nonlinear PROMs is based on the observation that foams are often made of polymeric material which is much softer than cells. Consequently, the vibration responses of foams are dominated by the two first plate-like modes of neighboring cells - one from each cell. The vibration responses predicted using nonlinear PROMs were validated using full-order models.

In Chapter IV, the effect of spacers was considered. Since spacers may have different equivalent stiffness, according to their design and material, PROMs capture this effect by considering different types of spacers as S2SV. The mechanical coupling between cells varies when different types of spacers are placed between cells, leading to changes in the vibration response of battery packs. Since stiffness matrices of cells are dependent on four parameters: PreV, C2CV, and two S2SVs of neighboring spacers, the stiffness matrix of a cell was obtained using a unique quadra-linear interpolation with respect to these four parameters. Since the vibration response is a key metric of reliability of battery packs, the goal is to minimize the vibration response. The arrangement of different types of spacers was chosen as the variable for the optimization problem with the vibration response as the cost function. Since the vibration response is a non-convex nonlinear function of the arrangement of spacers and the variables of the optimization problem are discrete numbers, a genetic algorithm was employed to solve the optimization problem. The genetic algorithm is a random random search approach which requires an extensive number of simulations;

hence, PROMs were applied to reduce the simulation time. The optimal solution was shown to reduce the vibration response of the academic battery packs.

5.2 Future work

Based on the work reported in this dissertation, some ideas for future research may be considered.

1. Extension of PROMs capturing first few plate-like modes

   Nonlinear PROMs developed in Chapter III show good accuracy and speed for predicting vibration responses of battery packs with nonlinear material in cells and foams. However, the vibration response may not be dominated by only the first plate-like mode or just one plate-like mode depending on the force excitation and the boundary conditions applied to the battery pack. Consequently, PROMs can be improved by including more plate-like modes. To include more plate-like modes, Eq. 3.29 and Eq. 3.36 can be rewritten so that the vibration response can be approximated as the summation of static deformation and multiple plate-like modes multiplied by a participation factor matrix. This provides nonlinear PROMs with a capability of capturing vibration responses with various types of boundary conditions and force excitation, while only slightly increasing the computational time.

2. Extension of PROMs capturing more types of spacers

   In Chapter IV, PROMs capturing two different types of spacers considered as S2SV were developed, and a genetic algorithm was applied to find the optimal arrangement of spacers. However, there are more than two types of spacers and the vibration responses of battery packs may be further minimized when more types of spacers are used. To capture more types of spacers, modes from more cases of extreme structural variation levels may need to be included when con-

structing the transformation matrix. The quadra-linear interpolation may need to be modified to a higher order interpolation. Additionally, the cost function of the optimization problem in Chapter IV was formulated without PreV and C2CV. In future studies, the effect of PreV and C2CV can be considered into the cost function.

3. Verification of PROMs on a industrial battery pack model

   In this dissertation, an academic battery pack model with 20 nominally identical cells was used. However, battery packs used in industry may include dozens or even hundreds of cells with more sophisticated structures. Compared to PROMs applied to the academic battery pack, PROMs applied to a more complicated system may show an even larger reduction in computational time, and the optimal arrangement of spacers may lower the vibration response even more.

4. Explore the physical explanation of the optimized of arrangement of spacers and provide design guidance to the industry

   The optimized arrangement of spacers in Fig. 4.9 shows the left 14 spacers are type 1 and the other spacers are type2. Is the ratio 14:9 remains a constant for a system with more cells? Is the optimized arrangement of spacers affected by the range of forcing frequency? Can we find a general design rule for the optimized arrangement of spacers? PROMs can be applied to explore the connection between the arrangement of spacers and the vibration response of battery packs.

BIBLIOGRAPHY

[1] O. van Vliet, A. S. Brouwer, T. Kuramochi, M. van den Broek, and A. Faaij, "Energy use, cost and co2 emissions of electric cars," *Journal of Power Sources*, vol. 196, no. 4, pp. 2298 – 2310, 2011.

[2] J. Gonder, T. Markel, M. Thornton, and A. Simpson, "Using global positioning system travel data to assess real-world energy use of plug-in hybrid electric vehicles," *Transportation Research Record: Journal of the Transportation Research Board*, vol. 2017, pp. 26–32, 2007.

[3] L. Lu, X. Han, J. Li, J. Hua, and M. Ouyang, "A review on the key issues for lithium-ion battery management in electric vehicles," *Journal of Power Sources*, vol. 226, pp. 272 – 288, 2013.

[4] G. L. Plett, "High-performance battery-pack power estimation using a dynamic cell model," *IEEE Transactions on Vehicular Technology*, vol. 53, pp. 1586–1593, Sept 2004.

[5] M. Einhorn, W. Roessler, and J. Fleig, "Improved performance of serially connected li-ion batteries with active cell balancing in electric vehicles," *IEEE Transactions on Vehicular Technology*, vol. 60, pp. 2448–2457, July 2011.

[6] F. Croce, M. L. Focarete, J. Hassoun, I. Meschini, and B. Scrosati, "A safe, high-rate and high-energy polymer lithium-ion battery based on gelled membranes prepared by electrospinning," *Energy & Environmental Science*, vol. 4, no. 3, pp. 921–927, 2011.

[7] J. Lepine, V. Rouillard, and M. Sek, "Review paper on road vehicle vibration simulation for packaging testing purposes," *Packaging Technology and Science*, vol. 28, no. 8, pp. 672–682, 2015.

[8] J. M. Hooper and J. Marco, "Understanding vibration frequencies experienced by electric vehicle batteries," in *IET Hybrid and Electric Vehicles Conference 2013 (HEVC 2013)*, pp. 1–6, Nov 2013.

[9] C. Yi, B. I. Epureanu, S.-K. Hong, T. Ge, and X. G. Yang, "Modeling, control, and performance of a novel architecture of hybrid electric powertrain system," *Applied Energy*, vol. 178, pp. 454 – 467, 2016.

[10] S.-I. Moon, I.-J. Cho, and D. Yoon, "Fatigue life evaluation of mechanical components using vibration fatigue analysis technique," *Journal of Mechanical Science and Technology*, vol. 25, pp. 631–637, Mar 2011.

[11] Y. Choi, D. Jung, K. Ham, and S. Bae, "A study on the accelerated vibration endurance tests for battery fixing bracket in electrically driven vehicles," *Procedia Engineering*, vol. 10, pp. 851 – 856, 2011. 11th International Conference on the Mechanical Behavior of Materials (ICM11).

[12] G. Kjell and J. F. Lang, "Comparing different vibration tests proposed for li-ion batteries with vibration measurement in an electric vehicle," in *2013 World Electric Vehicle Symposium and Exhibition (EVS27)*, pp. 1–11, Nov 2013.

[13] J. M. Hooper, J. Marco, G. H. Chouchelamane, J. S. Chevalier, and D. Williams, "Multi-axis vibration durability testing of lithium ion 18650 nca cylindrical cells," *Journal of Energy Storage*, vol. 15, pp. 103 – 123, 2018.

[14] G. Kjell and J. F. Lang, "Comparing different vibration tests proposed for li-ion batteries with vibration measurement in an electric vehicle," in *2013 World Electric Vehicle Symposium and Exhibition (EVS27)*, pp. 1–11, Nov 2013.

[15] M. Wang, A. V. Le, D. J. Noelle, Y. Shi, H. Yoon, M. Zhang, Y. S. Meng, and Y. Qiao, "Effects of electrode pattern on thermal runaway of lithium-ion battery," *International Journal of Damage Mechanics*, vol. 27, no. 1, pp. 74–81, 2018.

[16] Q. Wang, P. Ping, X. Zhao, G. Chu, J. Sun, and C. Chen, "Thermal runaway caused fire and explosion of lithium ion battery," *Journal of Power Sources*, vol. 208, pp. 210 – 224, 2012.

[17] Z. Rao and S. Wang, "A review of power battery thermal energy management," *Renewable and Sustainable Energy Reviews*, vol. 15, no. 9, pp. 4554 – 4571, 2011.

[18] P. Valdes-Dapena, "Gm recalls volts to fix fire risk," *CNN Money*, 2012.

[19] B. Johnson, ""major explosion" at gm plant near detroit," *CBS News*, 2012.

[20] C. Riley, "Tesla dodges full investigation after fiery crash," *CNN Money*, 2013.

[21] J. M. Hooper and J. Marco, "Characterising the in-vehicle vibration inputs to the high voltage battery of an electric vehicle," *Journal of Power Sources*, vol. 245, pp. 510 – 519, 2014.

[22] O. O. Bendiksen, "Mode localization phenomena in large space structures," *AIAA journal*, vol. 25, no. 9, pp. 1241–1248, 1987.

[23] O. Ezvan, A. Batou, C. Soize, and L. Gagliardini, "Multilevel model reduction for uncertainty quantification in computational structural dynamics," *Computational Mechanics*, vol. 59, pp. 219–246, Feb 2017.

[24] A. Batou, "A global/local probabilistic approach for reduced-order modeling adapted to the low- and mid-frequency structural dynamics," *Computer Methods in Applied Mechanics and Engineering*, vol. 294, pp. 123 – 140, 2015.

[25] A. Batou, C. Soize, and N. Brie, "Reduced-order computational model in nonlinear structural dynamics for structures having numerous local elastic modes in the low-frequency range. application to fuel assemblies," *Nuclear Engineering and Design*, vol. 262, pp. 276 – 284, 2013.

[26] S.-K. Hong, B. I. Epureanu, and M. P. Castanier, "Parametric reduced-order models of battery pack vibration including structural variation and prestress effects," *Journal of Power Sources*, vol. 261, no. 0, pp. 101 – 111, 2014.

[27] C. Hodges, "Confinement of vibration by structural irregularity," *Journal of Sound and Vibration*, vol. 82, no. 3, pp. 411–424, 1982.

[28] O. Bendiksen, "Localization phenomena in structural dynamics," *Chaos, Solitons & Fractals*, vol. 11, no. 10, pp. 1621–1660, 2000.

[29] D. S. Whitehead, "The maximum factor by which forced vibration of blades can increase due to mistuning," *Journal of Engineering for Gas Turbines and Power*, vol. 120, no. 1, pp. 115–119, 1998.

[30] D. Ewins, "The effects of detuning upon the forced vibrations of bladed disks," *Journal of Sound and Vibration*, vol. 9, no. 1, pp. 65 – 79, 1969.

[31] J. M. Hooper and J. Marco, "Experimental modal analysis of lithium-ion pouch cells," *Journal of Power Sources*, vol. 285, pp. 247 – 259, 2015.

[32] B. Kenney, K. Darcovich, D. D. MacNeil, and I. J. Davidson, "Modelling the impact of variations in electrode manufacturing on lithium-ion battery modules," *Journal of Power Sources*, vol. 213, pp. 391 – 401, 2012.

[33] A. K. Yuya Ishihara, Jumpei Terashima, "Battery pack spacer," *US Patents*, vol. US20160268573A1, 2015. Toyota Motor Corp.

[34] S. H. Yoshiaki Ogata, "Battery pack cooling structure," *US Patents*, vol. US6709783B2, 2000. Panasonic Corp.

[35] T. E. Shinji Hamada, "Cooling device for battery pack and rechargeable battery," *US Patents*, vol. US7618740B2, 2002. Panasonic Corp, Toyota Motor Corp.

[36] J. Jaguemont, L. Boulon, and Y. Dub, "A comprehensive review of lithium-ion batteries used in hybrid and electric vehicles at cold temperatures," *Applied Energy*, vol. 164, pp. 99 – 114, 2016.

[37] J. E. W. A. H. A. G. E. B. R. Brouns, "Electric vehicle battery pack," *US Patents*, vol. US5378555A, 1993. Motors Liquidation Co.

[38] R. S. B. M. J. D. D. Ploss, "Battery pack latching assembly for fastener driving tool," *US Patents*, vol. US6357534B1, 1998. Illinois Tool Works Inc.

[39] G. Kermani and E. Sahraei, "Review: Characterization and modeling of the mechanical properties of lithium-ion batteries," *Energies*, vol. 10, no. 11, 2017.

[40] W.-J. Lai, M. Y. Ali, and J. Pan, "Mechanical behavior of representative volume elements of lithium-ion battery cells under compressive loading conditions," *Journal of Power Sources*, vol. 245, pp. 609 – 623, 2014.

[41] C. Breitfuss, W. Sinz, F. Feist, G. Gstrein, B. Lichtenegger, C. Knauder, C. Ellersdorfer, J. Moser, H. Steffan, M. Stadler, P. Gollob, and V. Hennige, "A microscopic structural mechanics fe model of a lithium-ion pouch cell for quasi-static load cases," *SAE International Journal of Passenger Cars - Mechanical Systems*, vol. 6, pp. 1044–1054, apr 2013.

[42] E. Sahraei, R. Hill, and T. Wierzbicki, "Calibration and finite element simulation of pouch lithium-ion batteries for mechanical integrity," *Journal of Power Sources*, vol. 201, pp. 307 – 321, 2012.

[43] E. Sahraei, J. Meier, and T. Wierzbicki, "Characterizing and modeling mechanical properties and onset of short circuit for three types of lithium-ion pouch cells," *Journal of Power Sources*, vol. 247, pp. 503 – 516, 2014.

[44] M.-T. Yang and J. H. Griffin, "A reduced-order model of mistuning using a subset of nominal system modes," *Journal of Engineering for Gas Turbines and Power*, vol. 123, no. 4, pp. 893–900, 1999.

[45] W. C. HURTY, "Dynamic analysis of structural systems using component modes," *AIAA Journal*, vol. 3, pp. 678–685, Apr 1965.

[46] S. Rubin, "Improved component-mode representation for structural dynamic analysis," *AIAA Journal*, vol. 13, no. 8, pp. 995–1006, 1975.

[47] R. M. Hintz, "Analytical methods in component modal synthesis," *AIAA Journal*, vol. 13, no. 8, pp. 1007–1016, 1975.

[48] R. Craig and C. J. Chang, "Free-interface methods of substructure coupling for dynamic analysis," *AIAA Journal*, vol. 14, no. 11, pp. 1633–1635, 1976.

[49] W.-H. Shyu, J. Gu, G. M. Hulbert, and Z.-D. Ma, "On the use of multiple quasi-static mode compensation sets for component mode synthesis of complex structures," *Finite Elements in Analysis and Design*, vol. 35, no. 2, pp. 119–140, 2000.

[50] R. H. MacNeal, "A hybrid method of component mode synthesis," *Computers & Structures*, vol. 1, no. 4, pp. 581 – 601, 1971. Special Issue on Structural Dynamics.

[51] H. He, T. Wang, G. Chen, D. Sun, and R. Sun, "A real decoupled method and free interface component mode synthesis methods for generally damped systems," *Journal of Sound and Vibration*, vol. 333, no. 2, pp. 584 – 603, 2014.

[52] D. Sarsri, L. Azrar, A. Jebbouri, and A. E. Hami, "Component mode synthesis and polynomial chaos expansions for stochastic frequency functions of large linear fe models," *Computers & Structures*, vol. 89, no. 3, pp. 346 – 356, 2011.

[53] P. Seshu, "Substructuring and component mode synthesis," vol. 4, pp. 199–210, 01 1997.

[54] M. P. Castanier, Y.-C. Tan, and C. Pierre, "Characteristic constraint modes for component mode synthesis," *AIAA Journal*, vol. 39, no. 6, pp. 1182–1187, 2001.

[55] E. Balmés, "Parametric families of reduced finite element models. theory and applications," *Mechanical Systems and Signal Processing*, vol. 10, no. 4, pp. 381–394, 1996.

[56] S.-H. Lim, R. Bladh, M. P. Castanier, and C. Pierre, "Compact, generalized component mode mistuning representation for modeling bladed disk vibration," *AIAA Journal*, vol. 45, no. 9, pp. 2285–2298, 2007.

[57] S.-K. Hong, B. I. Epureanu, M. P. Castanier, and D. J. Gorsich, "Parametric reduced-order models for predicting the vibration response of complex structures with component damage and uncertainties," *Journal of Sound and Vibration*, vol. 330, no. 6, pp. 1091 – 1110, 2011.

[58] S.-K. Hong, B. I. Epureanu, and M. P. Castanier, "Next-generation parametric reduced-order models," *Mechanical Systems and Signal Processing*, vol. 37, no. 12, pp. 403 – 421, 2013.

[59] A. Cardona and M. Geradin, "Time integration of the equations of motion in mechanism analysis," *Computers & Structures*, vol. 33, no. 3, pp. 801 – 820, 1989.

[60] A. Cardona, T. Coune, A. Lerusse, and M. Geradin, "A multiharmonic method for nonlinear vibration analysis," *International Journal for Numerical Methods in Engineering*, vol. 37, no. 9, pp. 1593–1608, 1994.

[61] S. Baek and B. Epureanu, "Reduced-order modeling of bladed disks with friction ring dampers," *Journal of Vibration and Acoustics*, vol. 139, no. 6, pp. 061011–061011–9, 2017.

[62] M. Mitra, S. Zucca, and B. I. Epureanu, "Effects of contact mistuning on shrouded blisk dynamics," *Proceedings of ASME Turbo Expo 2016: Turbomachinery Technical Conference and Exposition, Seoul, South Korea*, June 13-17 2016.

[63] M. Mitra, S. Zucca, and B. I. Epureanu, "Adaptive microslip projection for reduction of frictional and contact nonlinearities in shrouded blisks," *Journal of Computational and Nonlinear Dynamics*, vol. 11, no. 4, pp. 041016–041016–15, 2016.

[64] J. Cannarella and C. B. Arnold, "Stress evolution and capacity fade in constrained lithium-ion pouch cells," *Journal of Power Sources*, vol. 245, pp. 745 – 751, 2014.

[65] K.-Y. Oh, N. A. Samad, Y. Kim, J. B. Siegel, A. G. Stefanopoulou, and B. I. Epureanu, "A novel phenomenological multi-physics model of li-ion battery cells," *Journal of Power Sources*, vol. 326, pp. 447 – 458, 2016.

[66] S. F. Schuster, M. J. Brand, P. Berg, M. Gleissenberger, and A. Jossen, "Lithium-ion cell-to-cell variation during battery electric vehicle operation," *Journal of Power Sources*, vol. 297, pp. 242 – 251, 2015.

[67] R. Yazami and Y. Reynier, "Thermodynamics and crystal structure anomalies in lithium-intercalated graphite," *Journal of Power Sources*, vol. 153, no. 2, pp. 312 – 318, 2006. Selected papers presented at the 2004 Meeting of the International Battery Association 2004 International Meeting of the International Battery Association.

[68] R. Fu, M. Xiao, and S.-Y. Choe, "Modeling, validation and analysis of mechanical stress generation and dimension changes of a pouch type high power li-ion battery," *Journal of Power Sources*, vol. 224, pp. 211 – 224, 2013.

[69] K.-Y. Oh, J. B. Siegel, L. Secondo, S. U. Kim, N. A. Samad, J. Qin, D. Anderson, K. Garikipati, A. Knobloch, B. I. Epureanu, C. W. Monroe, and A. Stefanopoulou, "Rate dependence of swelling in lithium-ion cells," *Journal of Power Sources*, vol. 267, pp. 197 – 202, 2014.

[70] K.-Y. Oh, J. B. Siegel, L. Secondo, S. U. Kim, N. A. Samad, J. Qin, D. Anderson, K. Garikipati, A. Knobloch, B. I. Epureanu, C. W. Monroe, and A. Stefanopoulou, "Rate dependence of swelling in lithium-ion cells," *Journal of Power Sources*, vol. 267, no. 0, pp. 197 – 202, 2014.

[71] K.-Y. Oh, B. I. Epureanu, J. B. Siegel, and A. G. Stefanopoulou, "Phenomenological force and swelling models for rechargeable lithium-ion battery cells," *Journal of Power Sources*, vol. 310, pp. 118 – 129, 2016.

[72] J.-C. Lu, D. Kiran, M. P. Castanier, and B. I. Epureanu, "Nonlinear parametric reduced-order model for the structural dynamics of hybrid electric vehicle batteries," *Journal of Vibration and Acoustics*, vol. 140, no. 2, pp. 021018–021018–9, 2017.

[73] S. Filippi and P. J. Torvik, "A methodology for predicting the response of blades with non-linear coatings," *ASME Proceedings*, vol. 6, pp. 729–737, 2010.